



Mélanie Burette

French, born 16th June 1993
melanie.burette@crbm.cnrs.fr
burette.melanie@gmail.fr

Position:

Post-doctoral researcher (since January 2021)
CRBM CNRS UMR5237 Montpellier, France
Supervisor : Dr. Cécile Gauthier-Rouvière

Academic achievements

- 2020: **Doctor of Philosophy in Cell Biology**
Université de Montpellier, France
IRIM CNRS UMR9004 Montpellier, France
Supervisor : Dr. Matteo Bonazzi
- 2017: **Master of Science in Microbiology and Immunology**
Université de Montpellier, France.
- 2015: **Bachelor of Science in Ecology and Organismal Biology**
Université de Montpellier, France.
- 2011: **A-level in Science**
Lycée Jean Renoir, France

Awards and honors

- 2019: **IRIM Institute Meeting Grant**
- 2019: **European Society of Endocrinology Meeting Grant** for the 44th symposium on Hormones and Cell Regulation.
- 2018: Winner “Prix du meilleur poster” of the 16th meeting of PhD students in Chemical and Biological Sciences for Health CBS2 Doctoral School, Montpellier, France.

List of Publications

1. **Burette M.** *, Bienvenu A. *, Inamdar K., Bordignon B., Swain J., Muriaux D., Martinez E., Bonazzi M. (*Submitted*) Identification of a new *Coxiella* lipid-binding effector protein by a vacuolar lipid profiling.

2. Martinez E., Huc-Brandt S., Brelle S., Allombert J., Cantet F., Gannoun-Zaki L., **BURETTE M.**, Martin M., Letourneur F., Bonazzi M. and Molle V. (2020) The *Coxiella burnetii* secreted protein kinase CstK influences vacuole development and interacts with the GTPase-activating protein TBC1D5. **Journal of Biological Chemistry**, 295(21): 7391-7403, doi: 10.1074/jbc.RA119.01011.
3. **Burette M.** *, Allombert J. *, Lambou K., Maarifi G., Nisole S., Case ED., Blanchet FP., Hassen-Khodja C., Cabantous S., Samuel J., Martinez E., Bonazzi M. (2020) Modulation of innate immune signaling by a *Coxiella burnetii* eukaryotic-like effector protein. **PNAS**, 117(24): 13708-13718, doi: 10.1073/pnas.1914892117.
4. Siadous FA., Cantet F., van Schaik E., **Burette M.**, Allombert J., Lakhani A., Bonaventure B., Goujon C., Samuel J., Bonazzi M., Martinez E. (2020) *Coxiella* effector protein CvpF subverts RAB26-dependent autophagy to promote vacuole biogenesis and virulence. **Autophagy**, 1 :1-17, doi: 10.1080/15548627.2020.1728098.

*: Co-first author

Reviews

1. **Burette M.** and Bonazzi M. (2020) From neglected to dissected: how technological advances are leading the way to the study of *Coxiella burnetii* pathogenesis. **Cellular Microbiology**, 22(4):e13180. doi: 10.1111/cmi.13180.

Mentoring

2018-2020 : Supervision of 2 middle school students in the context of the "Apprentis Chercheurs" initiative organised by the association "Arbre des Connaissances".

2020: Supervision of a M.Sc. student (Mr Arthur Bienvenu), UMR9004 IRIM CNRS, Montpellier, France.

2019: Supervision of a M.Sc. student (Ms Angélique Perret), UMR9004 IRIM CNRS, Montpellier, France.

2018: Supervision of a M.Sc. student (Mr Lucien Platon) and a B.Sc. student (Mr Matthéo Alcaraz) UMR9004 IRIM CNRS, Montpellier, France.

Teaching

Sept-Dec 2019 : Lecturer « Bacterial virulence factors » (2 hours), Licence professionnelle « Biologie analytique et expérimentale », IUT de Montpellier, France.

Jan-June 2019 : Supervision of mycology and microbial genetics practicals (20 hours) Licence professionnelle « Biologie analytique et expérimentale », IUT de Montpellier, France.

Sept-Dec 2018 : Lecturer « Experimental design for the study of host-pathogen interactions » (2 hours), Licence professionnelle « Biologie analytique et expérimentale », IUT de Montpellier, France.

Jan-June 2019 : Supervision of mycology and microbial genetics practicals (20 hours) Licence professionnelle « Biologie analytique et expérimentale », IUT de Montpellier, France.

Talks and seminars

01-10-19: Selected speaker at the 15th Annual meeting of the French Society for Microbiology, Paris, France.

29-05-19: Selected speaker at the 17th meeting of PhD students in Chemical and Biological Sciences for Health CBS2 Doctoral School, Montpellier, France.

19-02-19: Selected speaker at the 2nd MicrobiOccitanie meeting, Montpellier, France.

Posters

Burette M., Perret A., Martinez E. and Bonazzi M. (2019) 44th Symposium on Hormones and Cell Regulation - Inositol Lipids in Health and Diseases, Mont St Odile, France.

Burette M., Allombert J., Lambou K., Maarifi G., Nisole S., Hassen-Khodja C., Cabantous S., Martinez E. and Bonazzi M. (2018) 16th meeting of PhD students in Chemical and Biological Sciences for Health CBS2 Doctoral School, Montpellier, France.

Skills

1. Techniques :

1. **Molecular biology**: Cloning, expression and purification of recombinant proteins, *in vivo* and *in vitro* protein interaction analysis (Co-transfection, immunoprecipitation, co-immunoprecipitation, tripartite split-GFP assay, Western blot), siRNA, protein-lipid overlay assay (PIP strips, beads), cell fractionation.
2. **Cell biology**: Cell culture and handling (THP1, RAW, J774, HeLa, Vero, A431, U2OS, C2C12, MDA-MB-231), generation of stable cell

lines by transfection, flow cytometry, cellular infection, immunofluorescence.

3. **Microbiology**: Isolation, culture and handling of class 2 pathogens.
4. **Biophysics** : Confocal and epifluorescence microscopy, electronic microscopy.
5. **Bioinformatics** : TMHMM, RaptorX, I-Tasser, Phyre2, Metamorph, Serial Cloner, Cell Profiler, FlowJo
2. **Writing skills** : Writing, editing and proofreading scientific articles
3. **E-learning skills** : Writing and editing Massive Open Online Courses (MOOC)
4. **Softwares**: Windows, Mac OS, Word, Excel, Powerpoint.
5. **Languages** : French (mother tongue), English (intermediate).

Other Scientific activities

2018-2020: Member of the laboratory board (IRIM)

2018-2019: Elective representative of PhD students at the Doctoral College of the University of Montpellier.

2018-2019: Elective representative of PhD students at the CBS2 Doctoral School

Referees

Dr Matteo Bonazzi: matteo.bonazzi@irim.cnrs.fr

Dr Eric Martinez: eric.martinez@irim.cnrs.fr

Dr Cecile Squarizoni-Diaw: cecile.squarzonidiaw@cirad.fr

Modulation of innate immune signaling by a *Coxiella burnetii* eukaryotic-like effector protein

Melanie Burette^{a,1} , Julie Allombert^{a,1}, Karine Lambou^a , Ghizlane Maarifi^a, Sébastien Nisole^a , Elizabeth Di Russo Case^b , Fabien P. Blanchet^a , Cedric Hassen-Khodja^c , Stéphanie Cabantous^d , James Samuel^b , Eric Martinez^a , and Matteo Bonazzi^{a,2} 

^aInstitut de Recherche en Infectiologie de Montpellier (IRIM) UMR 9004, CNRS, Université de Montpellier, 34293 Montpellier, France; ^bDepartment of Microbial and Molecular Pathogenesis, Texas A&M Health Science Center College of Medicine, Bryan, TX 77807–3260; ^cMontpellier Ressources Imagerie (MRI), BioCampus Montpellier, CNRS, INSERM, Université de Montpellier, 34293 Montpellier, France; and ^dCentre de Recherche en Cancérologie de Toulouse, INSERM, Université Paul Sabatier-Toulouse III, CNRS, 31037 Toulouse, France

Edited by Ralph R. Isberg, Tufts University School of Medicine, Boston, MA, and approved April 21, 2020 (received for review August 27, 2019)

The Q fever agent *Coxiella burnetii* uses a defect in organelle trafficking/intracellular multiplication (Dot/Icm) type 4b secretion system (T4SS) to silence the host innate immune response during infection. By investigating *C. burnetii* effector proteins containing eukaryotic-like domains, here we identify NopA (nucleolar protein A), which displays four regulator of chromosome condensation (RCC) repeats, homologous to those found in the eukaryotic Ras-related nuclear protein (Ran) guanine nucleotide exchange factor (GEF) RCC1. Accordingly, NopA is found associated with the chromatin nuclear fraction of cells and uses the RCC-like domain to interact with Ran. Interestingly, NopA triggers an accumulation of Ran-GTP, which accumulates at nucleoli of transfected or infected cells, thus perturbing the nuclear import of transcription factors of the innate immune signaling pathway. Accordingly, qRT-PCR analysis on a panel of cytokines shows that cells exposed to the *C. burnetii* *nopA::Tn* or a Dot/Icm-defective *dotA::Tn* mutant strain present a functional innate immune response, as opposed to cells exposed to wild-type *C. burnetii* or the corresponding *nopA* complemented strain. Thus, NopA is an important regulator of the innate immune response allowing *Coxiella* to behave as a stealth pathogen.

Coxiella burnetii | effector proteins | innate immune sensing | host/pathogen interactions | nucleocytoplasmic transport

The nuclear factor kappa-light-chain-enhancer of activated B cells (NF- κ B) family of transcription factors regulates the expression of genes associated with diverse cellular functions and plays a central role in regulating the innate and acquired host immune response to bacterial infections (1, 2). Under physiological conditions, the transcription factors of the NF- κ B family are sequestered in the cytoplasm by specific interactions with nuclear factor kappa-light polypeptide gene enhancer in B cells inhibitor alpha (I κ B α), which mask the nuclear localization signal (NLS) on transcription factors. Exogenous signals, including recognition of the tumor necrosis factor (TNF) by TNF receptor or the bacterial lipopolysaccharide (LPS) by toll-like receptor 4 (TLR4), activate the NF- κ B signaling pathway by triggering the phosphorylation and proteasomal degradation of I κ B α , thus unmasking the NLS on transcription factors. The signal is then recognized by importin- α and members of the importin- β family, which mediate the translocation of transcription factors to the nucleus through nuclear pore complexes (1). Energy for nuclear transport of NLS-containing proteins is provided by intracellular gradients of the small GTPase Ras-related nuclear protein (Ran), which interacts with the importin complexes upon nuclear import. GDP-bound Ran is largely cytoplasmic and nuclear translocation triggers the conversion to the GTP-bound form by means of the Ran guanine nucleotide exchange factor (GEF) RCC-1 (regulator of chromosome condensation-1). In its GTP-bound form, Ran triggers the dissociation of importins from the cargo and importin complexes recycle back to the cytoplasm.

There, Ran GTPase activating protein (RanGAP) generates Ran-GDP, which dissociates from importin complexes (3).

Given its pivotal role in the antimicrobial response, it is not surprising to observe that a considerable number of bacterial pathogens deploy effector proteins that modulate the NF- κ B signaling pathway (1, 2). These are mostly involved in phosphorylation, ubiquitination, and proteasomal degradation of components of the NF- κ B complex, whereas others modulate NF- κ B-mediated transcription (1, 2). Interestingly, it has recently been reported that *Salmonella* and *Orientia tsutsugamushi* effector proteins can interfere with nucleocytoplasmic transport, thereby inhibiting nuclear translocation of the p65/RelA transcription factor (4, 5).

The Q fever pathogen *Coxiella burnetii* is an obligate intracellular bacterium that relies on the translocation of effector proteins by a defect in organelle trafficking/intracellular multiplication (Dot/Icm) type 4b secretion system (T4SS) to replicate within large autolysosomal-like compartments inside infected cells (6, 7). Bioinformatics analysis identified over 140 *C. burnetii* genes encoding candidate effector proteins (7); however, the majority of these remain underinvestigated due to the technical constraints associated with the genetic manipulation of this organism. A subset of effector proteins is involved in the biogenesis of *Coxiella*-containing vacuoles (CCVs), by rerouting membrane traffic to the bacterial replicative niche, while other effectors manipulate the

Significance

Coxiella burnetii is a stealth pathogen that evades innate immune recognition by inhibiting the NF- κ B signaling pathway. This process is mediated by the bacterial Dot/Icm secretion system; however, the bacterial effector/s, as well as the molecular mechanism involved in this process have remained unknown to date. Here, by investigating *C. burnetii* proteins with eukaryotic-like features (EUGENs), we discovered a new effector protein, NopA (nucleolar protein A), which localizes at nucleoli of infected cells and perturbs nucleocytoplasmic transport by manipulating the intracellular gradients of the GTPase Ran. In doing so, NopA reduces the nuclear levels of transcription factors involved in the innate immune sensing of pathogens and single-handedly down-modulates the expression of a panel of cytokines.

Author contributions: M. Burette, J.A., G.M., S.N., E.D.R.C., J.S., E.M., and M. Bonazzi designed research; M. Burette, J.A., K.L., G.M., S.N., E.D.R.C., and E.M. performed research; G.M., S.N., E.D.R.C., F.P.B., C.H.-K., and S.C. contributed new reagents/analytical tools; M. Burette, J.A., G.M., S.N., E.D.R.C., F.P.B., C.H.-K., J.S., E.M., and M. Bonazzi analyzed data; and M. Burette, E.M., and M. Bonazzi wrote the paper.

The authors declare no competing interest.

This article is a PNAS Direct Submission.

Published under the PNAS license.

¹M. Burette and J.A. contributed equally to this work.

²To whom correspondence may be addressed. Email: matteo.bonazzi@irim.cnrs.fr.

This article contains supporting information online at <https://www.pnas.org/lookup/suppl/doi:10.1073/pnas.1914892117/-DCSupplemental>.

First published June 1, 2020.

apoptotic and inflammatory pathways to ensure intracellular persistence (6). Importantly, *C. burnetii* behaves as a stealth pathogen, evading the host innate immune response by down-modulating the NF- κ B and the inflammasome signaling pathways (8, 9). The *C. burnetii* effector protein IcaA (inhibition of caspase activation A) inhibits NOD-like receptor family pyrin domain containing 3 (NLRP3)-mediated inflammasome activation induced by caspase-11 (8), whereas the NF- κ B signaling pathway is down-modulated in a Dot/Icm-dependent manner, by perturbing the nuclear translocation of the p65/RelA subunit, without affecting the overall cellular levels of p65 (9). However, the bacterial effector/s involved in this process remains uncharacterized (9). We have previously reported the large-scale phenotypic characterization of the *C. burnetii* transposon mutant library, which led to gaining important insights into the function of the Dot/Icm secretion system, and which highlight an important set of virulence determinants (10–12). Importantly, several genes involved in intracellular replication of *C. burnetii* encode proteins with predicted eukaryotic-like domains, which prompted us to investigate eukaryotic-like genes (EUGENS) on a genome-wide scale. Here, we identify and validate the Dot/Icm-mediated translocation of seven *C. burnetii* EUGENS. Among these, NopA (nucleolar protein A) displays four regulation of chromosome condensation (RCC) repeats, which are partially homologous to the seven repeats found in the bladed β -propeller structure of the Ran GEF RCC1 (13–15). Similarly to RCC1, NopA also localizes at the nucleus of infected or transfected cells; it is found associated with the chromatin nuclear fraction; and it uses the RCC-like domain to interact with Ran. Differently from RCC1, however, NopA accumulates at nucleoli and sequesters Ran, thus perturbing nucleocytoplasmic transport. Indeed, NopA perturbs nuclear translocation of p65 upon cell treatment with TNF- α or challenge with *C. burnetii*. Conversely, transposon insertions in the *nopA* gene restore nuclear translocation of p65 during infections, to levels that are similar to those observed with the Dot/Icm-deficient *C. burnetii* *dotA* mutant. Accordingly, myeloid cells challenged with the *C. burnetii* *nopA* or *dotA* mutant strains present a functional innate immune response, as opposed to myeloid cells exposed to wild-type (WT) *C. burnetii* or the *nopA* complemented strain.

Results

Identification of *C. burnetii* EUGENS. The searching algorithm for type IV effector proteins (S4TE) 2.0 (16) was used to identify *C. burnetii* eukaryotic-like genes (EUGENS) encoding candidate effector proteins. This allowed the identification of 56 genes, which were validated using the Protein families database (PFAM), Simple Modular Architecture Research Tool (SMART), Conserved Domain Database (CDD), and Eukaryotic Linear Motif (ELM) databases (SI Appendix, Table S1). Of these, 20 candidate EUGENS were retained for further analysis (SI Appendix, Table S2), based on the S4TE score (16), the eukaryotic-like domain encoded, and the presence of corresponding transposon mutants in our library (10). *cbu0072* (*ankA*), *cbu0201* (*ankC*), *cbu0447* (*ankF*), *cbu0781* (*ankG*), and *cbu1213* (*ankI*) encode ankyrin repeats (17, 18); *cbu0295*, *cbu0547*, and *cbu1457* (*cig43*) encode tetratricopeptide repeats; *cbu0175* and *cbu1379a* encode predicted Ser/Thr kinases; *cbu0801* (*rimI*), *cbu0505* (*cig14*), and *cbu1799* encode acetyltransferases; *cbu0096* encodes a predicted phospholipase D; *cbu0519* (*dedA*) encodes a SNARE-like domain-containing protein; *cbu1206* encodes a predicted sterol reductase; *cbu1217* encodes a protein with four regulation of chromosome condensation (RCC) repeats; *cbu1724* encodes a predicted F-box protein; *cbu1366* (*cig40*) encodes a coiled-coil domain-containing protein; and *cbu0542* (*ligA*) encodes a predicted DNA ligase (SI Appendix, Table S2). Of note, Dot/Icm-dependent translocation of proteins encoded by 8 of these genes has been previously validated using *Legionella pneumophila* as a surrogate system (17, 19, 20) (SI Appendix, Table S2). Selected genes were cloned into pXDC61K-*blaM* vector, thus generating N-terminal fusions with β -lactamase, and transformed into *C. burnetii* Nine Mile II (NMII) RSA439. The expression of 16 out of 20 chimeric proteins was validated by Western blot using an anti- β -lactamase antibody (SI Appendix, Fig. S1A). Candidate effector protein translocation was assessed at 6, 12, 24, 48, and 72 h postinfection using the β -lactamase assay. *C. burnetii* expressing β -lactamase alone or β -lactamase-tagged

CvpB (CBU0021) (12) were used as negative and positive controls, respectively. CvpB, CBU0295, and CBU1217 were efficiently translocated from 12 h postinfection, whereas AnkA, F, and G were translocated from 24 h postinfection (Fig. 1A and B). Finally, AnkC, CBU0175, and CBU1724 were also translocated, albeit less efficiently, at later time points of infection (Fig. 1A and B). Plasmids encoding translocated effectors were then transformed into the *C. burnetii* *dotA::Tn* strain to validate their Dot/Icm-dependent secretion at 72 h postinfection. The expression of 6 chimeric proteins was validated by Western blot using an anti- β -lactamase antibody (SI Appendix, Fig. S1B). None of the effector proteins were secreted by the Dot/Icm-defective mutant as expected (Fig. 1A). Next, *cbu0072* (*ankA*), *cbu0295*, *cbu0447* (*ankF*), *cbu0781* (*ankG*), and *cbu1217* were cloned into a pLVX-mCherry vector to tag effector proteins at their N-terminal domain and their localization was investigated in noninfected and *C. burnetii*-infected U2OS cells (Fig. 1C). AnkA and CBU0295 were mostly diffuse in the cytoplasm and did not localize at CCVs in infected cells. AnkF displayed a punctate pattern in the cytoplasm, which partially colocalized with the lysosomal marker LAMP1 in noninfected and infected cells alike (Fig. 1C). Differently from previous reports, indicating a translocation of AnkG from mitochondria to the nucleus of transfected cells following staurosporine treatment (21), in our hands, this effector protein displayed nuclear localization even in the absence of staurosporine, in both infected and noninfected cells (Fig. 1C). Of note, CBU1217 was exclusively localized at subnuclear structures in over 90% of either infected or noninfected cells (Fig. 1C).

The Effector Protein CBU1217 Localizes at Nucleoli in Infected and Transfected Cells.

The localization of CBU1217 was further investigated by cloning the gene into a pJA-LacO-4HA plasmid, to express the effector protein carrying an N-terminal 4xHA tag in *C. burnetii*, under the control of an isopropyl β -D-1-thiogalactopyranoside (IPTG) promoter, and monitor its localization during infection. GFP-expressing WT *C. burnetii* or the *dotIcm* mutant *dotA::Tn* (10) were transformed either with pJA-LacO-4HA or with pJA-LacO-4HA-*cbu1217*. Expression of 4HA-CBU1217 was validated by Western blot using an anti-HA antibody (SI Appendix, Fig. S1C). U2OS cells were challenged with the transformed *C. burnetii* strains and NopA localization was assessed, in the presence or absence of IPTG, using anti-HA and anti-fibrillarin antibodies, and Hoechst dye. Infections by *C. burnetii* transformed with pJA-LacO-4HA-*cbu1217* in the absence of IPTG did not show specific HA labeling (Fig. 2A). Addition of 1 mM IPTG triggered 4HA-CBU1217 expression, which colocalized with fibrillarin in over 90% of HA-positive cells (Fig. 2B). The intracellular localization of 4HA-CBU1217 was lost when cells were infected with the *dotA::Tn* mutant transformed with pJA-LacO-4HA-*cbu1217* in the presence of IPTG (Fig. 2D), confirming that CBU1217 is a Dot/Icm substrate. Induction of the expression of the HA tag alone did not show specific localization (Fig. 2C). We thus named the new *C. burnetii* EUGEN NopA, for nucleolar protein A.

As mentioned above, NopA encodes four RCC repeats in its C-terminal domain (Fig. 2E). In the eukaryotic protein RCC1, seven repeats are arranged in a seven-bladed propeller, which associates with nuclear chromatin and acts as a GEF for Ran, thus regulating nucleocytoplasmic protein transport (3). To determine the role of the RCC-like domain in NopA localization and function, the effector protein was cloned into a pRK5-HA plasmid to generate HA-tagged NopA. U2OS cells transfected with pRK5-HA-NopA were processed for immunofluorescence using Hoechst dye and anti-HA and anti-fibrillarin antibodies. In parallel, HA-NopA localization was investigated by Western blot using U2OS cells transfected as above and lysed and separated into cytoplasmic, nuclear, and chromatin fractions. Full-length NopA (NopA_{FL}) localized at nucleoli in over 90% of transfected cells, confirming our observations in the context of *C. burnetii* infections (Fig. 2E). Western blot analysis confirmed that NopA is excluded from the cytoplasmic fraction and localized at the soluble and chromatin nuclear fractions (Fig. 2E). Next, we generated HA-tagged NopA deletions to exclude (NopA_{N-ter}; amino acids [aa] 1 to 195, Fig. 2F) or include (NopA_{C-ter}; aa 196 to 497, Fig. 2G) the RCC repeats. Ectopically expressed HA-NopA_{N-ter} was

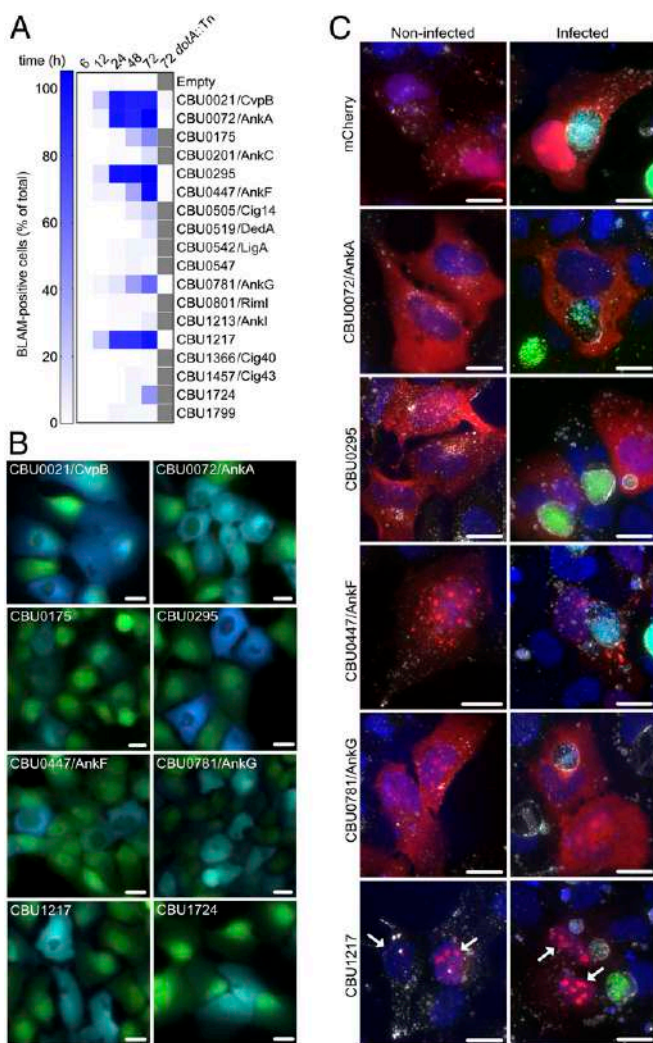


Fig. 1. Identification of *C. burnetii* EUGENs. (A) U2OS cells were challenged with *C. burnetii* strains expressing BLAM-tagged versions of candidate EUGENs for 6, 12, 24, 48, and 72 h. The percentage of BLAM-positive, infected cells was automatically calculated using CellProfiler over the total number of infected cells per each condition. Empty, BLAM empty vector. The Dot/Icm-dependent translocation of the effectors that were efficiently secreted was validated in the *dotA::Tn* mutant strain at 72 h postchallenge. (B) Representative images of positive (blue) cells treated as in A. (C) Non-infected or GFP-expressing *C. burnetii*-infected U2OS cells were transfected with plasmids encoding N-terminally tagged mCherry versions of the effector proteins validated in A (red). At 24 h after transfection, cells were fixed and labeled with Hoechst (blue) and an anti-LAMP1 antibody (white). White arrows point at CBU1217 subnuclear localization. (Scale bars, 10 μ m.)

excluded from nuclei and remained diffuse in the cytoplasm (Fig. 2F), whereas HA-NopA_{C-ter} retained the nucleolar localization (Fig. 2G). Cell fractionation confirmed the cytoplasmic localization of HA-NopA_{N-ter} and the nuclear localization of HA-NopA_{C-ter}, as well as the association with the chromatin fraction (Fig. 2F and G). Thus, despite the lack of typical nuclear or nucleolar localization signals, the C-terminal domain of NopA encoding the RCC-like domain, is necessary and sufficient for the nucleolar targeting of the effector protein. The role of the RCC repeats in the intracellular localization of NopA was further dissected by generating increasing deletions of single RCC repeats (numbered from 1 to 4 from the N-terminal) from either the N-terminal or C-terminal ends of HA-NopA_{C-ter} (SI Appendix, Fig. S2A). The intracellular localization of each construct was tested by immunofluorescence and cell fractionation following ectopic expression in U2OS cells. Interestingly,

this revealed that the first RCC repeat is critical for targeting NopA to the nucleus as removal of this repeat from NopA_{C-ter} displaces the protein to the cytoplasm (SI Appendix, Fig. S2B and C). The first two RCC repeats (RCC12; aa 196 to 310) alone localize within the nucleus but are excluded from nucleoli (SI Appendix, Fig. S2E) and instead localize at promyelocytic leukemia (PML) bodies (SI Appendix,

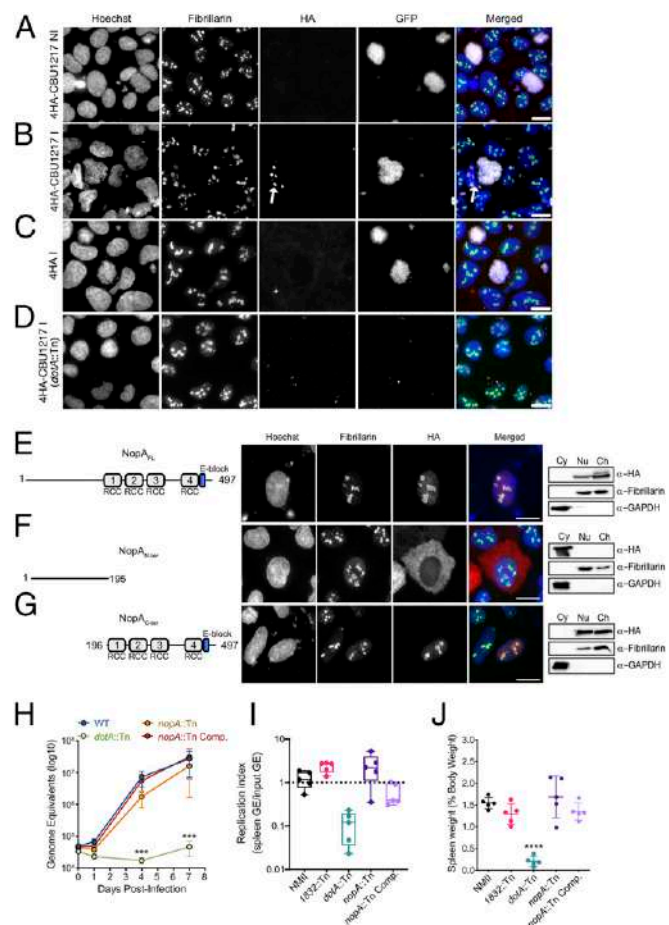


Fig. 2. Intracellular localization of CBU1217/NopA and role in *C. burnetii* replication during infection. U2OS cells were challenged either with WT GFP-tagged *C. burnetii* (white) transformed with plasmids encoding 4HA-tagged CBU1217/NopA (A and B, red) or the 4HA tag alone (C, red), or with the GFP-tagged *dotA::Tn* mutant (D, white), transformed with plasmids encoding 4HA-tagged CBU1217/NopA, all under the control of an IPTG-inducible promoter. At 72 h postinfection, cells were fixed and labeled with Hoechst (blue) and anti-fibrillarin antibodies (green). I, IPTG-induced; NI, noninduced. Arrow points at 4HA-CBU1217/NopA localization in infected cell. U2OS cells were transfected with plasmids encoding HA-tagged versions of either full-length (E) or the indicated deletion mutants (F and G) of HA-tagged NopA. At 24 h after transfection, cells were either fixed and labeled with Hoechst (blue), an anti-fibrillarin antibody (green) and an anti-HA antibody (red, Center), or lysed and processed for cell fractionation (Right). Cell fractions were analyzed by Western blotting using anti-fibrillarin and anti-GAPDH antibodies as nuclear and chromatin (Nu and Ch) and cytoplasmic (Cy) markers, respectively, and anti-HA antibodies to reveal NopA localization. (Scale bars, 10 μ m.) (H) Genome equivalents (GEs) calculated using TaqMan real-time PCR with DNA purified from infected spleens of 5 SCID mice per group on day 14 after challenge with 1×10^6 GEs of the strains shown. (I) Replication index calculated as the ratio between spleen GE at the time of necropsy and the input GE of the strains listed in the figure legend. (J) Spleen weight as a percentage of total body weight at the time of necropsy on day 14 after infection with 1×10^6 GEs of the strains listed in the figure legend. Values are the mean of three independent infections, with error bars indicating SDs from the mean. **** $P < 0.0001$, *** $P < 0.001$, two-way ANOVA (H) and one-way ANOVA (J), Dunnett's multiple comparisons test.

Fig. S2G). This localization remains unchanged with the addition of the third RCC repeat (SI Appendix, Fig. S2 D and F), and it is only with the addition of the complete NopA_{C-ter} that the protein localizes at nucleoli (Fig. 2G), suggesting the presence of a nucleolar-targeting motif in the fourth RCC repeat. Unfortunately, we were unable to express detectable amounts of single RCC repeats (RCC1 and RCC4, SI Appendix, Fig. S24).

NopA Is Not Involved in *C. burnetii* Intracellular Replication. Given the early translocation of NopA observed using the β -lactamase assay, we determined the time course of NopA production during infection. To this aim, we have complemented the *nopA* mutation, using a mini Tn7 transposon to integrate a WT copy of HA-tagged *nopA*, under the regulation of its predicted endogenous promoter, in the chromosome of the *C. burnetii* Tn227 strain, which carries the transposon insertion closest to the *nopA* start codon (10). Protein expression was then monitored by Western blot, using an anti-HA antibody, from cells challenged with the complemented *nopA*::Tn strain for 12, 24, 48, and 72 h. By this approach, detectable amounts of NopA were observed from 12 h postinfection (SI Appendix, Fig. S1D).

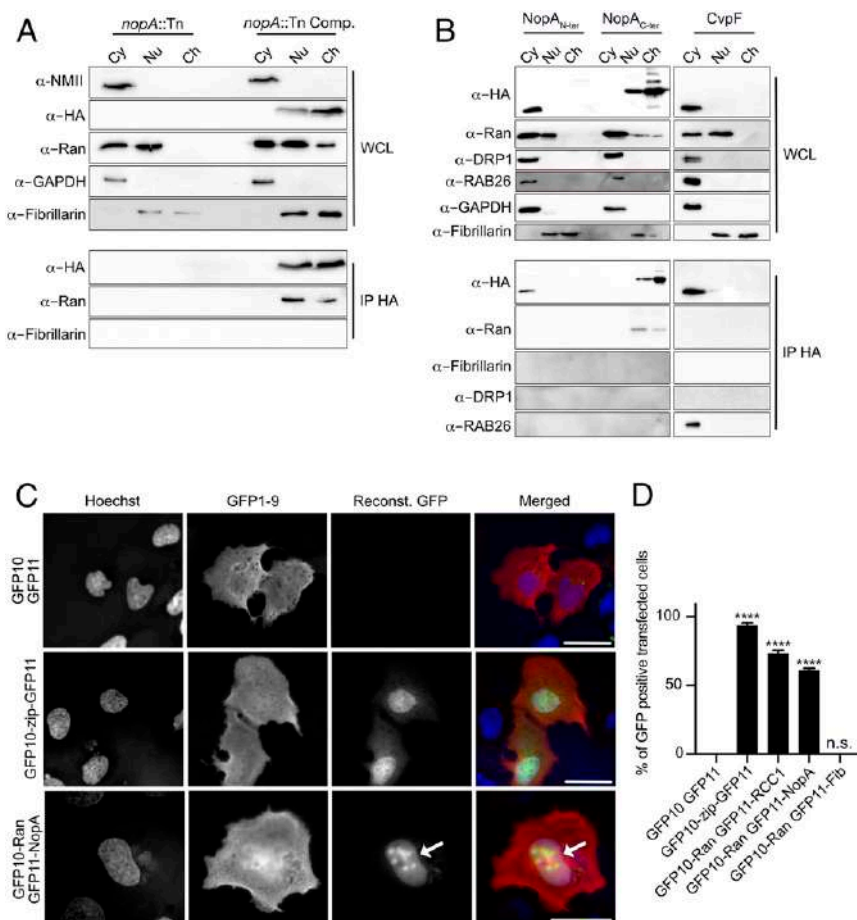
We previously reported that transposon insertions in *nopA* do not affect bacterial replication in Vero cells (10). To further investigate the role of NopA in *C. burnetii* infections, bacterial replication and virulence of the wild-type, *dotA*::Tn, *nopA*::Tn, and the *nopA*::Tn complemented strain (*nopA*::Tn Comp.) described above, were tested using either bone marrow-derived macrophages (BMDMs) or a severe combined immunodeficiency (SCID) mouse model of infection. Confirming our initial observations, transposon insertions in

nopA do not affect *C. burnetii* replication (Fig. 2 H and I) or virulence (as determined here by splenomegaly measurements, Fig. 2J).

NopA Interacts with the Small GTPase Ran. Given that NopA localizes at nucleoli and presents four out of the seven RCC repeats present in the eukaryotic Ran-GEF RCC1, we investigated whether NopA can interact with Ran. To this aim, U2OS cells incubated either with the *nopA*::Tn mutant or the complemented strain expressing 4HA-tagged NopA under the control of the predicted endogenous promoter (*nopA*::Tn Comp.). Twenty-four hours postinfection, cells were lysed, separated into cytoplasmic, nuclear, and chromatin fractions, and NopA was immunoprecipitated from cell fractions using an anti-HA antibody. As expected, NopA was not detected in cells infected with the *nopA*::Tn mutant strain, whereas it was efficiently isolated from the nuclear and chromatin fractions of cells challenged with the complemented strain (Fig. 3A). Of note, whole cell lysates of cells incubated with the complemented strain also presented an accumulation of Ran in the chromatin fraction, which was not observed in cells challenged with the *nopA*::Tn mutant strain (Fig. 3A). Importantly, Ran was efficiently detected, together with NopA, in immunoprecipitates from the nuclear and chromatin fractions of cells challenged with the *nopA*::Tn complemented strain, indicating indeed an interaction with the *C. burnetii* effector protein (Fig. 3A). The NopA/Ran interaction was further investigated in U2OS cells, following the ectopic expression of either HA-tagged NopA_{N-ter}, NopA_{C-ter}, or the *C. burnetii* effector protein CvpF as negative control (22). Unfortunately, under these conditions, we were unable to immunoprecipitate full-length NopA from transfected cells. Similarly to infected cells, 24 h posttransfection, cells were lysed,

Fig. 3. NopA interacts with the small GTPase Ran.

(A) U2OS cells challenged for 24 h with either the *C. burnetii* *nopA* transposon mutant (*nopA*::Tn) or the corresponding complemented strain (*nopA*::Tn Comp.) were lysed and processed for cell fractionation. Whole cell lysates (WCLs) were probed with the indicated antibodies, as well as anti-GAPDH and anti-fibrillarin antibodies as cytoplasmic (Cy), and nuclear/chromatin (Nu/Ch) markers, respectively. Following immunoprecipitation with anti-HA-coated magnetic beads, the presence of Ran and that of fibrillarin (as a negative control) was assessed using specific antibodies (IP HA). (B) U2OS cells transfected with HA-tagged versions of either the N-terminal domain (NopA_{N-ter}), the C-terminal domain (NopA_{C-ter}) of NopA, or CvpF as negative control were lysed and processed for cell fractionation. WCLs were probed with the indicated antibodies, as well as anti-GAPDH and anti-fibrillarin antibodies as cytoplasmic (Cy), nuclear/chromatin (Nu/Ch) markers, respectively. Following immunoprecipitation with anti-HA-coated magnetic beads, the presence of candidate interacting proteins was assessed using specific antibodies (IP HA). (C) U2OS cells were transfected with plasmids encoding GFP1-9 in combination with plasmids encoding either the GFP10 and GFP11 tags alone as negative control (Top row), GFP10 and GFP11 linked by a leucine zipper motif (GFP10-zip-GFP11) as positive control (Middle row), or GFP10-Ran and GFP11-NopA (Bottom row). At 24 h after transfection, cells were fixed and labeled with Hoechst (blue) and anti-GFP antibodies (red) to reveal nuclei and the expression of GFP1-9, respectively. Protein/protein interaction was assessed following the reconstitution of GFP (Reconst. GFP, green). Arrows point at nuclei in which Ran and NopA interact. (D) The percentage of cells presenting GFP reconstitution over the total number of GFP1-9-positive cells was calculated. Values are means \pm SD from two independent experiments. Asterisks indicate statistically significant variations (n.s., nonsignificant, **** P < 0.0001, one-way ANOVA, Dunnett's multiple comparison test). (Scale bars, 20 μ m.)



separated into cytoplasmic, nuclear, and chromatin fractions, and NopA truncations and CvpF were immunocaptured from cell fractions using an anti-HA antibody. As expected, NopA_{N-ter} and CvpF were efficiently isolated from the cytoplasmic fractions, whereas NopA_{C-ter} was isolated from the nuclear and cytoplasmic fractions (Fig. 3B). In agreement with what we observed in infected cells, the ectopic expression of NopA_{C-ter} triggered an accumulation of Ran to the chromatin fractions (Fig. 3B). Moreover, Ran was specifically detected in the nuclear and chromatin fractions upon immunocapturing of NopA_{C-ter}, confirming an interaction between the two proteins (Fig. 3B). Of note, no interaction was detected between Ran and NopA_{N-ter}, despite their shared cytoplasmic localization (Fig. 3B). Furthermore, NopA_{C-ter} did not interact with other small GTPases such as DRP1 or RAB26, nor with the nucleolar marker fibrillarin (Fig. 3B). Conversely, the *C. burnetii* effector protein CvpF (22), was readily immunocaptured from the cytoplasm of transfected cells and interacted with RAB26 as reported (22) (Fig. 3B).

Finally, the direct interaction between NopA and Ran was further investigated using the tripartite split-GFP interaction sensor (23). Briefly, the assay is based on a tripartite association between two GFP β -strands (GFP10 and GFP11), fused to proteins of interest, and the complementary GFP1-9 detector. If proteins interact, GFP10 and GFP11 self-associate with GFP1-9 to reconstitute a functional GFP. pCDNA3-zipper-GFP10 and pCDNA3-zipper-GFP11 were used as negative control, whereas a plasmid encoding GFP10 and GFP11 linked by a zipper motif (GFP10-zip-GFP11) was used as positive control (23). *ran* cDNA was cloned into the pCDNA3-GFP10-zipper plasmid to generate the GFP10-Ran, whereas *nopA*, *rcc1*, and *fbl* (the gene encoding fibrillarin) were cloned into the pCDNA3-zipper-GFP11 plasmid to generate the corresponding GFP11 fusion proteins. Combinations of the above-mentioned constructs with a pCMV plasmid encoding GFP1-9 were used for triple transfections in U2OS cells. After fixation, an anti-GFP antibody was used to identify cells expressing GFP1-9 (which is not fluorescent) and protein interactions were analyzed by monitoring GFP reconstitution. As expected, coexpression of GFP1-9 with GFP10 and GFP11 did not result in the reconstitution of GFP (Fig. 3C, Top row, and 3D). The coexpression of GFP1-9 with GFP10-zip-GFP11 led to the

reconstitution of GFP fluorescence in over 93% of transfected cells, demonstrating the functionality of the assay (Fig. 3C, Center row, and 3D). Importantly, over 60% of cells expressing GFP1-9 in combination with GFP10-Ran and GFP11-NopA showed reconstitution of GFP, with a fluorescent signal detected at nuclei, with a strong accumulation at nucleoli (Fig. 3C, Bottom row, and 3D). On the contrary, the expression of GFP1-9 in combination with GFP10-Ran and GFP11-RCC1 allowed reconstitution of GFP fluorescence, which was homogeneously detected in the nucleus in over 73% of transfected cells (SI Appendix, Fig. S3A and D). Lack of GFP reconstitution upon expression of GFP1-9 in combination with GFP10-Ran and GFP11-fibrillarin indicated that the shared nucleolar localization was not sufficient for GFP reconstitution (SI Appendix, Fig. S3A and D).

Ectopic expression of either mCherry-NopA_{FL} or mCherry-NopA_{C-ter} in combination with GFP-Ran in U2OS cells also confirmed the colocalization of both proteins at nucleolar structures labeled with the anti-fibrillarin antibody (SI Appendix, Fig. S3B). Conversely, Ran-GFP accumulation at nucleoli was lost when the small GTPase was ectopically expressed in U2OS cells in combination either with mCherry alone or mCherry-NopA_{N-ter} (SI Appendix, Fig. S3B). Collectively, these observations indicate that NopA specifically interacts with Ran and may sequester it at nucleoli.

NopA Preferentially Interacts with GDP-Bound Ran and Triggers an Increase in Ran-GTP. To determine whether NopA displays preferential binding to Ran in its GDP- versus GTP-bound form, a GFP-trap assay was carried out on U2OS cells cotransfected with plasmids encoding HA-NopA_{C-ter} in combination with either GFP alone, GFP-Ran, GFP-Ran_{T24N} (GDP-locked), GFP-Ran_{Q69L} (GTP-locked), or GFP-Ran_{N122I} (nucleotide-free form). Similar to RCC1, NopA displayed preferential binding to either GDP-locked Ran_{T24N} or the nucleotide-free form Ran_{N122I} (Fig. 4A).

Next, we investigated whether NopA binding to Ran can affect the Ran GDP/GTP ratio that is required to fuel nucleocytoplasmic transport. U2OS cells were challenged either with WT *C. burnetii*, the *dotA::Tn*, *nopA::Tn*, or the *nopA::Tn* complemented strains.

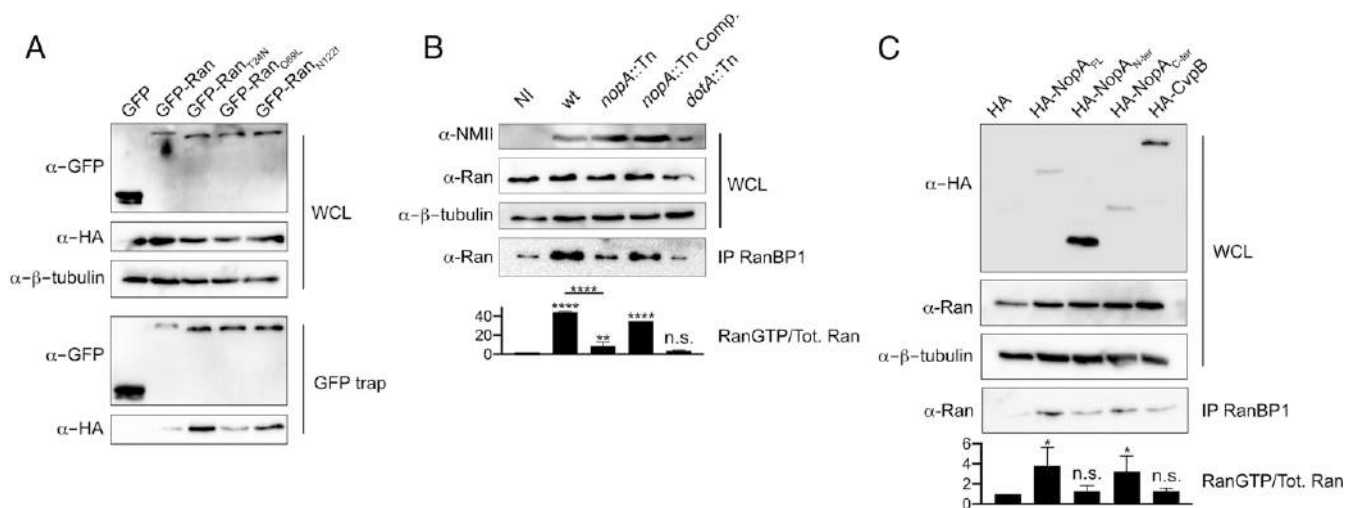


Fig. 4. NopA increases the intracellular levels of Ran-GTP. (A) The GFP-trap assay was carried out in U2OS cells expressing HA-tagged NopA_{C-ter} in combination with either GFP alone, GFP-Ran, GFP-Ran_{T24N} (GDP-locked), GFP-Ran_{Q69L} (GTP-locked), or GFP-Ran_{N122I} (guanosine-free). WCLs (Upper) were probed with anti-GFP and anti-HA antibodies to assess the expression of the GFP-tagged proteins and HA-tagged NopA_{C-ter}, and anti-tubulin antibodies as loading control. Protein/protein interactions were assessed using anti-GFP and anti-HA antibodies following GFP capture (GFP-trap, Lower). (B) GTP-bound Ran was pulled down using RanBP1-coated beads from cell lysates of U2OS cells challenged for 24 h with either WT *C. burnetii* (WT), a *nopA* transposon mutant (*nopA::Tn*), the corresponding complemented strain (*nopA::Tn Comp.*), or the *Dot/Icm*-defective mutant (*dotA::Tn*). Noninfected cells (NI) were used as control. WCLs were probed with anti-*C. burnetii* (NMII), anti-Ran, and anti- β -tubulin antibodies. GTP-bound Ran was revealed using an anti-Ran antibody (IP RanBP1). (C) GTP-bound Ran was pulled down using RanBP1-coated beads from cell lysates of U2OS cells expressing either the HA tag alone, HA-tagged versions of either full-length (NopA_{FL}), the N-terminal domain (NopA_{N-ter}), the C-terminal domain (NopA_{C-ter}), or CvpB. WCLs were probed with anti-HA antibodies to assess the expression of the HA-tagged versions of NopA and anti-Ran and anti-tubulin antibodies as loading controls. GTP-bound Ran was revealed using an anti-Ran antibody (IP RanBP1). The signal ratio of GTP-bound Ran over the total amount of Ran is indicated for experiments illustrated in B and C. Values are mean \pm SD from three independent experiments. n.s., nonsignificant, **** P < 0.0001, ** P < 0.007, * P < 0.02, one-way ANOVA, Dunnett's multiple comparison test.

Noninfected cells were used as control. Twenty-four hours post-infection, cells were lysed and incubated with agarose beads coated with the Ran effector Ran-binding protein 1 (RanBP1), to specifically pull down the GTP-bound form of Ran. Indeed, infection with WT *C. burnetii* triggered a 40-fold increase in the intracellular levels of Ran-GTP, as compared to noninfected cells (Fig. 4B). This phenotype was lost in cells challenged with the *dotA::Tn* mutant strain and only an 8.5-fold increase was observed in cells challenged with the *nopA::Tn* mutant strain. Increased levels of Ran-GTP were largely restored (35-fold increase) in cells exposed to the complemented strain (*nopA::Tn* Comp., Fig. 4B). The effects of NopA on the intracellular levels of Ran-GTP were further investigated in U2OS cells transfected with plasmids encoding either HA alone, HA-NopA, HA-NopA_{N-ter}, HA-NopA_{C-ter}, or the *C. burnetii* effector protein CvpB (12) used here as negative control. A threefold increase in the intracellular levels of Ran-GTP was observed in cells expressing either HA-NopA or HA-NopA_{C-ter}, as compared to cells transfected with HA alone or HA-NopA_{N-ter} (Fig. 4C). As expected, ectopic expression of CvpB had negligible impact on the intracellular levels of Ran-GTP (Fig. 4C). These observations suggest that NopA sequestration of Ran at nucleoli leads to an increase in the intracellular levels of Ran-GTP, which may negatively regulate nuclear import (24).

NopA Perturbs Protein Translocation to the Nucleus. Given the role of Ran in nucleocytoplasmic traffic, and the previously reported observation that *C. burnetii* infections modulate nuclear translocation of p65 by a Dot/Icm-dependent mechanism (9), we investigated whether NopA affects the nuclear localization of p65, which follows the activation of the NF- κ B signaling pathway. U2OS cells transfected with plasmids encoding either HA- or mCherry-tagged versions of NopA were either left untreated or challenged with 10 ng/mL TNF- α for 30 min, and the nuclear translocation of p65 was monitored using an anti-p65 antibody either by fluorescence microscopy or Western blot following cell fractionation. Cells expressing either HA- or mCherry-tagged CvpB or the tags alone were used as controls. TNF- α treatment efficiently activated the NF- κ B pathway, as indicated by the significant degradation of I κ B α (Fig. 5A). Accordingly, p65 was readily relocalized to the nucleus of cells expressing either the HA or mCherry tags alone or tagged versions of the *C. burnetii* effector CvpB (Fig. 5B–D). However, p65 translocation was largely inhibited in cells expressing either HA-NopA or mCherry-NopA (Fig. 5B–D). In all cases, the intracellular levels of p65 remained largely unaltered. To determine whether NopA modulates the intracellular levels of p65 by perturbing its nuclear import or by accelerating its nuclear export, U2OS cells expressing either mCherry-NopA, mCherry-CvpB, or mCherry alone as controls, were incubated for 4 h with 5 nM leptomycin B (LMB), a fungal metabolite that blocks nuclear export by covalently binding to exportin 1. As p65 shuttles continuously between the nucleus and the cytoplasm, treatment with LMB in mCherry or mCherry-CvpB expressing cells led to an accumulation of the transcription factor in the nucleus (Fig. 5D and SI Appendix, Fig. S4). Interestingly however, ectopic expression of mCherry-NopA significantly prevented p65 nuclear accumulation in response to LMB treatment (Fig. 5D and SI Appendix, Fig. S4). A similar phenotype was observed in cells treated with LMB for 4 h, followed by a 30-min incubation with TNF- α (Fig. 5D and SI Appendix, Fig. S4). These data indicate that indeed, NopA perturbs nuclear import.

Next, we tested whether the perturbation of nuclear import triggered by NopA was specific to p65 and *C. burnetii* infections. The nuclear translocation of the transcription factor IRF3 was monitored in U2OS cells cotransfected with 3FLAG-tagged IRF3 in combination with either mCherry alone, mCherry-NopA, or mCherry-CvpB, and infected with the Sendai virus for 18 h. Noninfected cells were used as control (SI Appendix, Fig. S5A). Similar to what we reported for p65, IRF3 was readily translocated to the nuclei of cells expressing either mCherry alone or mCherry-CvpB but remained largely cytoplasmic in cells expressing mCherry-NopA (SI Appendix, Fig. S5A and B).

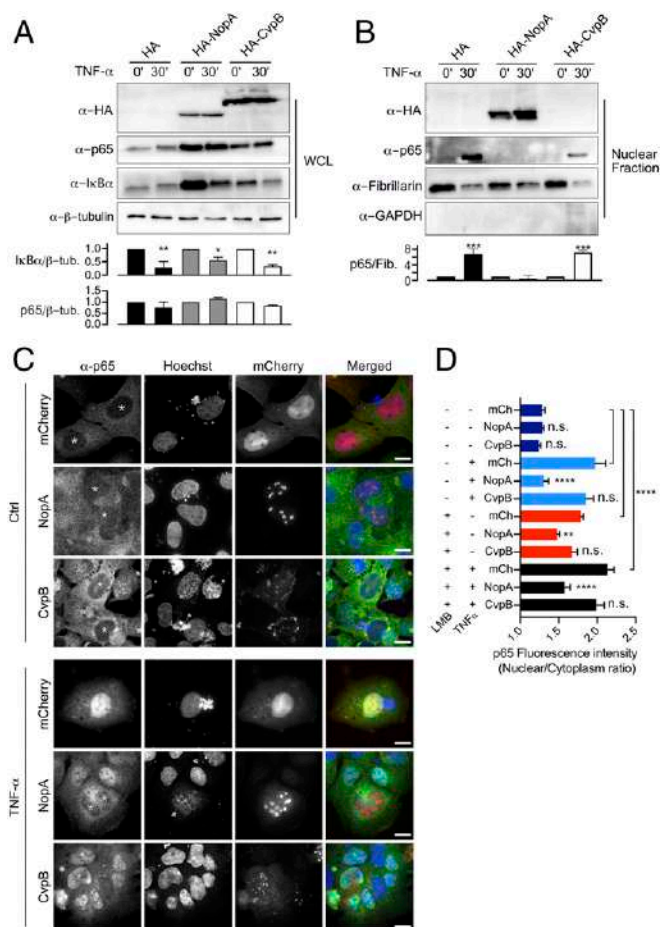


Fig. 5. Overexpression of NopA interferes with the nuclear translocation of p65. Representative Western blot of U2OS cells expressing either the HA tag alone, HA-NopA, or HA-CvpB left untreated or incubated with 10 ng/mL TNF- α for 30 min, lysed, and processed for cell fractionation. Whole cell lysates (A, WCLs) were used to assess the overall levels of p65 and I κ B α and nuclear fractions (B) to monitor p65 translocation to the nucleus (nuclear fraction). The signal ratio of p65 over tubulin or fibrillarin and of I κ B α over tubulin is indicated for experiments illustrated in A and B. Values are mean \pm SD from three independent experiments. (C) Representative images of U2OS cells expressing mCherry-NopA or mCherry-CvpB and treated as in A. The localization of p65 was monitored using an anti-p65 antibody and Hoechst staining of nuclei. Asterisks indicate transfected cells. (D) CellProfiler was used to identify mCherry-expressing U2OS cells and to measure the median of the ratios of p65 fluorescence intensity at nuclei versus cytoplasm. Values are means \pm SEM from two independent experiments where a minimum of 200 nuclei were measured per condition. Asterisks indicate statistically significant variations [n.s., nonsignificant, **** P < 0.0001, *** P < 0.001, ** P < 0.01, * P < 0.1, one-way ANOVA, Dunnett's (A and B) and Bonferroni (D) multiple comparison test]. (Scale bars, 10 μ m.)

NopA Is Involved in the Silencing of the Innate Immune Response during *C. burnetii* Infections. p65 nuclear translocation was further monitored in U2OS cells noninfected or challenged either with 10 ng/mL TNF- α for 30 min, WT *C. burnetii*, the Dot/Icm-defective mutant *dotA::Tn*, the *nopA::Tn*, or the complemented strain (*nopA::Tn* Comp.), for 24, 48, and 72 h by fluorescence microscopy and, for the 72 h time point, by Western blot following cell fractionation. I κ B α was significantly degraded in all conditions as compared to noninfected cells, indicating an efficient activation of the NF- κ B pathway (Fig. 6A). Translocation of p65 to the nucleus was readily detected in cells treated with TNF- α , either by Western blotting (Fig. 6B) or by immunofluorescence (Fig. 6C and D). Cells challenged with WT *C. burnetii* or the *nopA::Tn* complemented

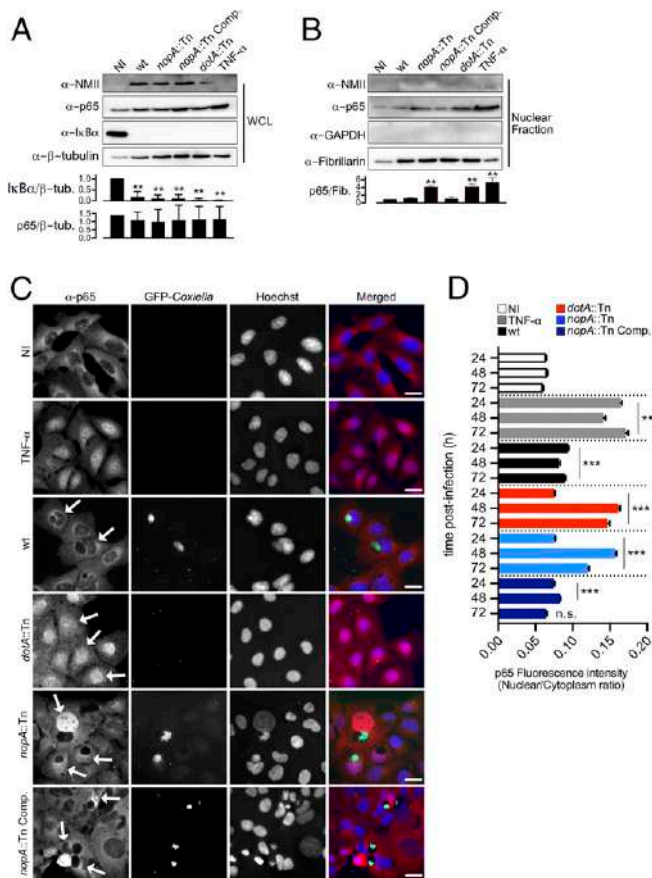


Fig. 6. NopA interferes with the nuclear translocation of p65 during *C. burnetii* infections. Representative Western blot of U2OS cells challenged for 72 h with GFP-tagged strains of WT *C. burnetii* (WT), the Dot/Icm-defective *dotA* transposon mutant (*dotA::Tn*), the *nopA* transposon mutant (*nopA::Tn*), or the corresponding complemented strain (*nopA::Tn Comp.*). Noninfected cells (NI) and cells treated with 10 ng/mL TNF- α (TNF- α) for 30 min were used as negative and positive controls, respectively. Cells were lysed and fractionated to isolate nuclear fractions. Whole cell lysates (A, WCL) were used to assess the overall levels of p65 and I κ B α and nuclear fractions (B) to monitor p65 translocation to the nucleus (nuclear fraction). Normalized densitometry of indicated protein ratios was calculated. Values are means \pm SD from two independent experiments. (C) Representative images of U2OS cells treated as in A. The localization of p65 (red) was monitored using an anti-p65 antibody and Hoechst staining of nuclei (blue). White arrows indicate nuclei of infected cells. (D) U2OS cells were treated as in A for 24, 48, and 72 h. CellProfiler was used to identify infected and total U2OS cells and to measure the median of the ratios of p65 fluorescence intensity at nuclei versus cytoplasm. Values are means \pm SEM from two independent experiments where a minimum of 400 nuclei were measured per condition. In all cases, n.s., nonsignificant, *** P < 0.0001, one-way ANOVA, Dunnett's multiple comparison test. (Scale bars, 10 μ m.)

strain showed a small but significant increase in nuclear p65 fluorescence as compared to noninfected, untreated cells (Fig. 6B–D). However, incubation with either the *dotA::Tn* or the *nopA::Tn* mutants triggered an accumulation of p65 to the nucleus which was comparable to the TNF- α treatment (Fig. 6B–D). Measurement of p65 nuclear translocation by immunofluorescence, which was specifically measured in infected cells, resulted in a stronger phenotype as compared to Western blot analysis, which was carried out on the total cell population.

To investigate the downstream effects of perturbing the nuclear translocation of transcription factors involved in the immune response to *C. burnetii* infections, differentiated THP-1 macrophages were exposed to either WT *C. burnetii*, the Dot/Icm-deficient *dotA::Tn* mutant, the *nopA::Tn* mutant, or the corresponding complemented

strain (*nopA::Tn Comp.*) for 24, 48, and 72 h. Total RNA was extracted from cell lysates and qRT-PCR analysis was used to monitor the expression of a panel of cytokines (Fig. 7A and *SI Appendix, Fig. S64*). A slight increase in the mRNA expression levels of all tested cytokines was observed in cells exposed to WT *C. burnetii* or the *nopA::Tn* complemented strain, as compared to noninfected cells. Interestingly however, cells exposed to either the *dotA::Tn* mutant or the *nopA::Tn* mutant displayed a comparable, significant increase in the production of the majority of the cytokines tested, ranging from a 2-fold increase to a 100-fold increase for IL8 (Fig. 7A and *SI Appendix, Figs. S64 and S7*). Down-modulation of the innate immune response was further confirmed by monitoring TNF- α and IFN- α production in THP-1 macrophages infected as above for 72 and 96 h. As *C. burnetii* effectors are known to perturb the secretory pathway of infected cells (20, 25), THP-1 cells were treated with brefeldin A (BFA) 24 h prior to fixation and the intracellular levels of TNF- α and IFN- α were assessed by flow cytometry (Fig. 7B and C), following the application of a specific gating to isolate the population of infected cells (*SI Appendix, Fig. S6B*). A significant increase in the intracellular levels of both cytokines was observed in cells infected either with the *nopA::Tn* or the *dotA::Tn* strains as compared to cells infected with WT *C. burnetii* or the *nopA::Tn* complemented strain (Fig. 7B and C). Overall, our data indicate that *C. burnetii* uses the Dot/Icm secretion system to down-modulate the NF- κ B signaling pathway as previously reported (9), and that NopA is a key effector for this process.

Discussion

Intracellular bacterial pathogens and symbionts establish intimate interactions with their eukaryotic hosts, which have evolved by co-evolution over time. Part of their adaptation to their intracellular niches has been mediated by transkingdom acquisition and functional integration of eukaryotic genes in bacterial genomes (26). Indeed, EUGENS represent a hallmark of intracellular bacteria, and are rarely observed in free-living bacteria. Importantly, many EUGENS from intracellular bacteria produce candidate or validated effector proteins that are translocated into host cells through dedicated type III or type IV secretion systems (27). Thus, EUGENS are predicted to play an important role in the establishment of parasitic or symbiotic bacterial lifestyles.

In this study, bioinformatics analysis combined with translocation assays led to the identification of seven *C. burnetii* effector proteins encoding eukaryotic-like domains involved in protein/protein interactions, protein/chromatin interactions, and posttranslational modifications. CBU0447 and CBU0175 are conserved among *C. burnetii* strains, whereas the remaining five EUGENS present some degree of polymorphism (7). Upon ectopic expression in epithelial cells of translocated ankryrin repeat-containing proteins, AnkA (CBU0072) was largely cytoplasmic, whereas AnkF (CBU0447) seemed to associate with membranes that partially colocalized with the lysosomal marker LAMP1. AnkG (CBU0781), which was previously reported to localize at mitochondria and translocate to the nucleus upon staurosporine treatment of transfected cells (21), partially localized to the nucleus even in the absence of staurosporine in our hands. It is thus possible that other Ank proteins modify their intracellular localization at different stages of infection.

Here, we have focused our study on CBU1217, which encodes four RCC repeats in its C-terminal domain (aa 196 to 497). RCC repeats are found in the regulation of chromosome condensation 1 (RCC1) eukaryotic protein (28). In eukaryotes, the RCC domain consists of seven homologous repeats of 51 to 68 amino acid residues, arranged in a β -propeller fold (15). A single RCC domain constitutes the majority of the protein in the case of the RCC1 subgroup of the RCC1 superfamily, whereas multiple RCC domains can be found, either alone or in combination with other functional domains of the other subgroups of the superfamily (13). As such, RCCs are versatile domains that can be involved in protein/protein or protein/chromatin interactions, guanine nucleotide exchange factor (GEF), and posttranslational modifications including ubiquitination and phosphorylation (13). RCC1 is primarily found in association with histones H2A and H2B on chromatin (29) and acts as a GEF for the small GTPase Ran, a master regulator of nucleocytoplasmic

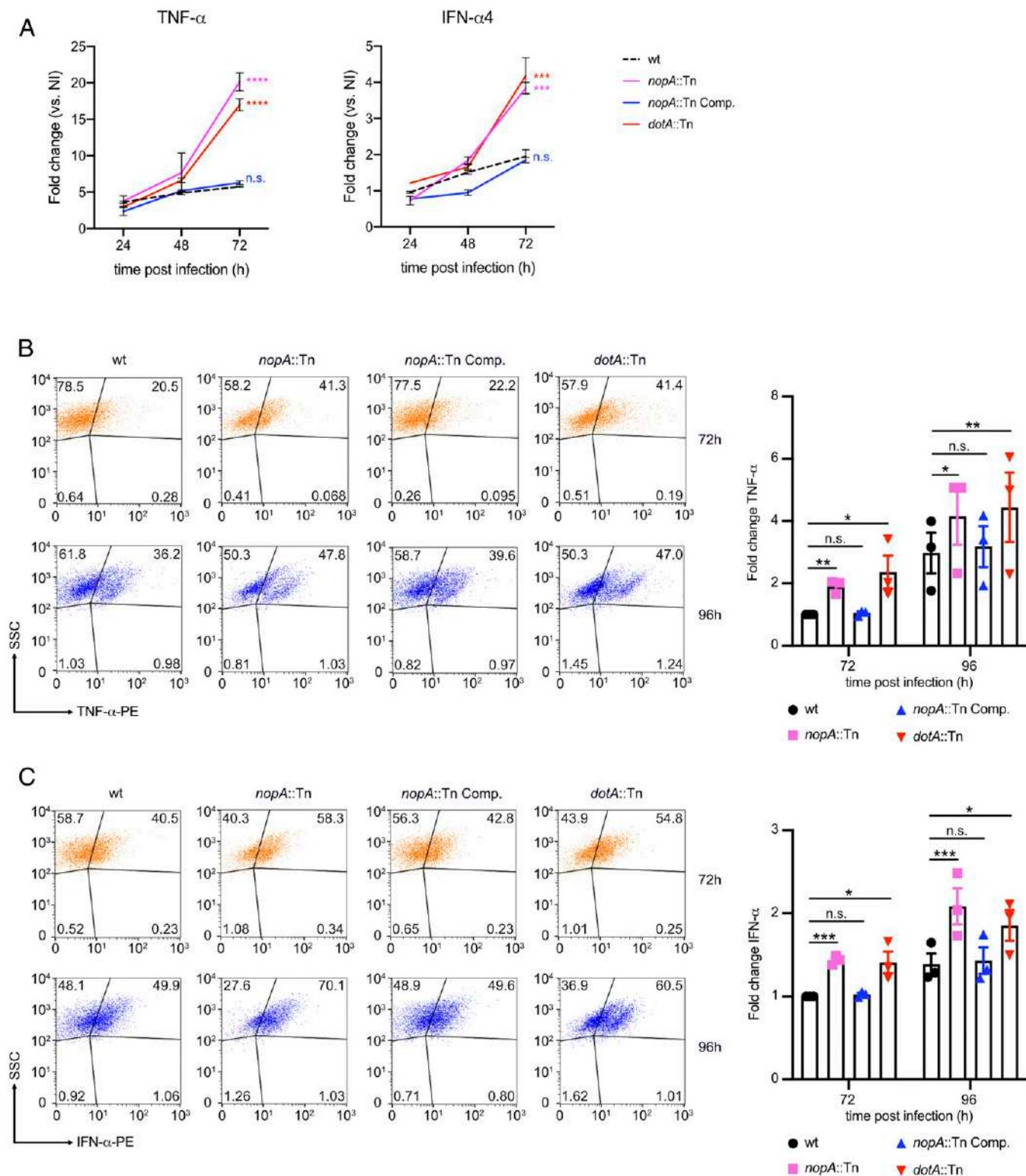


Fig. 7. NopA inhibits cytokines production. (A) Differentiated THP-1 cells were challenged either with GFP-expressing WT *C. burnetii* (WT), the Dot/Icm-defective *dotA* transposon mutant (*dotA::Tn*), the *nopA* transposon mutant (*nopA::Tn*), or the corresponding complemented strain (*nopA::Tn Comp.*) for 24, 48, 72, and 96 h. The expression of TNF- α and IFN- α 4 cytokines was assessed by RT-qPCR for the indicated time points. Dot plots from a representative experiment showing intracellular staining of TNF- α (B) and IFN- α (C) in cells infected for 72 and 96 h and treated with BFA for the last 24 h. Infected cells were first gated on the GFP⁺ population and the percentage of cells expressing TNF- α and IFN- α was assessed. Flow cytometry data are presented on graphs as fold relative to WT. Values are means \pm SD from three independent experiments. n.s., nonsignificant, **** P < 0.0001, *** P < 0.001, ** P < 0.01, * P < 0.1. Full statistical analysis for the 72-h time point illustrated in A is available in [SI Appendix, Fig. S7](#).

transport during interphase and mitotic spindle assembly during mitosis (30).

Among vacuolar bacterial pathogens, the *L. pneumophila* effector protein LegG1 encodes an RCC-like domain (RLD) consisting of three out of the seven RCC repeats typically found in eukaryotes (31). Of note, LegG1 localizes at *Legionella*-containing vacuoles (LCVs) where it recruits and activates Ran to promote microtubule polymerization and LCV mobility (32). Differently from LegG1, *C. burnetii* NopA encodes an additional RCC repeat and, despite the lack of typical nuclear or nucleolar localization signals, exclusively localizes at nuclei with a strong enrichment in the chromatin fraction, which is consistent with RCC1 localization. NopA RCC repeats are necessary and sufficient to target the protein to nucleoli and exert its functions. Moreover, the first RCC repeat seems to be critical for targeting NopA to the nucleus, as removal of this repeat from NopA_{C-term} displaces the protein to the cytoplasm. Interestingly, the first two RCC repeats (aa 196–310) alone localize at PML bodies. This localization remains unchanged with the addition of the third RCC repeat and it is only the expression of the complete NopA_{C-term} that triggers protein localization at nucleoli, suggesting the presence of a nucleolar-targeting motif in the fourth RCC repeat.

Similarly to the eukaryotic protein RCC1, NopA interacts with Ran, with preferential affinity for the GDP-bound form and promotes the activation of Ran. Differently from RCC1, however, NopA also triggers a nucleolar accumulation of Ran. Thus, the observed increase in the intracellular levels of GTP-bound Ran may result from either GEF activity of NopA (which has been reported for RCC1), or via the observed sequestration of Ran at nucleoli, which would prevent GTP-bound Ran to recycle back to the cytoplasm, where Ran GTPase-activating proteins (GAPs) stimulate GTP to GDP conversion. As we were unable to purify sufficient amounts of either full-length NopA or NopA_{C-term}, we could not assess for the moment whether NopA has intrinsic GEF activity. Interestingly, a residual increase in the intracellular levels of Ran-GTP was still observed in cells challenged with the *nopA*::Tn mutant strain, as compared to infections with the Dot/Icm-defective *dotA*::Tn strain. This may suggest that other *C. burnetii* effectors may have a role in the modulation of Ran activity.

Of note, mutations in *nopA* do not affect *C. burnetii* intracellular replication (10). However, increasing the intracellular levels of Ran-GTP results in a global alteration in the nucleocytoplasmic transport of proteins (24). It has been reported that during infections, *C. burnetii* requires Dot/Icm activity to down-modulate the NF- κ B pathway by perturbing the nuclear translocation of the p65 transcription factor (9). Here we demonstrate that NopA is one of the effector proteins involved in this process, as indicated by the strong inhibition of nuclear translocation of p65 upon treatment of cells with TNF- α or infection. The modulation of the NF- κ B signaling pathway has been reported for a number of bacterial pathogens and viruses (1, 2). In most cases, bacteria interfere with the degradation of I κ B α and the release of p65 or by triggering the proteasomal degradation of p65 itself. Other bacteria, including *L. pneumophila* and *Shigella flexneri* may also inhibit the innate immune response downstream of p65 nuclear translocation, at the level of transcription and mRNA processing, respectively (2). Finally, an emerging number of bacterial effectors inhibit NF- κ B activation by modulating the nuclear translocation and/or accumulation of p65, by interfering with nucleocytoplasmic protein transport. The *Salmonella* SPI-2 T3SS effector protein SpvD accumulates importin- α in the nucleus by binding exportin Xpo2, thereby preventing p65 nuclear import (4). *O. tsutsugamushi* uses ankyrin repeat-containing effector proteins Ank1 and 6 by coopting the function of both importin- β and exportin 1, thus accelerating p65 nuclear export (5). Here we show that the NF- κ B pathway is readily activated upon *C. burnetii* infections as shown by efficient I κ B α degradation. However, NopA perturbs nuclear accumulation of p65 by triggering the nuclear accumulation of GTP-bound Ran, resulting in an imbalanced Ran gradient across cells. In turn, this leads to a defective nuclear import of proteins, as also demonstrated by challenging cells ectopically expressing NopA with leptomycin B to block nuclear export.

Considering that these bacterial effectors manipulate common adaptors and GTPases involved in nucleocytoplasmic transport, it would be of interest to monitor their effect on a broader panel of proteins and investigate how infected cells respond to these perturbations. For example, other *C. burnetii* effector proteins have been described to localize at the nucleus of infected cells (21, 33, 34). In this perspective, it is important to note that nuclear translocation of p65 is not completely ablated during *C. burnetii* infections, and that the strongest phenotypes are observed at 48 and 72 h post-infection, which is compatible with a reduced, but still detectable translocation of protein to the nucleus at earlier time points. Here we show that indeed the perturbation of nuclear import by NopA affects a broader class of proteins, also outside the context of *C. burnetii* infections, as indicated by the perturbation of nuclear translocation of IRF3 in response to Sendai virus infection, in cells ectopically expressing NopA.

To monitor the downstream effects of inhibiting the nuclear accumulation of transcription factors involved in immune sensing, we challenged differentiated THP-1 cells with WT *C. burnetii* or strains carrying mutations either in the Dot/Icm secretion system or in *nopA*. As expected, infections by the WT strain elicited a minor response in the expression of a panel of cytokines, including TNF- α , interleukins, and interferons, in agreement with the observation that *C. burnetii* is a stealth pathogen. Evasion of the innate immune response was unmasked by infections with the Dot/Icm-defective strain *dotA*::Tn, which triggered a significant cytokine response. Interestingly, infections by the *nopA*::Tn mutant strain largely phenocopied the *dotA*::Tn mutation, suggesting that NopA is critical for the down-modulation of the innate immune response.

Together, this work highlighted a number of *C. burnetii* eukaryotic-like effector proteins and showed that one of them, NopA, is responsible for evading the host innate immune response by interfering with nucleocytoplasmic transport.

Materials and Methods

Antibodies, reagents, bacterial strains, cell lines, and growth conditions used in this study are listed in [SI Appendix](#).

Plasmids. Plasmids used in this study are listed in [SI Appendix, Table S4](#). DNA sequences were amplified by PCR using Phusion polymerase (New England Biolabs) and gene-specific primers (Sigma).

Plasmid Design for Secretion Assay in *C. burnetii*. Selected genes from [SI Appendix, Table S2](#) were amplified from *C. burnetii* RSA439 NMII genomic DNA using primer pairs indicated in [SI Appendix, Table S5](#). PCR products were cloned into the pXDC61-BLAM plasmid to generate N-terminal-tagged fusion version of all candidate effector proteins.

Plasmid Design for Mammalian Cells Transfection. Effector-coding genes were amplified from *C. burnetii* RSA439 NMII genomic DNA using primer pairs indicated in [SI Appendix, Table S5](#). PCR products were cloned either into pLVX-mCherry-N2 or pRK5-HA plasmids to generate N-terminal-tagged mCherry or HA fusion versions of all effector proteins, respectively. For cloning of Ran in pCDNA3-GFP10-zipper, Ran was amplified using forward primers Ran-BspEI and reverse primers Ran-XbaI-rev. For cloning of NopA, RCC1, and fibrillarin in pCDNA3-zipper-GFP11, genes were amplified using forward primers NopA-NotI, RCC1-NotI, or FBL-NotI and reverse primers NopA-Clal-rev, RCC1-Clal-rev, or FBL-Clal-rev. pGBKT7-containing eukaryotic sequence of Ran WT, RanT24N/Q69L/N122I mutants were kindly provided by Aymelt Itzen, Zentrum für Experimentelle Medizin Institut für Biochemie und Signaltransduktion, Hamburg, Germany. Ran WT and mutants were amplified from pGBKT7-Ran-WT, pGBKT7-Ran-T24N, pGBKT7-Ran-Q69L, and pGBKT7-Ran-N122I using primer pairs XhoI-Ran-F and Ran-XmaI-rev, and the PCR products were cloned into pLVX-GFP-N2.

Plasmid Design for *nopA* Complementation in *C. burnetii*. For *nopA* complementation, the *nopA* putative promoter and *nopA* sequences were amplified using the primer pairs *NheI*-prom1217-fw/*PstI*-prom1217-Rev and CBU1217-BamHI/CBU1217-EcoRI-rev, respectively ([SI Appendix, Table S5](#)). The PCR products were cloned into pUCR6K-miniTn7-Kan-tetRA-4HA. Plasmids were electroporated in the *nopA*::Tn mutant strain Tn227 (10).

Beta-Lactamase Translocation Assay. For *C. burnetii* effector translocation assays, cells were cultured in black, clear-bottomed, 96-well plates and infected with the appropriate *C. burnetii* strain (multiplicity of infection [MOI] of 100) for 24 and 48 h. *C. burnetii*-expressing BLAM alone or BLAM-tagged CBU0021 were used as negative and positive controls, respectively. Cell monolayers were loaded with the fluorescent substrate CCF4/AM (LiveBLAzer-FRET B/G loading kit; Invitrogen) in a solution containing 20 mM Hepes, 15 mM probenecid (Sigma) pH 7.3, in Hank's balanced salt solution (HBSS). Cells were incubated in the dark for 1 h at room temperature and imaged using an EVOS inverted fluorescence microscope. Images were acquired using DAPI and GFP filter cubes. The image analysis software CellProfiler was used to segment and count total cells and positive cells in the sample using the 520-nm and 450-nm emission channels, respectively, and to calculate the intensity of fluorescence in each channel. Following background fluorescence subtraction using negative control samples, the percentage of positive cells was then calculated and used to evaluate effector translocation. A threshold of 20% of positive cells was applied to determine efficient translocation of bacterial effector proteins.

Immunofluorescence Staining and Microscopy. Cells were fixed in 4% (wt/vol) paraformaldehyde in phosphate-buffered saline (PBS) solution at room temperature for 20 min. Samples were then rinsed in PBS solution and incubated in blocking solution (0.5% bovine serum albumine [BSA], 50 mM NH₄Cl in PBS solution, pH 7.4). Cells were then incubated with the primary antibodies diluted in blocking solution for 1 h at room temperature, rinsed five times in PBS solution, and further incubated for 1 h with the secondary antibodies diluted in the blocking solution. To visualize HA-tagged NopA or nuclear/nucleolar proteins, cells were fixed as previously described in 4% (wt/vol) paraformaldehyde in PBS solution. Then, cells were permeabilized with 0.5% Triton X-100 in PBS solution for 3 min at room temperature. Sample were then rinsed in PBS solution and incubated with blocking solution (0.1% Triton X-100, 5% [wt/vol] milk in PBS solution) for 1 h at room temperature. Cells were then incubated with the primary antibodies diluted in blocking solution for 1 h at 37 °C, rinsed five times in PBS solution, and incubated with the secondary antibodies for 1 h at room temperature. For all conditions, coverslips were mounted by using Fluoromount mounting medium (Sigma) supplemented with Hoechst 33258 for DNA staining. Samples were imaged with a Zeiss Axio Imager Z1 epifluorescence microscope (Carl Zeiss) connected to a CoolSNAP HQ² charge-coupled device (CCD) camera (Photometrics). Images were acquired alternatively with 100×, 63×, or 40× oil immersion objectives and processed with MetaMorph (Universal Imaging). ImageJ and CellProfiler software were used for image analysis and quantifications.

Immunoprecipitations and Pull-Down Assays. For coimmunoprecipitation experiments, pLVX-GFP-N2-tagged WT Ran, RanT24N/Q69L/N122I mutants, or vector control were cotransfected with pRK5-HA-NopA_{C-ter} in U2OS cells. At 24 h posttransfection, cells were lysed in lysis buffer (10 mM Tris HCl, pH 7.5, 150 mM NaCl, 0.5 mM ethylenediaminetetraacetic acid [EDTA] 1% Nonidet P-40) supplemented with a protease inhibitor tablet (Complete; Roche) and incubated with 25 μ L of GFP-Trap magnetic beads (Chromotek) for 2 h at 4 °C with rotation. The beads were then washed three times with wash buffer (10 mM Tris HCl, pH 7.5, 150 mM NaCl, 0.5 mM EDTA), resuspended in Laemmli buffer 4×, and analyzed by Western blot.

Tripartite Split-GFP Assay. U2OS were grown in Dulbecco's modified Eagle medium (DMEM) supplemented in 10% (vol/vol) fetal calf serum (FCS) at 37 °C and 5% CO₂. For the interaction assay, U2OS cells were cotransfected with Lipofectamine 2000 (Gibco, Invitrogen) with plasmids encoding for GFP1-9, GFP10, and GFP11 fusions. At 24 h posttransfection, cells were fixed in 4% paraformaldehyde in PBS solution and processed for immunofluorescence. Protein/protein interactions were scored by calculating the percentage of GFP-positive cells over the total number of cells positive for the anti-GFP antibody.

Cell Fractionation. U2OS cells were grown to 60% confluence in 100-mm Petri dishes before being transfected with 10 μ g of pRK5-HA-NopA_{N-ter} or pRK5-HA-NopA_{C-ter} in JetPEI reagent (Polyplus-Transfection) according to the manufacturer's recommendations. At 24 h after transfection, cells were washed in PBS and pelleted at 4 °C. U2OS cells cultured in 100-mm dishes were infected with the *nopA::Tn* mutant or the corresponding complemented strain (*nopA::Tn* Comp.) expressing a 4HA-tagged version of NopA. After 24 h of infection, cells were washed in PBS and pelleted at 4 °C.

Transfected or infected cell pellets were subjected to cell fractionation as previously described (35). Where appropriate, cytoplasmic, nuclear, and chromatin fractions were subjected to immunoprecipitation using 40 μ L of anti-HA magnetic beads (Sigma) for 2 h at 4 °C with rotation. Bound proteins were eluted using 80 μ L of 100 μ g/mL⁻¹ HA-peptide (Sigma) and then resuspended in Laemmli buffer 4× and analyzed by Western blot.

Ran Activation Assay. For the analysis of enzymatic activity of NopA, U2OS cells were either infected or transfected and lysed with lysis buffer (25 mM Hepes, pH 7.5, 150 mM NaCl, 1% Nonidet P-40, 10 mM MgCl₂, 1 mM EDTA, 2% glycerol) containing a protease inhibitor tablet (Complete; Roche). Cell lysates were then centrifuged for 10 min at 14,000 × *g* at 4 °C. For Ran-GTP immunoprecipitation, 40 μ L of RanBP1 beads (Cell Biolabs, Inc.) were incubated with cell lysates for 1 h at 4 °C, and then washed three times with lysis buffer, subjected to sodium dodecyl sulfate-polyacrylamide gel electrophoresis (SDS/PAGE), and visualized by Western blotting using an anti-Ran antibody (1:4,000, Sigma). GTP-bound Ran levels were determined by calculating the signal ratio of GTP-bound Ran over the total amount of Ran.

NF- κ B/IRF3 Translocation Assays. To analyze NF- κ B translocation, U2OS cells were grown to 60% confluence before being transfected as previously described. At 24 h posttransfection, cells were incubated with media containing 10 ng/mL TNF- α for 30 min at 37 °C. Alternatively, cells were preincubated with media containing 5 nM LMB for 4 h at 37 °C, followed by a TNF- α treatment as indicated above where needed. For *C. burnetii* infection assays, cells were infected with *C. burnetii* and incubated at 37 °C for 1 to 3 d. Cells were then fixed in 4% paraformaldehyde in PBS solution and processed for NF- κ B immunostaining. The image analysis software CellProfiler was used to segment all nuclei using the Hoechst staining and cell contours using nuclei as seeds and p65 labeling. Cytoplasm was segmented by subtracting nuclei from cell objects. Next, mCherry signal was used to identify and isolate the subpopulation of transfected cells, and single cell measurements of the ratio of the mean p65 fluorescence in the nucleus versus cytoplasm were calculated for each condition. For infection assays, CellProfiler was used to identify and isolate the population of infected cells based on the GFP fluorescence associated with the strains of *C. burnetii* used in this study and nuclear p65 fluorescence was specifically measured as described above in the subpopulation of infected cells. To analyze IRF3 translocation, pLVX-mCherry-N2-tagged NopA, CvpB, or empty vector were cotransfected with pcDNA3-3×FLAG-tagged IRF-3 in U2OS cells. At 24 h posttransfection, cells were infected with a defective-interfering H4 Sendai virus (36) provided by D. Garcin, Department of Microbiology and Molecular Medicine, University of Geneva, Geneva Switzerland, and used at 50 hemagglutination units (HAU)/mL for 18 h at 37 °C. Cells were then fixed in 4% paraformaldehyde in PBS solution and processed for FLAG immunostaining. IRF3 nuclear translocation was measured as described above for p65.

Densitometry. Regions of Interest (ROIs) were obtained from each band of interest and the intensity was measured using ImageJ. For each band, the same ROI was used for background calculation and removal from areas adjacent to each band. For the experiments illustrated in Fig. 5, the intensity of bands from samples treated with TNF- α were normalized for the intensity of the corresponding untreated sample. For the experiments illustrated in Fig. 6, the intensity of bands from samples challenged with *C. burnetii* or treated with TNF- α were normalized for the intensity of the noninfected (NI) sample.

qRT-PCR Analysis of Cytokine mRNA. Total RNA was extracted from THP-1 cells using the RNeasy Micro kit and submitted to DNase treatment (Qiagen), following manufacturer's instructions. RNA concentration and purity were evaluated by spectrophotometry (NanoDrop 2000c, Thermo Fisher Scientific). A total of 500 ng of RNA was reverse transcribed with both oligo-dT and random primers, using PrimeScript RT Reagent Kit (Perfect Real Time, Takara) in a 10-mL reaction. Real-time PCR reactions were performed in duplicates using Takyon ROX SYBR MasterMix blue dTTP (Eurogentec) on an Applied Biosystems QuantStudio 5, using the following program: 3 min at 95 °C followed by 40 cycles of 15 s at 95 °C, 20 s at 60 °C, and 20 s at 72 °C. Cycle threshold (Ct) values for each transcript were normalized to the geometric mean of the expression of RPL13A, B2M, and ACTB (i.e., reference genes) and the fold changes were determined by using the 2^{- $\Delta\Delta$ Ct} method. Primers used for quantification of transcripts by real-time quantitative PCR are indicated in *SI Appendix, Table S5*.

SCID Mouse Infections. SCID (C.B-17/LcrHsd-Prkdcscid) mice were purchased from Envigo and housed in the Texas A&M Health Science Center (TAMHSC) animal facility. All animal procedures were done in compliance with Texas A&M University Institutional Animal Care and Use Committee (Animal Use Protocol, AUP 2016–0370). Infections were performed as described previously (37). Briefly, 6- to 8-wk-old female mice (SCID or C57BL/6) were infected with 1×10^6 viable *C. burnetii* phase II strain via intraperitoneal (i.p.) injection. Inoculum concentrations were confirmed by serial dilution spot plating on acidified citrate cysteine medium-2-defined (ACCM-D) agarose as described previously (38).

Mouse Tissue Collection, Processing, and DNA Purification. At 10 d (competitive infections) or 14 d postinfection (single infections), the mouse spleens were removed and weighed at necropsy to determine splenomegaly (spleen weight/body weight). Each spleen was added to 1 mL PBS and homogenized using an Omni tissue homogenizer equipped with plastic tips. A total of 100 μ L of homogenate was added to 400 μ L of TriZol LS (Invitrogen) for RNA extraction. For DNA extraction, 100 μ L of homogenate was added to 900 μ L tissue lysis buffer (Roche) plus 100 μ L of proteinase K and incubated at 55 °C overnight. The following day 100 μ L of 10% SDS (wt/vol) was added and incubated at room temperature for 1 h. Lysed tissue samples were then processed using the Roche High Pure PCR template preparation kit according to the manufacturer's instructions.

Enumeration of *Coxiella* in Mouse Spleens. DNA purified from infected organs was used as template for TaqMan real-time PCR using primers and probe for *com1* or primers and probe of *IS1111* as described previously (37). Quantitative PCR was performed in 20- μ L reactions with ABI TaqMan universal PCR mastermix run on an ABI StepOne Plus machine. The replication index reported for each mouse was calculated by dividing the number of genome

copies recovered from spleens by the number of genome copies in the original inoculum.

Flow Cytometry. For intracellular human TNF- α /IFN- α 4 staining, 5×10^4 THP-1 cells differentiated in phorbol 12-myristate 13-acetate (PMA) (200 ng/mL) for 2 d seeded in 24-well plates were infected with the indicated *C. burnetii* strain for 72 and 96 h. Cells were then treated with 1 μ g/mL of BFA for the last 24 h. The following day, cells were fixed using 2% paraformaldehyde in PBS solution for 20 min at 4 °C. After washing with fluorescence-activated cell sorting (FACS) buffer (1% BSA in PBS solution), cells were permeabilized in FACS buffer supplemented with 0.1% saponin for 30 min at 4 °C and then stained with anti-TNF- α -PE and IFN- α -PE antibodies for 1 h at 4 °C. Infected cells were analyzed based on the GFP fluorescence associated with the strains of *C. burnetii*. Flow cytometry analyses were performed on a BD FACSCalibur flow cytometer using flow cytometry (CellQuest software, BD Biosciences). FlowJo software (Tree Star) was used to analyze data.

Data Availability. All data discussed in the paper are available to readers either in the manuscript or in *SI Appendix*.

ACKNOWLEDGMENTS. This work was supported by the European Research Area Net (ERA-NET) Infect-ERA (ANR-13-IFEC-0003), the French National Research Agency (ANR; ANR-14-CE14-0012-01, ANR-10-LABX-12-01). G.M. is the recipient of a fellowship from the Agence National de la Recherche sur le SIDA et les Hépatites virales. We acknowledge the imaging facility MRI, member of the national infrastructure France-BioImaging supported by the French National Research Agency (ANR-10-INBS-04, "Investments for the Future"). We thank Dr. Caroline Goujon, Dr. Marylene Mougél (IRIM), Prof. Hubert Hilbi and Leoni Swart (University of Zurich), and Prof. Aymelt Itzen (University of Hamburg) for scientific advice and for sharing materials.

1. M. M. Rahman, G. McFadden, Modulation of NF- κ B signalling by microbial pathogens. *Nat. Rev. Microbiol.* **9**, 291–306 (2011).
2. S. Asrat, K. M. Davis, R. R. Isberg, Modulation of the host innate immune and inflammatory response by translocated bacterial proteins. *Cell. Microbiol.* **17**, 785–795 (2015).
3. M. Stewart, Molecular mechanism of the nuclear protein import cycle. *Nat. Rev. Mol. Cell Biol.* **8**, 195–208 (2007).
4. N. Rolhion *et al.*, Inhibition of nuclear transport of NF- κ B p65 by the *Salmonella* type III secretion system effector SpvD. *PLoS Pathog.* **12**, e1005653 (2016).
5. S. M. Evans, K. G. Rodino, H. E. Adcox, J. A. Carlyon, *Orientia tsutsugamushi* uses two Ank effectors to modulate NF- κ B p65 nuclear transport and inhibit NF- κ B transcriptional activation. *PLoS Pathog.* **14**, e1007023 (2018).
6. A. Lührmann, H. J. Newton, M. Bonazzi, Beginning to understand the role of the Type IV secretion system effector proteins in *Coxiella burnetii* pathogenesis. *Curr. Top. Microbiol. Immunol.* **413**, 243–268 (2017).
7. C. L. Larson *et al.*, Right on Q: Genetics begin to unravel *Coxiella burnetii* host cell interactions. *Future Microbiol.* **11**, 919–939 (2016).
8. L. D. Cunha *et al.*, Inhibition of inflammasome activation by *Coxiella burnetii* type IV secretion system effector IcaA. *Nat. Commun.* **6**, 10205 (2015).
9. S. Mahapatra *et al.*, *Coxiella burnetii* employs the Dot/Icm type IV secretion system to modulate host NF- κ B/RelA activation. *Front. Cell. Infect. Microbiol.* **6**, 188 (2016).
10. E. Martinez, F. Cantet, L. Fava, I. Norville, M. Bonazzi, Identification of OmpA, a *Coxiella burnetii* protein involved in host cell invasion, by multi-phenotypic high-content screening. *PLoS Pathog.* **10**, e1004013 (2014).
11. E. Martinez, F. Cantet, M. Bonazzi, Generation and multi-phenotypic high-content screening of *Coxiella burnetii* transposon mutants. *J. Vis. Exp.* **2015**, e52851 (2015).
12. E. Martinez *et al.*, *Coxiella burnetii* effector CvpB modulates phosphoinositide metabolism for optimal vacuole development. *Proc. Natl. Acad. Sci. U.S.A.* **113**, E3260–E3269 (2016).
13. O. Hadjebi, E. Casas-Terradellas, F. R. Garcia-Gonzalo, J. L. Rosa, The RCC1 superfamily: From genes, to function, to disease. *Biochim. Biophys. Acta* **1783**, 1467–1479 (2008).
14. T. Seki, N. Hayashi, T. Nishimoto, RCC1 in the Ran pathway. *J. Biochem.* **120**, 207–214 (1996).
15. L. Renault *et al.*, The 1.7 Å crystal structure of the regulator of chromosome condensation (RCC1) reveals a seven-bladed propeller. *Nature* **392**, 97–101 (1998).
16. C. Noroy, T. Lefrançois, D. F. Meyer, Searching algorithm for Type IV effector proteins (S4TE) 2.0: Improved tools for Type IV effector prediction, analysis and comparison in proteobacteria. *PLOS Comput. Biol.* **15**, e1006847 (2019).
17. X. Pan, A. Lührmann, A. Satoh, M. A. Laskowski-Arce, C. R. Roy, Ankyrin repeat proteins comprise a diverse family of bacterial type IV effectors. *Science* **320**, 1651–1654 (2008).
18. D. E. Voth *et al.*, The *Coxiella burnetii* ankyrin repeat domain-containing protein family is heterogeneous, with C-terminal truncations that influence Dot/Icm-mediated secretion. *J. Bacteriol.* **191**, 4232–4242 (2009).
19. C. Chen *et al.*, Large-scale identification and translocation of type IV secretion substrates by *Coxiella burnetii*. *Proc. Natl. Acad. Sci. U.S.A.* **107**, 21755–21760 (2010).
20. K. L. Carey, H. J. Newton, A. Lührmann, C. R. Roy, The *Coxiella burnetii* Dot/Icm system delivers a unique repertoire of type IV effectors into host cells and is required for intracellular replication. *PLoS Pathog.* **7**, e1002056 (2011).
21. R. A. Eckart *et al.*, Antiapoptotic activity of *Coxiella burnetii* effector protein AnkG is controlled by p32-dependent trafficking. *Infect. Immun.* **82**, 2763–2771 (2014).
22. F. Ayeunoue Siadou *et al.*, *Coxiella* effector protein CvpF subverts RAB26-dependent autophagy to promote vacuole biogenesis and virulence. *Autophagy*, 10.1080/15548627.2020.1728098 (2020).
23. S. Cabantous *et al.*, A new protein-protein interaction sensor based on tripartite split-GFP association. *Sci. Rep.* **3**, 2854 (2013).
24. I. Palacios, K. Weis, C. Klebe, I. W. Mattaj, C. Dingwall, RAN/TC4 mutants identify a common requirement for snRNP and protein import into the nucleus. *J. Cell Biol.* **133**, 485–494 (1996).
25. E. M. Campoy, F. C. M. Zoppino, M. I. Colombo, The early secretory pathway contributes to the growth of the *Coxiella*-replicative niche. *Infect. Immun.* **79**, 402–413 (2011).
26. K. S. de Felipe *et al.*, Evidence for acquisition of Legionella type IV secretion substrates via interdomain horizontal gene transfer. *J. Bacteriol.* **187**, 7716–7726 (2005).
27. K. S. de Felipe *et al.*, Legionella eukaryotic-like type IV substrates interfere with organelle trafficking. *PLoS Pathog.* **4**, e1000117 (2008).
28. M. Ohtsubo, H. Okazaki, T. Nishimoto, The RCC1 protein, a regulator for the onset of chromosome condensation locates in the nucleus and binds to DNA. *J. Cell Biol.* **109**, 1389–1397 (1989).
29. I. G. Macara, M. E. Nemerut, C. A. Mizzen, T. Stukenberg, C. D. Allis, Chromatin docking and exchange activity enhancement of RCD by histones H2A and H2B. **292**, 1540–1543 (2001).
30. P. R. Clarke, C. Zhang, Spatial and temporal coordination of mitosis by Ran GTPase. *Nat. Rev. Mol. Cell Biol.* **9**, 464–477 (2008).
31. S. Ninio, J. Celli, C. R. Roy, A Legionella pneumophila effector protein encoded in a region of genomic plasticity binds to Dot/Icm-modified vacuoles. *PLoS Pathog.* **5**, e1000278 (2009).
32. E. Rothmeier *et al.*, Activation of Ran GTPase by a Legionella effector promotes microtubule polymerization, pathogen vacuole motility and infection. *PLoS Pathog.* **9**, e1003598 (2013).
33. W. Schäfer *et al.*, Nuclear trafficking of the anti-apoptotic *Coxiella burnetii* effector protein AnkG requires binding to p32 and Importin- α . *Cell. Microbiol.* **19**, e12634 (2017).
34. M. M. Weber *et al.*, Modulation of the host transcriptome by *Coxiella burnetii* nuclear effector Cbu1314. *Microbes Infect.* **18**, 336–345 (2016).
35. A. Prokop *et al.*, Orfx, a nucleomodulin required for *Listeria monocytogenes* virulence. *MBio* **8**, e01550-17 (2017).
36. L. Strahle, D. Garcin, D. Kolakofsky, Sendai virus defective-interfering genomes and the activation of interferon-beta. *Virology* **351**, 101–111 (2006).
37. E. J. van Schaik, E. D. Case, E. Martinez, M. Bonazzi, J. E. Samuel, The SCID mouse model for identifying virulence determinants in *Coxiella burnetii*. *Front. Cell. Infect. Microbiol.* **7**, 25 (2017).
38. K. M. Sandoz, P. A. Beare, D. C. Cockrell, R. A. Heinzen, Correction for Sandoz *et al.*, Complementation of Arginine Auxotrophy for Genetic Transformation of *Coxiella burnetii* by Use of a Defined Axenic Medium. *Appl. Environ. Microbiol.* **82**, 3695 (2016).

From neglected to dissected: How technological advances are leading the way to the study of *Coxiella burnetii* pathogenesis

Melanie Burette | Matteo Bonazzi 

IRIM, UMR 9004 CNRS, Université de Montpellier, Montpellier, France

Correspondence

Matteo Bonazzi, IRIM, UMR 9004 CNRS, Université de Montpellier, Montpellier, France.
Email: matteo.bonazzi@irim.cnrs.fr

Funding information

Agence Nationale de la Recherche, Grant/Award Numbers: ANR-17-CE15-0021, ANR-13-IFEC-0003, ANR-14-CE14-0012-01

Abstract

Coxiella burnetii is an obligate intracellular bacterial pathogen responsible for severe worldwide outbreaks of the zoonosis Q fever. The remarkable resistance to environmental stress, extremely low infectious dose and ease of dissemination, contributed to the classification of *C. burnetii* as a class B biothreat. Unique among intracellular pathogens, *C. burnetii* escapes immune surveillance and replicates within large autophagolysosome-like compartments called *Coxiella*-containing vacuoles (CCVs). The biogenesis of these compartments depends on the subversion of several host signalling pathways. For years, the obligate intracellular nature of *C. burnetii* imposed significant experimental obstacles to the study of its pathogenic traits. With the development of an axenic culture medium in 2009, *C. burnetii* became genetically tractable, thus allowing the implementation of mutagenesis tools and screening approaches to identify its virulence determinants and investigate its complex interaction with host cells. Here, we review the key advances that have contributed to our knowledge of *C. burnetii* pathogenesis, leading to the rise of this once-neglected pathogen to an exceptional organism to study the intravacuolar lifestyle.

KEYWORDS

Coxiella burnetii, effector proteins, host-pathogen interactions, molecular genetics, phenotypic screening

1 | INTRODUCING COXIELLA BURNETII

Coxiella burnetii is a Gram negative obligate intracellular pathogen, and the causative agent of Q fever, a worldwide zoonotic disease (Eldin et al., 2017). Animal coxiellosis is mostly associated with abortion, stillbirths and weak offspring (Figure 1). Desiccation of placental materials, excretions of birthing fluids, urine, faeces and milk from infected animals contribute to shed *C. burnetii* into the environment (Eldin et al., 2017). Transmission to humans results from exposure to contaminated aerosols and dust (Figure 1). In humans, *C. burnetii* infections are often asymptomatic and self-limiting, however, 40% of individuals infected with *C. burnetii* develop an acute disease which is associated with a flu-like syndrome, pneumonia, hepatitis and chronic fatigue (Eldin et al., 2017) (Figure 1). Acute disease may convert into a chronic illness with severe complications, including endocarditis

(Eldin et al., 2017). An important risk factor for Q fever outbreaks is the multiple zoonotic reservoirs of *C. burnetii*, which include domestic livestock and wild animals (mammals, reptiles, birds and ticks) (Eldin et al., 2017). *C. burnetii* is extremely infectious, with 1-to-10 bacteria being sufficient to cause disease (Brooke et al., 2013). The low infectious dose coupled to remarkable environmental stability contribute to the significant spreading of *C. burnetii* infections well away from the outbreak source and led to the classification of *C. burnetii* as a category B biothreat (Madariaga et al., 2003).

Coxiella burnetii is a stealth pathogen that actively escapes innate immune recognition by inhibiting the NF- κ B pathway (Mahapatra et al., 2016) and inflammasome activation (Cunha et al., 2015). Infected cells are also protected from apoptosis, thereby preserving the bacterial replicative niche over long periods (Lührmann et al., 2017). *C. burnetii* enters macrophages by phagocytosis through the

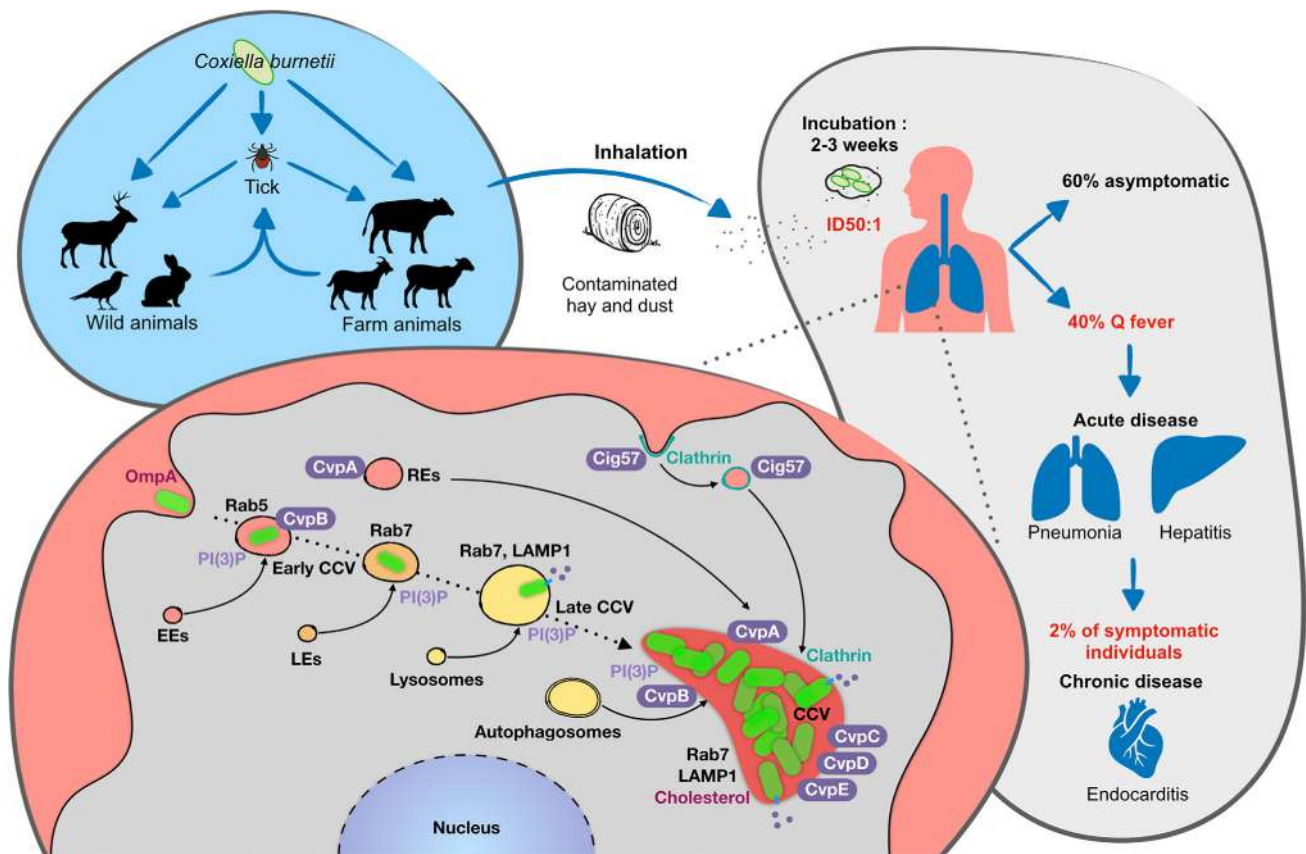


FIGURE 1 Overview of *C. burnetii* infections. *C. burnetii* is an obligate intracellular pathogen which infects wild and farm animals. Bacteria are shed in the environment with birth products and excretions leading to the contamination of hay and dust. Human infection occurs 2–3 weeks after the inhalation of contaminated particles, followed by the internalisation of *C. burnetii* by alveolar macrophages. Human Q fever remains asymptomatic in 60% of infected individuals, whereas 40% develop an acute, febrile disease, which can turn into a chronic disease with more severe symptoms including endocarditis. *C. burnetii* invades eukaryotic cell through phagocytosis, which is facilitated by the bacterial invasin OmpA. Early CCVs mature along the endocytic pathway by successive fusion events with early endosomes (EEs), late endosomes (LEs) and lysosomes. Acidification of the CCV activates bacterial metabolism and the translocation of bacterial effector proteins (purple circles and ovals) by the Dot/Icm secretion system. Several effector proteins are collectively beneficial for the biogenesis of the mature CCV where bacterial replication occurs. These include the Cvp family (for *Coxiella* vacuolar proteins) of effectors that localise at CCV membranes and manipulate host membrane trafficking pathways. CvpA interacts with the clathrin adaptor AP2 at recycling endosomes (REs), re-routing these compartments to the forming CCV. CvpB binds PI(3)P at early endosomes and enriches this phospholipid at CCVs. This is required to favour the autophagy-mediated homotypic fusion between CCVs. Although not a Cvp, Cig57 interacts with the clathrin adaptor FCHO2 at clathrin-coated pits and re-routes clathrin-mediated membrane traffic to the CCV

interaction with $\alpha V\beta 3$ integrins (Capo et al., 1999). In contrast, in non-phagocytic cells, internalisation is facilitated by the invasin OmpA (Outer membrane protein A) (Martinez et al., 2014) (Figure 1). Following internalisation, bacteria reside within early endosomal compartments, also called early CCVs, that passively mature along the endocytic pathway by successive fusion events with early and late endosomes and lysosomes (Figure 1). Maturation is accompanied by the acidification of the CCV lumen (Heinzen et al., 1996), which is required to activate bacterial metabolism (Hackstadt and Williams, 1981) and the translocation of bacterial effector proteins by a Dot/Icm Type 4b Secretion System (T4SS) (Newton et al., 2013). Thus, by 48 h post-infection, cells display a single, large, mature CCV, where markers of multiple membrane compartments co-exist (Dragan and Voth, 2019), which is indicative of the capacity of *C. burnetii* to hijack multiple host membrane trafficking pathways (Figure 1).

Importantly, the biogenesis of these remarkable compartments is a two-step process requiring both cellular and bacterial factors. This review will focus on the recent technological advances that fostered remarkable progress in our understanding of the complex host/pathogen interplay that controls the generation of the *C. burnetii* replicative niche.

2 | THE LONG AND WINDING ROAD (TO GENETIC MANIPULATION)

Together with its high infectivity, the obligate intracellular nature of *C. burnetii* has imposed severe constraints on the study of its pathogenesis. An important step towards the development of tools to investigate *C. burnetii* infection was the isolation of a Phase II variant

(NMII) of the Nine Mile Phase I strain (NMI), presenting a single deletion of 21 genes involved in lipopolysaccharide biosynthesis and displaying loss-of-virulence phenotype in animal models (Moos and

Hackstadt, 1987; Hoover et al., 2002). Thus, NMII was allowed for manipulation in biosafety level-2 (BSL-2) environments (Figure 2D), as opposed to other *C. burnetii* strains that require manipulation in

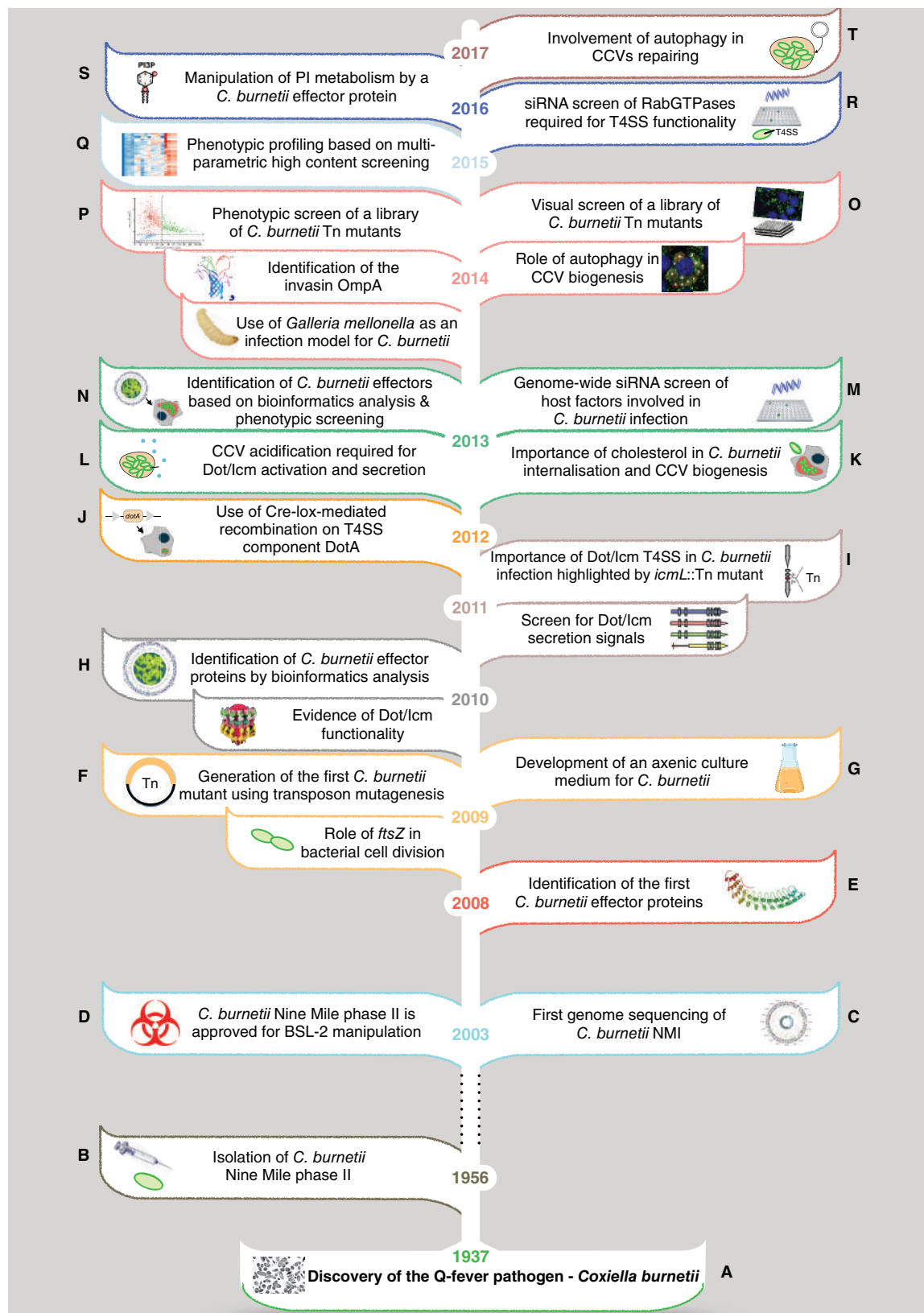


FIGURE 2 Milestone discoveries that have contributed to the knowledge of *C. burnetii* pathogenesis

biosafety level-3 (BSL-3) confinement. Importantly, loss-of-virulence of NMII has no impact either on intracellular growth kinetics or development of CCVs in cultured cells, making NMII a relevant model to study host-pathogen interactions (Howe et al., 2010).

Nevertheless, bacterial amplification of *C. burnetii* in embryonated eggs and/or cultured cells represented a real obstacle for its genetic manipulation. Indeed, transposon mutagenesis allowed the generation of *C. burnetii* mutants (Beare et al., 2009); however, amplification and isolation of these from infected cells ruled out the possibility of isolating mutations in virulence genes. Thus, until 2011, *ftsZ* was the only *C. burnetii* gene characterised using Himar1 transposon mutagenesis (Beare et al., 2009) (Figure 2F).

Whole-genome sequencing of *C. burnetii* NMI RSA493 in 2003 allowed the identification of typical features, including a Dot/Icm secretion system, which is highly homologous to that of *L. pneumophila* (Seshadri et al., 2003) (Figure 2C). This finding was pivotal to develop bioinformatics-based approaches to predict effector proteins-coding genes. These revealed that similar to *L. pneumophila*, effector proteins translocated by *C. burnetii* encode a C-terminal secretion signal called the E-block motif and are mostly under the control of a PmrA response regulator (Zusman et al., 2007). Due to the genetic intractability of *C. burnetii* at that time, candidate effector proteins were tested for secretion using *L. pneumophila* as a surrogate model, exploiting the homologies between the Dot/Icm secretion systems of the two pathogens. This approach allowed the Roy laboratory to validate the translocation of four *C. burnetii* effector proteins encoding ankyrin repeat homology domains (ARHDs) (Pan et al., 2008) (Figure 2E). Later work from the Samuel laboratory reported the first large-scale, bioinformatics-based identification of *C. burnetii* effector proteins and used the *L. pneumophila* system to validate the secretion of 32 new T4SS substrates (Chen et al., 2010) (Figure 2H). Moreover, using a shuttle plasmid system for the expression of recombinant proteins in *C. burnetii*, Chen and colleagues also demonstrated that the functionality of the Dot/Icm secretion system (Chen et al., 2010).

One year later, a genetic screen of *C. burnetii* proteins carrying C-terminal secretion signals led to the identification of additional effector proteins (Carey et al., 2011) (Figure 2I). For this study, wild type (wt) *L. pneumophila* or the T4SS-defective $\Delta dotA$ mutant were transformed with a library containing adenylate cyclase enzyme (CyaA)-tagged random fragments of *C. burnetii* genome, leading to the validation of seven additional *C. burnetii* effectors (Carey et al., 2011). These were further tested for their intracellular localization and function, which indicated a possible implication in the manipulation of host membrane trafficking. Of note, this is the first study to report a replication phenotype associated with a transposon insertion in the *C. burnetii* Dot/Icm gene *icmL* (*icmL::Tn*), thus demonstrating the importance of *C. burnetii* effector protein translocation for infection (Carey et al., 2011) (Figure 2I). Today, the development of tailored bioinformatics algorithms for the identification of T4SS effector proteins led to the identification of over 140 candidate *C. burnetii* T4SS effectors (Voth et al., 2009; Chen et al., 2010; Carey et al., 2011; Maturana et al., 2013; Weber et al., 2013). Recent genome

comparison of the *C. burnetii* strains NMII RSA493, Henzerling RSA331, G Q212, K Q154 and Dugway 5J108-111, revealed that many genes encoding candidate effector proteins are either pseudo-genised or missing altogether, leaving only 44 out of the 143 identified effector protein-coding genes intact across all strains (Larson et al., 2016). Despite these significant advances, functional analysis of *C. burnetii* genes involved in virulence was still limited by the genetic intractability of this pathogen.

A game-changer in the study of *C. burnetii* infections has been the development of a synthetic medium (ACCM for Acidified Citrate Cysteine Medium), followed by the development of ACCM-2, allowing the extracellular culture of this obligate intracellular bacterium (Omsland et al., 2009, 2011) (Figure 2G). ACCM-2 development stems from metabolic requirement studies using microarrays, genomic reconstruction of metabolic pathways and metabolite typing (Omsland et al., 2009, 2011). These studies highlighted that *C. burnetii* requires acid activation buffer (pH 4.75), to reproduce the CCV micro-environment (Heinzen et al., 1996) and increase its metabolic potential as well as low oxygen levels (2.5%) to facilitate the bacterial micro-aerophilic respiration (Omsland et al., 2009, 2011). This scientific milestone finally enabled genetic manipulation of *C. burnetii*, leading to a new era in our understanding of its pathogenesis (Figure 2).

3 | FROM GENES TO FUNCTION: CHARACTERISATION OF *C. BURNETII* EFFECTORS INVOLVED IN VACUOLE BIOGENESIS

With the development of axenic culture, targeted deletion of *C. burnetii* was formally achievable (albeit remaining extremely challenging), and the role of *C. burnetii* effector proteins in infection could be tested directly. The Heinzen laboratory first exploited axenic culture with the generation of a *dotA* deletion mutant (Beare et al., 2012) (Figure 2J) and with the identification and characterisation of CvpA (for *Coxiella* vacuolar protein A). This effector protein localises at CCVs and reroutes recycling endosomes to this compartment by interacting with the clathrin adaptor protein AP2 (Larson et al., 2013) (Figure 1). In a follow-up study, the Heinzen laboratory identified four additional members of what constitutes today the Cvp sub-class of *C. burnetii* effector proteins (CvpA, CvpB/Cig2 and CvpC-to-E, Figure 1) (Larson et al., 2015). Accordingly, targeted deletion of *C. burnetii* vacuolar proteins severely affects the biogenesis of CCVs (Larson et al., 2013, 2015).

If targeted deletion of *C. burnetii* genes remains challenging, *Himar1*-based transposon mutagenesis has been extensively applied to the generation of libraries of *C. burnetii* mutants. Thus, by 2013, the Samuel laboratory reported the first study that combined bioinformatics-mediated identification of candidate effector proteins with transposon mutagenesis (Weber et al., 2013) (Figure 2N). Searching the *C. burnetii* genome for T4SS features (PmrA consensus sequences, E-block motifs and homologies with known effectors), led to the identification of 234 genes encoding putative *C. burnetii*

effector proteins. β -lactamase translocation assay in *L. pneumophila* validated 53 T4SS substrates, most of which were never reported before. Transposon mutagenesis showed that 10 effector proteins were involved in the biogenesis of CCVs and bacterial replication (Weber et al., 2013) (Figure 2N).

The following year, two independent studies reported the large-scale identification of *C. burnetii* virulence determinants based on the generation of two libraries of *C. burnetii* transposon mutants (Martinez et al., 2014; Newton et al., 2014) (Figure 2O, (r)). The Bonazzi library consisted of 3,000 GFP-tagged mutants, among which over 1,000 were sequenced, annotated and screened using quantitative, multiparametric image analysis to identify bacterial factors involved in host cell invasion, intracellular replication and persistence (Martinez et al., 2014, 2015). This approach allowed to validate the function of 16 out of the 22 genes constituting the *C. burnetii* Dot/Icm secretion system, characterise the phenotype associated with transposon insertions in 31 genes encoding effector proteins and identify the first *C. burnetii* invasin OmpA (for Outer membrane protein A), which is necessary and sufficient to trigger internalisation by non-phagocytic cells (Martinez et al., 2014) (Figures 1 and 2P). This study was also the first to report the use of the insect model *Galleria mellonella* to investigate *C. burnetii* virulence in vivo (Martinez et al., 2014).

The Roy laboratory used a modified-Himar1 expressing mCherry fluorescent protein to generate over 3200 mutants. These were visually screened in HeLa cells to identify genes important in the biogenesis of CCVs and bacterial replication using the lysosomal marker LAMP-1 to visualise the membranes of the *C. burnetii* replicative compartment (Newton et al., 2014) (Figure 2O). This approach allowed the isolation of mutants characterised by different intracellular phenotypes, including defects in intracellular replication and homotypic fusion of independent CCVs or the appearance of filamentous bacteria. Of note, mutants carrying a transposon insertion in gene encoding *CBU1751* (*cig57*) displayed a severe vacuole biogenesis defect (Newton et al., 2014). The Newton laboratory has further characterised the role of this effector protein in the development of CCVs and intracellular replication, showing that Cig57 subverts clathrin-mediated traffic by interacting with FCHO2, an accessory protein of clathrin-coated pits (Latomanski et al., 2016) (Figure 1). More recently, CTLC (clathrin heavy chain) has been observed at CCVs, where it plays an essential role in vacuole expansion (Latomanski and Newton, 2018). Importantly, CTLC recruitment to the CCV is related to autophagy, and conversely, the fusion of autophagosomes with CCVs is dependent on CTLC (Latomanski and Newton, 2018). The Roy visual screen also highlighted a multivacuolar phenotype associated with transposon insertions in the gene *CBU0021* (*cig2*), identical to that previously observed following the knockdown of autophagy-related genes (McDonough et al., 2013), suggesting a functional link between a bacterial effector protein and the manipulation of a specific host cell function (Figure 2O). This hypothesis was further investigated, demonstrating that Cig2 contributes to the recruitment of the autophagy machinery to CCVs (Figure 1), thus facilitating their homotypic fusion and contributing to

an enhanced bacterial virulence in the *Galleria mellonella* infection model (Kohler et al., 2016).

4 | IT TAKES TWO TO TANGO: ROLE OF HOST CELL PATHWAYS IN *C. BURNETII* VACUOLE BIOGENESIS

If on one hand effector proteins translocation is critical for pathogenesis, host cell proteins, lipids and membrane trafficking pathways also play a significant role in *C. burnetii* infections. As mentioned above, the maturation of CCVs along the endocytic pathway is a prerequisite for effector proteins translocation (Newton et al., 2013) (Figure 2L); thus, Rab GTPases of the endocytic pathway play a key role in *C. burnetii* intracellular replication (Figure 1) (Beron et al., 2002; Romano et al., 2007; Campoy et al., 2011). Indeed, silencing of either Rab5 or Rab7 correlates with effector protein translocation defects (Newton et al., 2016) (Figure 2R).

A comprehensive characterisation of the host cell components required for the biogenesis of CCVs was provided for the first time by a genome-wide screen using siRNA targeting eukaryotic genes in *C. burnetii*-infected HeLa cells (McDonough et al., 2013) (Figure 2M). Host determinants required for *C. burnetii* infection were identified by the analysis of the number and size of CCVs, revealing the importance of several eukaryotic pathways in critical infection events. As expected, the silencing of genes encoding pH-regulating proteins CLN3 and CLCN5, as well as components of the vacuolar ATPase resulted in a defect in the biogenesis of CCVs (McDonough et al., 2013). Besides, the depletion of the retromer cargo complex VPS26-VPS29-VPS35 leads to defective bacterial replication, revealing a role for retrograde membrane trafficking in *C. burnetii* infections (McDonough et al., 2013). Interestingly, seminal work from the Colombo laboratory in the past decade demonstrated that the induction of autophagy favours the biogenesis of CCVs and that *C. burnetii* actively manipulates autophagy during infections (Gutierrez et al., 2005; Romano et al., 2007). However, the precise role of autophagy in CCVs' development remained to be characterised. The genome-wide screening approach of the Roy laboratory revealed that knockdown of autophagy proteins syntaxin-17, ATG5 and ATG12 results in the formation of multiple CCVs of smaller size as compared to control cells (McDonough et al., 2013). It was later demonstrated that this multivacuolar phenotype is the result of the defective homotypic fusion of CCVs (Newton et al., 2014; Martinez et al., 2016).

The Voth and Heinzen laboratories have further explored the complex interplay between *C. burnetii* and autophagy by. The autophagy-associated cargo receptor p62 is actively recruited at CCVs, independently of LC3-interacting domains (Winchell et al., 2018). Interestingly, *C. burnetii* infections seem to preserve p62 from degradation upon induction of autophagy (Winchell et al., 2018). Accordingly, *C. burnetii* infections inhibit mTORC1, a master regulator of autophagy, by a non-canonical mechanism that does not result in accelerated autophagy, nor a block of the autophagic flux (Larson et al., 2019). Finally, autophagy is also involved in repairing the

membranes of CCVs during expansion, which are subject to transitory damage and loss-of-acidification (Mansilla Pareja et al., 2017) (Figure 2T).

Besides host cell proteins, lipids also play a significant role in the development of CCVs, which are rich in sterols (Gilk et al., 2010). Indeed, cholesterol homeostasis regulates CCVs biogenesis and intracellular survival of *C. burnetii* (Gilk et al., 2013; Mulye et al., 2017) (Figure 2K). Accordingly, *C. burnetii* actively manipulates cholesterol metabolism via a eukaryotic-like $\Delta 24$ sterol reductase (Gilk et al., 2010). Furthermore, an image-based supervised machine learning approach led to the identification of CvpB/Cig2 as the first *C. burnetii* effector protein to bind phosphoinositides and manipulate their metabolism (Martinez et al., 2016) (Figure 2S). Indeed, CvpB/Cig2 binds phosphatidylinositol-3-phosphate (PI[3]P) and phosphatidylserine (PS) and perturbs the activity of the PI3-kinase PIKFYVE. This inhibition results in an enrichment of PI(3)P at CCVs, which is essential for their homotypic fusion (Martinez et al., 2016). Importantly, despite the apparent defect in the biogenesis of CCVs, *cvpB* transposon mutants were unaffected in their capacity of replicating within infected cells. However, *cvpB* mutants are attenuated in the in vivo models *Galleria mellonella* (Martinez et al., 2016) and SCID mice (van Schaik et al., 2017), demonstrating that the biogenesis of CCVs can modulate *C. burnetii* virulence, independently of bacterial replication.

5 | TO INFINITY AND BEYOND (CONCLUSIONS)

As of today, *C. burnetii* stands as the sole example of an obligate intracellular bacterial pathogen for which a specific axenic culture medium has been developed. Consequently, research on this dangerous and complex pathogen has bloomed during this decade, with the development of genetic tools and phenotypic screening approaches to better understand the complex interactions established between *C. burnetii* and its host. The generation of libraries of *C. burnetii* transposon mutants combined with the development of multi-parametric screening approaches have allowed the rapid and unbiased identification of microbial genes involved in specific steps of the infectious process. This has been facilitated by the fact that the majority of *C. burnetii* transposon mutants isolated to date display a significant phenotype during infection (Martinez et al., 2014), suggesting a milder functional gene redundancy as compared to the closely related pathogen *L. pneumophila*. Accordingly, bioinformatics predicted ~150 effector proteins compared to the 300 translocated by *Legionella*.

Nevertheless, understanding how these newly identified virulence determinants manipulate host cell functions remains exceptionally challenging. Probably due to the complex nature of this compartment, a large proportion of the *C. burnetii* effector proteins identified and characterised to date are involved in the biogenesis of the CCV; however, proteins involved in the manipulation of other signalling pathways including apoptosis and inflammation have been identified and partially characterised. With the development of advanced

bioinformatics approaches such as unsupervised machine learning, hierarchical clustering and Bayesian network analysis, we can now compare microbial-targeted and host-targeted phenotypic screens, to identify sets of bacterial and eukaryotic genes predicted to be involved in the same biological process during infection.

Despite the giant leaps taken since the development of axenic culture, many technical barriers still exist today. Directed mutagenesis remains challenging, limiting our studies to the mutants available in the transposon libraries hosted in the laboratories that undertook this endeavour. Nevertheless, our knowledge of this once-neglected pathogen is ever increasing. This will allow, in the near future, to address burning questions on *C. burnetii* pathogenesis, including a characterisation of the strategies used to evade immune recognition, cell-to-cell spread and, consequently, dissemination to distant organs (heart and liver) following infection of alveolar macrophages.

ACKNOWLEDGEMENTS

Work in our laboratory is supported by the Agence Nationale de la Recherche (ANR; ANR-14-CE14-0012-01, project AttaQ and ANR-17-CE15-0021, project QPID) and by the ERA-NET Infect-ERA (ANR-13-IFEC-0003, project EUGENPATH). We apologise to all colleagues whose work was not discussed in this review.

CONFLICT OF INTEREST

The authors declare no conflict of interest.

ORCID

Matteo Bonazzi  <https://orcid.org/0000-0001-5499-8759>

REFERENCES

- Beare, P. A., Larson, C. L., Gilk, S. D., & Heinzen, R. A. (2012). Two systems for targeted gene deletion in *Coxiella burnetii*. *Applied and Environmental Microbiology*, 78, 4580–4589.
- Beare, P. A., Howe, D., Cockrell, D. C., Omsland, A., Hansen, B., & Heinzen, R. A. (2009). Characterization of a *Coxiella burnetii* *ftsZ* mutant generated by Himar1 transposon mutagenesis. *Journal of Bacteriology*, 191, 1369–1381.
- Beron, W., Gutierrez, M. G., Rabinovitch, M., & Colombo, M. I. (2002). *Coxiella burnetii* localizes in a Rab7-labeled compartment with autophagic characteristics. *Infection and Immunity*, 70, 5816–5821.
- Brooke, R.J., Kretzschmar, M.E.E., Mutters, N.T., and Teunis, P.F. (2013). Human dose response relation for airborne exposure to *Coxiella burnetii*. *BMC Infectious Diseases* 13: 488 BMC Infectious Diseases.
- Campoy, E. M., Zoppino, F. C. M., & Colombo, M. I. (2011). The early secretory pathway contributes to the growth of the *Coxiella* replicative niche. *Infection and Immunity*, 79, 402–413.
- Capo, C., Lindberg, F. P., Meconi, S., Zaffran, Y., Tardei, G., Brown, E., ... Mege, J. L. (1999). Subversion of monocyte functions by *Coxiella burnetii*: Impairment of the cross-talk between α 5 β 3 integrin and CR3. *Journal of Immunology*, 163, 6078–6085.
- Carey, K. L., Newton, H. J., Lührmann, A., & Roy, C. R. (2011). The *Coxiella burnetii* dot/lcm system delivers a unique repertoire of type IV effectors into host cells and is required for intracellular replication. *PLoS Pathogens*, 7, e1002056.
- Chen, C., Banga, S., Mertens, K., Weber, M. M., Gorbashlieva, I., Tan, Y., ... Samuel, J. E. (2010). Large-scale identification and translocation of type IV secretion substrates by *Coxiella burnetii*. *Proceedings of the National Academy of Sciences*, 107, 21755–21760.

- Cunha, L. D., Ribeiro, J. M., Fernandes, T. D., Massis, L. M., Khoo, C. A., Moffatt, J. H., ... Zamboni, D. S. (2015). Inhibition of inflammasome activation by *Coxiella burnetii* type IV secretion system effector IcaA. *Nature Communications*, 6, 10205.
- Dragan, A. L., & Voth, D. E. (2019). *Coxiella burnetii*: International pathogen of mystery. *Microbes and Infection*, 1–11.
- Eldin, C., Mélenotte, C., Mediannikov, O., Ghigo, E., Million, M., Edouard, S., ... Raoult, D. (2017). From Q fever to *Coxiella burnetii* infection: A paradigm change. *Clinical Microbiology Reviews*, 30, 115–190.
- Gilk, S. D., Beare, P. A., & Heinzen, R. A. (2010). *Coxiella burnetii* expresses a functional $\Delta 24$ sterol reductase. *Journal of Bacteriology*, 192, 6154–6159.
- Gilk, S. D., Cockrell, D. C., Luterbach, C., Hansen, B., Knodler, L. A., Ibarra, J. A., ... Heinzen, R. A. (2013). Bacterial colonization of host cells in the absence of cholesterol. *PLoS Pathogens*, 9, e1003107.
- Gutierrez, M. G., Vázquez, C. L., Munafó, D. B., Zoppino, F. C. M., Berón, W., Rabinovitch, M., & Colombo, M. I. (2005). Autophagy induction favours the generation and maturation of the *Coxiella*-replicative vacuoles. *Cellular Microbiology*, 7, 981–993.
- Hackstadt, T., & Williams, J. C. (1981). Biochemical stratagem for obligate parasitism of eukaryotic cells by *Coxiella burnetii*. *Proceedings of the National Academy of Sciences*, 78, 3240–3244.
- Heinzen, R. A., Scidmore, M. A., Rockey, D. D., & Hackstadt, T. (1996). Differential interaction with endocytic and exocytic pathways distinguish parasitophorous vacuoles of *Coxiella burnetii* and *Chlamydia trachomatis*. *Infection and Immunity*, 64, 796–809.
- Hoover, T. A., Culp, D. W., Vodkin, M. H., Williams, J. C., & Thompson, H. A. (2002). Chromosomal DNA deletions explain phenotypic characteristics of two antigenic variants, phase II and RSA 514 (crazy), of the *Coxiella burnetii* nine mile strain. *Infection and Immunity*, 70, 6726–6733.
- Howe, D., Shannon, J. G., Winfree, S., Dorward, D. W., & Heinzen, R. A. (2010). *Coxiella burnetii* phase I and II variants replicate with similar kinetics in degradative phagolysosome-like compartments of human macrophages. *Infection and Immunity*, 78, 3465–3474.
- Kohler, L. J., Reed, S. R., Sarraf, S. A., Arteaga, D. D., Newton, H. J., & Roy, C. R. (2016). Effector protein Cig2 decreases host tolerance of infection by directing constitutive fusion of autophagosomes with the *Coxiella*-containing vacuole. *MBio*, 7, 1–14.
- Larson, C. L., Beare, P. A., Howe, D., & Heinzen, R. A. (2013). *Coxiella burnetii* effector protein subverts clathrin-mediated vesicular trafficking for pathogen vacuole biogenesis. *Proceedings of the National Academy of Sciences*, 110, E4770–E4779.
- Larson, C. L., Beare, P. A., Voth, D. E., Howe, D., Cockrell, D. C., Bastidas, R. J., ... Heinzen, R. A. (2015). *Coxiella burnetii* effector proteins that localize to the Parasitophorous vacuole membrane promote intracellular replication. *Infection and Immunity*, 83, 661–670.
- Larson, C. L., Martinez, E., Beare, P. A., Jeffrey, B., Heinzen, R. A., & Bonazzi, M. (2016). Right on Q: Genetics begin to unravel *Coxiella burnetii* host cell interactions. *Future Microbiology*, 11, 919–939.
- Larson, C. L., Sandoz, K. M., Cockrell, D. C., & Heinzen, R. A. (2019). Non-canonical inhibition of mTORC1 by *Coxiella burnetii* promotes replication within a phagolysosome-like vacuole. *MBio*, 10, 1–16.
- Latomanski, E. A., & Newton, H. J. (2018). Interaction between autophagic vesicles and the *Coxiella*-containing vacuole requires CLTC (clathrin heavy chain). *Autophagy*, 14, 1710–1725.
- Latomanski, E. A., Newton, P., Khoo, C. A., & Newton, H. J. (2016). The effector Cig57 hijacks FCHO-mediated vesicular trafficking to facilitate intracellular replication of *Coxiella burnetii*. *PLoS Pathogens*, 12, 1–24.
- Lührmann, A., Newton, H. J., & Bonazzi, M. (2017). Beginning to understand the role of the type IV secretion system effector proteins in *Coxiella burnetii* pathogenesis. *Current Topics in Microbiology and Immunology*, 413, 243–268.
- Madariaga, M. G., Rezai, K., Trenholme, G. M., & Weinstein, R. A. (2003). Q fever: A biological weapon in your backyard. *The Lancet Infectious Diseases*, 3, 709–721.
- Mahapatra, S., Gallaher, B., Smith, S. C., Graham, J. G., Voth, D. E., & Shaw, E. I. (2016). *Coxiella burnetii* employs the dot/Icm type IV secretion system to modulate host NF- κ B/RelA activation. *Frontiers in Cellular and Infection Microbiology*, 6, 1–13.
- Mansilla Pareja, M. E., Bongiovanni, A., Lafont, F., & Colombo, M. I. (2017). Alterations of the *Coxiella burnetii* replicative vacuole membrane integrity and interplay with the autophagy pathway. *Frontiers in Cellular and Infection Microbiology*, 7, 1–17.
- Martinez, E., Allombert, J., Cantet, F., Lakhani, A., Yandrapalli, N., Neyret, A., ... Bonazzi, M. (2016). *Coxiella burnetii* effector CvpB modulates phosphoinositide metabolism for optimal vacuole development. *Proceedings of the National Academy of Sciences*, 113, E3260–E3269.
- Martinez, E., Cantet, F., & Bonazzi, M. (2015). Generation and multi-phenotypic high-content screening of *Coxiella burnetii* transposon mutants. *Journal of Visualized Experiments*, 2015, 1–11.
- Martinez, E., Cantet, F., Fava, L., Norville, I., & Bonazzi, M. (2014). Identification of OmpA, a *Coxiella burnetii* protein involved in host cell invasion, by multi-phenotypic high-content screening. *PLoS Pathogens*, 10, e1004013.
- Maturana, P., Graham, J. G., Sharma, U. M., & Voth, D. E. (2013). Refining the plasmid-encoded type IV secretion system substrate repertoire of *Coxiella burnetii*. *Journal of Bacteriology*, 195, 3269–3276.
- McDonough, J. A., Newton, H. J., Klum, S., Swiss, R., Agaisse, H., & Roy, C. R. (2013). Host pathways important for *Coxiella burnetii* infection revealed by genome-wide RNA interference screening. *MBio*, 4, 1–13.
- Moos, A., & Hackstadt, T. (1987). Comparative virulence of intra- and interstrain lipopolysaccharide variants of *Coxiella burnetii* in the Guinea pig model. *Infection and Immunity*, 55, 1144–1150.
- Mulye, M., Samanta, D., Winfree, S., Heinzen, R. A., & Gilk, S. D. (2017). Elevated cholesterol in the *Coxiella burnetii* intracellular niche is bacteriolytic. *MBio*, 8, 1–18.
- Newton, H. J., Kohler, L. J., McDonough, J. A., Temoche-Diaz, M., Crabill, E., Hartland, E. L., & Roy, C. R. (2014). A screen of *Coxiella burnetii* mutants reveals important roles for dot/Icm effectors and host autophagy in vacuole biogenesis. *PLoS Pathogens*, 10, e1004286.
- Newton, H. J., McDonough, J. A., & Roy, C. R. (2013). Effector protein translocation by the *Coxiella burnetii* dot/Icm type IV secretion system requires Endocytic maturation of the pathogen-occupied vacuole. *PLoS One*, 8, e54566.
- Newton, P., Latomanski, E. A., & Newton, H. J. (2016). Applying fluorescence resonance energy transfer (FRET) to examine effector translocation efficiency by *Coxiella burnetii* during siRNA silencing. *Journal of Visualized Experiments*, 113, 54210.
- Omsland, A., Beare, P. A., Hill, J., Cockrell, D. C., Howe, D., Hansen, B., ... Heinzen, R. A. (2011). Isolation from animal tissue and genetic transformation of *Coxiella burnetii* are facilitated by an improved axenic growth medium. *Applied and Environmental Microbiology*, 77, 3720–3725.
- Omsland, A., Cockrell, D. C., Howe, D., Fischer, E. R., Virtaneva, K., Sturdevant, D. E., ... Heinzen, R. A. (2009). Host cell-free growth of the Q fever bacterium *Coxiella burnetii*. *Proceedings of the National Academy of Sciences*, 106, 4430–4434.
- Pan, X., Lührmann, A., Satoh, A., Laskowski-Arce, M. A., and Roy, C. R. (2008) Ankyrin repeat proteins comprise a diverse family of bacterial type IV effectors. *Science* (80-) 320: 1651–1654.
- Romano, P. S., Gutierrez, M. G., Berón, W., Rabinovitch, M., & Colombo, M. I. (2007). The autophagic pathway is actively modulated by phase II *Coxiella burnetii* to efficiently replicate in the host cell. *Cellular Microbiology*, 9, 891–909.
- van Schaik, E. J., Case, E. D., Martinez, E., Bonazzi, M., & Samuel, J. E. (2017). The SCID mouse model for identifying virulence determinants

- in *Coxiella burnetii*. *Frontiers in Cellular and Infection Microbiology*, 7, 1–10.
- Seshadri, R., Paulsen, I. T., Eisen, J. A., Read, T. D., Nelson, K. E., Nelson, W. C., ... Heidelberg, J. F. (2003). Complete genome sequence of the Q-fever pathogen *Coxiella burnetii*. *Proceedings of the National Academy of Sciences*, 100, 5455–5460.
- Voth, D. E., Howe, D., Beare, P. A., Vogel, J. P., Unsworth, N., Samuel, J. E., & Heinzen, R. A. (2009). The *Coxiella burnetii* ankryrin repeat domain-containing protein family is heterogeneous, with C-terminal truncations that influence dot/Icm-mediated secretion. *Journal of Bacteriology*, 191, 4232–4242.
- Weber, M. M., Chen, C., Rowin, K., Mertens, K., Galvan, G., Zhi, H., ... Samuel, J. E. (2013). Identification of *Coxiella burnetii* type IV secretion substrates required for intracellular replication and *Coxiella*-containing vacuole formation. *Journal of Bacteriology*, 195, 3914–3924.
- Winchell, C. G., Dragan, A. L., Brann, K. R., Onyilagha, F. I., Kurten, R. C., & Voth, D. E. (2018). *Coxiella burnetii* subverts p62/Sequestosome 1 and activates Nrf2 Signaling in human macrophages. *Infection and Immunity*, 86, 1–12.
- Zusman, T., Aloni, G., Halperin, E., Kotzer, H., Degtyar, E., Feldman, M., & Segal, G. (2007). The response regulator PmrA is a major regulator of the icm/dot type IV secretion system in *Legionella pneumophila* and *Coxiella burnetii*. *Molecular Microbiology*, 63, 1508–1523.

How to cite this article: Burette M, Bonazzi M. From neglected to dissected: How technological advances are leading the way to the study of *Coxiella burnetii* pathogenesis. *Cellular Microbiology*. 2020;22:e13180. <https://doi.org/10.1111/cmi.13180>

RESEARCH ARTICLE



Coxiella effector protein CvpF subverts RAB26-dependent autophagy to promote vacuole biogenesis and virulence

Fernande Ayenoue Siadous, Franck Cantet, Erin Van Schaik, Mélanie Burette, Julie Allombert, Anissa Lakhani, Boris Bonaventure, Caroline Goujon, James Samuel, Matteo Bonazzi, and Eric Martinez

^aInstitut de Recherche en Infectiologie de Montpellier (IRIM) UMR 9004 CNRS, Université de Montpellier, Montpellier, France; ^bDepartment of Microbial and Molecular Pathogenesis, Texas A&M Health Science Center College of Medicine, Bryan, TX, USA

ABSTRACT

Coxiella burnetii, the etiological agent of the zoonosis Q fever, replicates inside host cells within a large vacuole displaying autolysosomal characteristics. The development of this compartment is mediated by bacterial effectors, which interfere with a number of host membrane trafficking pathways. By screening a *Coxiella* transposon mutant library, we observed that transposon insertions in *cbu0626* led to intracellular replication and vacuole biogenesis defects. Here, we demonstrate that CBU0626 is a novel member of the *Coxiella* vacuolar protein (Cvp) family of effector proteins, which is translocated by the Dot/Icm secretion system and localizes to vesicles with autolysosomal features as well as *Coxiella*-containing vacuoles (CCVs). We thus renamed this effector CvpF for *Coxiella* vacuolar protein F. CvpF specifically interacts with the host small GTPase RAB26, leading to the recruitment of the autophagosomal marker MAP1LC3B/LC3B (microtubule associated protein 1 light chain 3 beta) to CCVs. Importantly, *cvpF::Tn* mutants were highly attenuated compared to wild-type bacteria in the SCID mouse model of infection, highlighting the importance of CvpF for *Coxiella* virulence. These results suggest that CvpF manipulates endosomal trafficking and macroautophagy/autophagy induction for optimal *C. burnetii* vacuole biogenesis.

Abbreviations: ACCM: acidified citrate cysteine medium; AP: adaptor related protein complex; CCV: *Coxiella*-containing vacuole; Cvp: *Coxiella* vacuolar protein; GDI: guanosine nucleotide dissociation inhibitor; GDF: GDI dissociation factor; GEF: guanine exchange factor; LAMP1: lysosomal associated membrane protein 1; MAP1LC3B/LC3B: microtubule associated protein 1 light chain 3 beta; MTORC1: mechanistic target of rapamycin kinase MTOR complex 1; PBS: phosphate-buffered saline; PMA: phorbol myristate acetate; SQSTM1/p62: sequestosome 1; WT: wild-type.

ARTICLE HISTORY

Received 7 June 2019
Revised 28 January 2020
Accepted 4 February 2020

KEYWORDS


Autophagy; *Coxiella burnetii*; effector protein; LC3B; RAB GTPase


Introduction

Coxiella burnetii is the causative agent of animal coxiellosis and human Q fever, considered as one of the most relevant reemerging zoonosis in Europe [1]. The symptoms of Q fever range from fatigue, long-lasting fever, and hepatitis in the acute form of the disease, to severe endocarditis in its chronic form [2]. Upon internalization by phagocytic and non-phagocytic cells, *Coxiella* remains in endosomes that progress in the endocytic pathway. Endosomal acidification triggers the activation of a defect in organelle trafficking genes/intracellular multiplication (Dot/Icm) type 4 secretion system (T4SS) and the translocation of bacterial effectors, which are essential for the biogenesis of the *Coxiella*-containing vacuole (CCV) [3–5]. Bioinformatics analysis and secretion assays using either *Legionella* [6] or *Coxiella* [7] have identified approximately 143 candidate *Coxiella* effectors [8]. However, very few host cell partners have been identified [9,10], and the role of *Coxiella* effectors in CCV biogenesis remains poorly characterized. *Coxiella* vacuolar proteins (Cvps) constitute a class of effectors that localize to endosomal compartments and CCVs

in cells infected with wild type *Coxiella*. These effectors play an important role in *Coxiella* vacuole biogenesis, as the mutation of their corresponding genes leads to smaller CCVs [11]. CvpA interacts with adaptor related protein complex 2 (AP2) and clathrin [10]. CvpB (or Cig2) interacts with cellular lipids phosphatidylinositol 3-phosphate (PtdIns3P) and phosphatidylserine (PS) and interferes with PIKfyve (phosphoinositide kinase, FYVE-type zinc finger containing) activity to promote autophagy-mediated homotypic fusion of CCVs [12]. The functions of CvpC, CvpD, and CvpE remain undetermined. Besides CvpB, additional effector proteins manipulate the autophagy machinery for optimal vacuole biogenesis: effectors CpeB and CpeL colocalize with the autophagosomal marker LC3B [13,14] and mutants of the effector proteins CBU0513, and Cig57 display decreased presence of LC3B at their respective vacuoles [15,16].

Macroautophagy (hereafter termed autophagy) is a highly conserved eukaryotic process used by cells to recycle and degrade cargos, such as damaged organelles and misfolded proteins, in order to acquire nutrients during periods of

CONTACT Eric Martinez  eric.martinez@irim.cnrs.fr; Matteo Bonazzi matteo.bonazzi@irim.cnrs.fr Institut de Recherche en Infectiologie de Montpellier (IRIM) UMR 9004 CNRS, Université de Montpellier, Montpellier, France

 Supplemental data for this article can be accessed [here](#).

© 2020 The Author(s). Published by Informa UK Limited, trading as Taylor & Francis Group.

This is an Open Access article distributed under the terms of the Creative Commons Attribution-NonCommercial-NoDerivatives License (<http://creativecommons.org/licenses/by-nc-nd/4.0/>), which permits non-commercial re-use, distribution, and reproduction in any medium, provided the original work is properly cited, and is not altered, transformed, or built upon in any way.

deprivation. It can also act as a cell defense mechanism capable of targeting invading pathogens for degradation. The mechanistic target of rapamycin kinase complex 1 (MTORC1) mediates the nutrient-sensing and regulatory functions of lysosomes. Under normal conditions, phosphorylated MTOR (mechanistic target of rapamycin kinase) localizes to the lysosome surface and downregulates autophagy. Upon starvation or treatment with the MTOR inhibitor torin1, MTOR is inactivated and delocalizes to the cytosol, which triggers a signaling cascade leading to autophagy. RAB GTPases, the key regulators of vesicular sorting and trafficking in the endocytic and secretory pathways, could regulate autophagy membrane dynamics. While RAB1, RAB5, RAB7, RAB9A, RAB11, RAB23, RAB32 and RAB33B act at different stages of autophagosome formation, RAB7, RAB8B and RAB24 participate in autophagosome maturation [17]. Recently, additional RAB GTPases, such as RAB26 and RAB37, have also been shown to participate in the autophagy process [18–21]. RAB GTPases shuttle between a cytosolic inactive GDP-bound state and a membrane-anchored active GTP-bound state. Once inserted into the membranes, these proteins can interact with other partner proteins to mediate vesicular trafficking and maturation events. Their central role in membrane dynamics and immunity made them ideal targets for intracellular bacterial pathogens, which divert their function for the development of optimal intracellular niches [22–24]. In the context of *Coxiella* infections, inhibiting the function or expression of RAB1, RAB5, RAB7, and RAB24 affects the vacuole biogenesis and impairs intracellular replication [12,25–29].

Multi-parametric phenotypic analysis of a *Coxiella* transposon library revealed that transposon insertions in the gene *cbu0626* affect *Coxiella* vacuole biogenesis and intracellular replication [30]. Here, we demonstrate that CBU0626 is a new *Coxiella* vacuolar effector protein interacting with RAB26 to trigger LC3B recruitment at CCVs. Decreased LC3B recruitment at CCVs in cells challenged with *cbu0626* mutants is associated with altered replication *in vitro* and *in vivo*, suggesting that diversion of autophagy by this effector is crucial for *Coxiella* virulence.

Results

CvpF is a Dot/Icm vacuolar effector protein required for LC3B recruitment to CCVs and for *Coxiella* virulence *in vivo*

Our phenotypic screen of a *Coxiella* transposon mutant library identified a significant number of genes encoding candidate *Coxiella* effector proteins with a role in CCV biogenesis [30]. Among these, the mutant *Tn248* with a transposon insertion in the gene *cbu0626* displayed a severe replication defect in epithelial cells [30]. Bioinformatics analysis indicated that *cbu0626* is likely part of a PmrA-regulated operon, together with *cbu0625* (also known as *cig17*) [31], and possesses a C-terminal E-Block motif found in type 4-secreted effectors [32] (Figure S1A). Southern blot analysis confirmed that transposon insertion in the genome of *Tn248* is unique and occurs in the gene

cbu0626 (Figure S1B). Complementation of the *cbu0626::Tn* mutation in *Tn248* by the introduction of the full *cbu0625-cbu0626* operon under the control of the endogenous PmrA promoter (*Tn248* Comp.) restored the expression of the full *cbu0626* mRNA (Figure S1C and D). We validated CBU0626 translocation by transforming either a control *Coxiella* transposon mutant (WT) or a T4SS-defective *dotA::Tn* mutant with a β -lactamase-*cbu0626* fusion construct and comparing the secretion of CBU0626 with that of the previously reported effector protein CvpB [12], using the β -lactamase secretion assay. We verified the expression of all β -lactamase-tagged constructs by western blot (Figure S1E). CBU0626 secretion was comparable with that of CvpB after 24, 48, and 72 h of infection by the control *Coxiella* strain (Figure S1F). The absence of detectable secretion of either protein by the T4SS-defective *dotA::Tn* mutant indicated that CBU0626 is indeed a Dot/Icm secreted protein. Of note, T4SS-dependent translocation was still functional in the *Tn248* mutant strain (Figure S1F).

To determine the subcellular localization and targets of CBU0626, we transfected U2OS cells infected with WT *Coxiella Tn1832* for 4 d with a plasmid coding for mCherry-tagged CBU0626 (mCh-CBU0626, Figure 1A). The *Coxiella* effector colocalized with the lysosomal marker LAMP1 at CCVs, indicating that CBU0626 is a newly identified member of the Cvp family of *Coxiella* effector proteins. We, thus, renamed this protein CvpF for *Coxiella* vacuolar protein F. Next, we used our implemented image analysis algorithm [33] to validate the replication phenotypes previously observed with the *cvpF::Tn* mutant in our transposon library [30]. U2OS and PMA-treated THP-1 cells infected for 6 d with either the control *Coxiella* mutant *Tn1832* (WT). We fixed and processed the *cvpF::Tn* transposon mutant or the complemented *cvpF* transposon mutant (*cvpF::Tn* Comp.) for immunofluorescence and quantitative PCR. Automated image analysis indicated that *cvpF* transposon mutant generated smaller CCVs and colonies in U2OS and THP1 cells, respectively (Figure 1B,D), and replicated less efficiently than WT bacterium (Figure 1C,E). Interestingly, in ACCM-2 axenic media, replication of the *cvpF::Tn* mutant was similar to WT *Coxiella*, the T4SS-defective *dotA::Tn* mutant and the *cvpF::Tn* complemented strain (Figure 1F), indicating that transposon insertion in *cvpF* only affects intracellular development of the bacterium.

We, then, investigated the *in vivo* relevance of CvpF using the recently developed SCID mice model [34]. Mice challenged via the IP route either with the control *Coxiella* strain NMII, the *cvpF::Tn* mutant, the complemented *cvpF::Tn* strain and the *dotA::Tn* mutant, were culled at 14 d post-infection and we assessed bacterial genome equivalents (GE) in the spleen, as well as splenomegaly (Figure 1G,H). In agreement with the observations on cultured cells, the number of *cvpF::Tn* mutant GE in the spleen of infected animals was significantly lower than those found for the WT bacterium and complementation of the *cvpF::Tn* mutant partially restored this replication defect (Figure 1G). The splenomegaly induced by the *cvpF::Tn* mutant was also much lower than the one provoked by WT bacterium (Figure 1H), strongly suggesting that the virulence of the *cvpF::Tn*

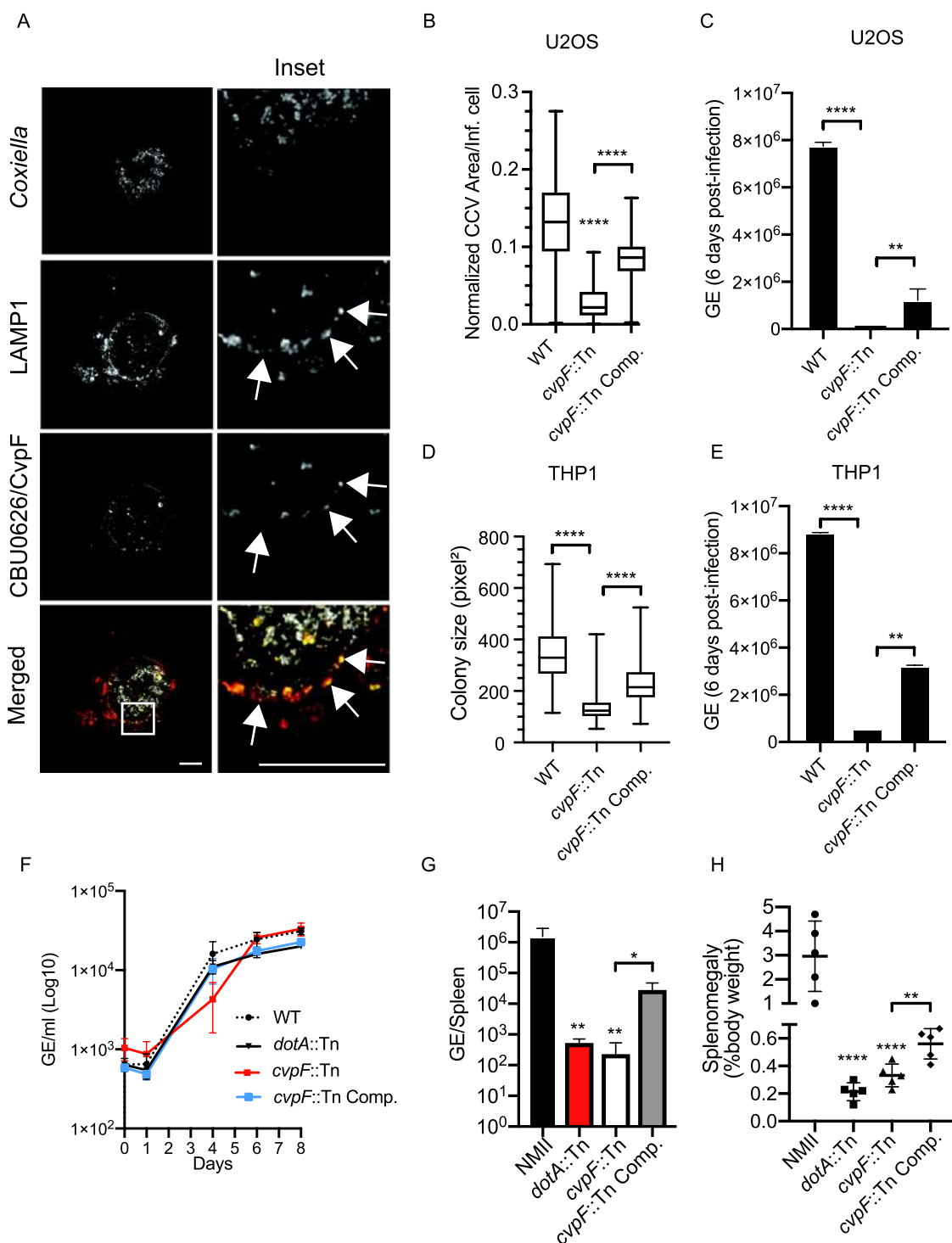


Figure 1. CvpF is a Dot/Icm T4BSS vacuolar effector protein important for *Coxiella* intracellular growth, CCV biogenesis, and virulence. (A) U2OS cells were infected with *Coxiella* WT GFP (gray) and transfected with pLVX-mCherry-CBU0626/CvpF (red) 4 d post-infection. We fixed cells 12 h post-transfection and labeled with an anti-LAMP1 antibody (green). White arrows indicate discrete regions of the *Coxiella* vacuole where CvpF and LAMP1 colocalize. (B) U2OS cells were challenged for 6 d either with *Coxiella* WT GFP (WT), *cvpF::Tn* mutant, or the complemented *cvpF::Tn* strain (*cvpF::Tn Comp.*). CCV area for each strain was determined using the Cell Profiler software. (C) U2OS cells were challenged as in B, and Genome Equivalents (GE) were determined by quantitative PCR. (D) PMA-treated THP1 cells were challenged for 6 d either with *Coxiella* WT GFP (WT), *cvpF::Tn* mutant, or the complemented *cvpF::Tn* strain (*cvpF::Tn Comp.*). The colony area for each strain was determined using the Cell Profiler software. (E) THP1 cells were challenged as in D and Genome Equivalents (GE) were determined by quantitative PCR. (F) *Coxiella* WT GFP (WT), *dotA::Tn* mutant, *cvpF::Tn* mutant and the complemented *cvpF::Tn* strain (*cvpF::Tn Comp.*) were grown for 8 d in ACCM-2 and Genome Equivalents (GE)/ml were determined by Pico Green assay. (G) Genome Equivalents (GE) calculated using TaqMan real-time PCR with DNA purified from infected spleens of 5 SCID mice per group on day 14 after challenge with 1×10^6 GE equivalents of the strains shown. (H) Splenomegaly calculated as spleen weight as a percentage of total body weight at the time of necropsy on day 14 after infection with 1×10^6 GE equivalents of the strains listed in the figure legend. Values are mean \pm SD from 3 independent experiments (n.s. = non-significant, **** = $P < 0.0001$, ** = $P < 0.0021$, * = $P < 0.033$, one-way ANOVA, Sidak's multiple comparison test). Scale bars: 10 μ m.

mutant is severely attenuated *in vivo* and could be partially restored using the *cvpF*::Tn-complemented strain.

As CvpF appears to be important for CCV biogenesis, we investigated whether the absence of CvpF affects typical CCVs markers. More than 80% of vacuoles generated by *WT Coxiella*, *cvpF*::Tn and *cvpF*::Tn Comp. strains were positive for the acidification marker LysoTracker and the lysosomal/late endosomal protein LAMP1 (Figure 2A,B). However, $15.77 \pm 6.8\%$ of CCVs generated by the *cvpF*::Tn mutant was positive for LC3B (Figure 2C,D), while $93.56 \pm 3.4\%$ of CCVs generated by *WT Coxiella* and $70.13 \pm 10.2\%$ of CCVs generated by the *cvpF*::Tn-complemented strain were positive for LC3B (Figure 2C,D). Colocalization analysis between LAMP1 and LC3B on CCVs generated by *WT*, *cvpF*::Tn, and *cvpF*::Tn complemented strains (Figure 2E) showed that significantly less LC3B is found on CCVs generated by the *cvpF*::Tn mutant, strongly suggesting that CvpF plays a role in the recruitment of this autophagosomal marker on CCVs.

Ectopically expressed CvpF localizes to vesicular structures with autolysosomal features

The defective vacuole biogenesis phenotype observed with the *cvpF* transposon mutants, accompanied by the loss of LC3B at CCVs, suggested a role for this bacterial effector in re-routing autophagy components to the forming CCV. We, thus, further investigated CvpF localization in cells overexpressing either mCherry- or HA-tagged versions of the effector protein. CvpF was excluded from the Golgi complex either labeled by an anti-GM130 antibody or by expression of GFP-tagged M6PR (mannose-6-phosphate receptor, cation dependent) (Figure S2), whereas we observed partial colocalization of CvpF with markers of the endosomal sorting complex required for transport (ESCRT) complex (GFP-TSG101, GFP-VPS4A and FLAG-CHMP4B) (Figure S2). Conversely, CvpF signal overlapped with the lysosomal marker LAMP1, but also with the early endosomal and autophagosomal markers phosphatidylinositol 3-phosphate (PtdIns3P) probe 2xFYVE-GFP and LC3B (Figure 3A). Importantly, all compartments labeled by CvpF displayed a clustered perinuclear localization (Figure 3A), as opposed to cells expressing either the HA or the mCherry tags alone (Figure S3).

To understand how CvpF is targeted to host cell membranes, we carried out a mutational analysis of this *Coxiella* effector protein. We transfected U2OS cells with mCherry- or HA-tagged versions of incremental deletions either from the N-terminal or the C-terminal of CvpF, and we assessed the localization of the bacterial effector fragments, with respect to 2xFYVE-GFP, LC3B, and LAMP1 (Figure 3B,C). The deletion of the first 370 amino acids did not affect CvpF localization nor the formation of perinuclear clusters of CvpF-labeled compartments (Figure 3B). Conversely, CvpF₅₀₀₋₆₉₅ failed to localize at cellular membranes and remained diffused in the cytoplasm (Figure 3B). Accordingly, the expression of CvpF₅₀₀₋₆₉₅ also failed to reposition cellular compartments to the perinuclear area (Figure 3B). Deletion of the last 195 amino acids (CvpF₁₋₅₀₀) did not affect membrane targeting of CvpF; however, the localization with LAMP1- and LC3B-positive vesicles was lost, together with the effect on the

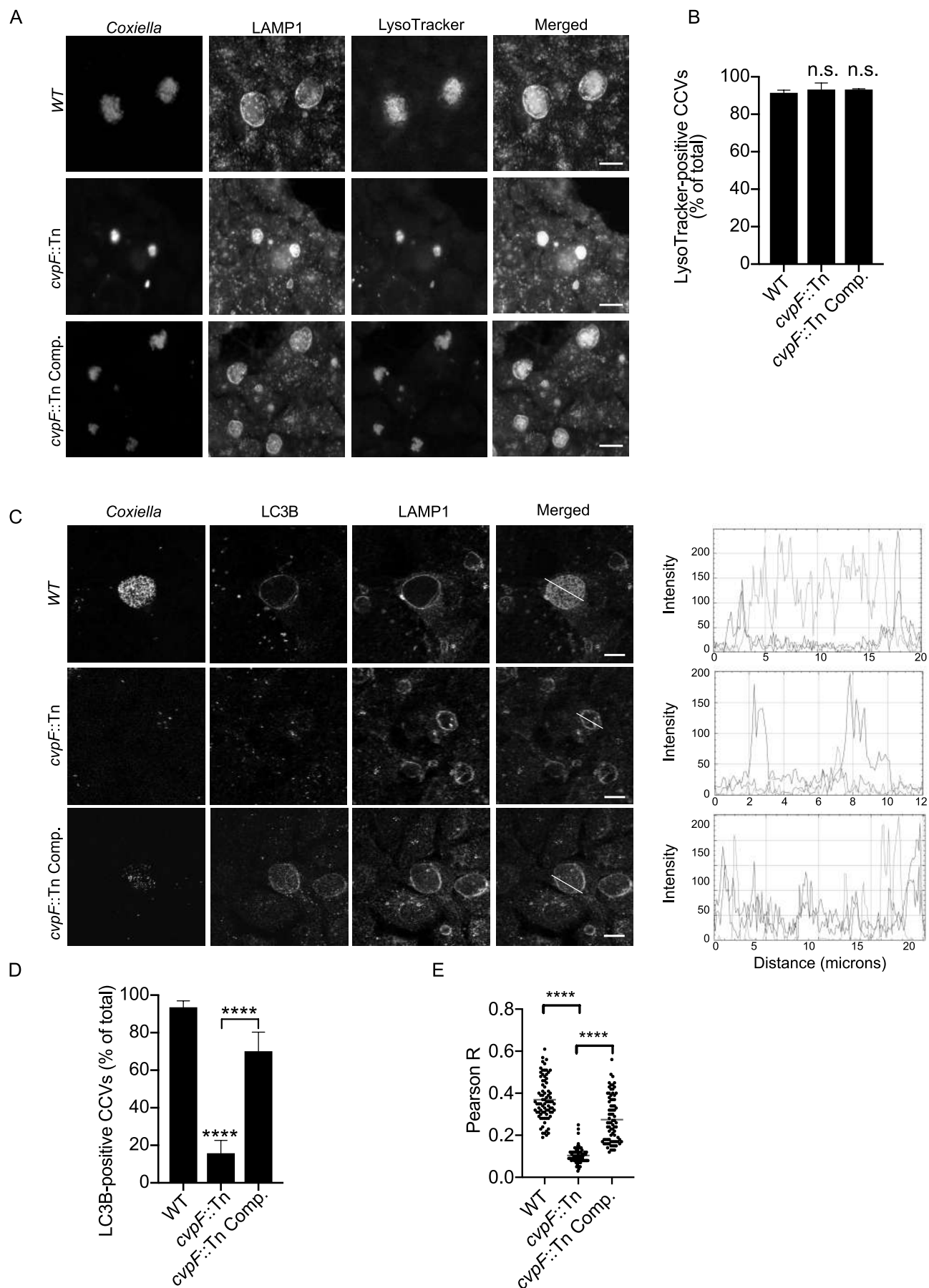
perinuclear positioning of these two markers. Of note, CvpF₁₋₅₀₀ still localized at PtdIns3P-positive structures, which retained the perinuclear localization. Further C-terminal deletions of CvpF resulted in a loss of membrane localization and the cytoplasmic redistribution of membrane markers. This result indicated that the membrane-binding domain (MBD) of CvpF is located between amino acids 370 and 500 and that the C-terminal domain of CvpF (effector domain, ED) may play a role either in the re-routing of early endosomes to autophagosomes or the maturation of autophagosomes to autolysosomes (Figure 3C).

Bioinformatics analysis of the CvpF MBD revealed the presence of one [DERQ]XXX[LI] and 2 YXXΦ endocytic sorting motifs (Figure S4A), involved in the interaction with clathrin adaptor complexes. We, thus, generated di-leucine and tyrosine mutants to validate the functionality of these motifs. The di-leucine LLAA mutant, and the Y440A mutant, failed to affect the membrane targeting and perinuclear localization of CvpF, whereas the Y425A mutation sufficiently displaced CvpF to the cytoplasm with concomitant loss of LAMP1 and LC3B repositioning (Figure S4B and C). Accordingly, Tyr425 is required for CvpF localization at the CCV (Figure S4D). These observations suggest that Tyr425 could be part of a functional endocytic sorting motif. To date, however, we could not detect any interaction or colocalization between CvpF and adaptor complexes or clathrin (data not shown).

CvpF stimulates LC3B-II formation

Several studies have shown that *Coxiella* stimulates the formation of LC3B-II in a T4SS-dependent manner during infection [15,35,36]. To determine whether the secretion of CvpF participates in the formation of LC3B-II, we infected U2OS cells either with the *WT GFP Coxiella* strain (*Tn1832*), the *cvpF*::Tn mutant, or the complemented *cvpF*::Tn mutant (*cvpF*::Tn Comp.). Given the intracellular replication defect of the *cvpF*::Tn mutant *Tn248*, and to rule out the possibility that LC3B-II increase is dependent on the bacterial load, we also infected cells with an excess of *cvpF*::Tn mutant (*cvpF*::Tn x10) (Figure 4A). We observed an increase in LC3B-II levels for cells infected with *WT Coxiella* and the complemented *cvpF*::Tn mutant, in the presence of bafilomycin A₁. We observed no LC3B-II increase for cells infected with the *cvpF*::Tn mutant (Figure 4A). Next, we infected the cells as in Figure 4A and starved for 3 h to determine whether the LC3B-II increase observed with *WT Coxiella* and the complemented *cvpF*::Tn mutant was not due to a blockade of the autophagy flux. We analyzed levels of SQSTM1/p62 (sequestosome 1) by western blot, which revealed that upon starvation, SQSTM1 is degraded for all conditions, indicating that CvpF does not block the starvation-induced autophagy flux but stimulates the formation of LC3B-II (Figure 4B).

The vacuolar localization of CvpF, together with the decreased presence of LC3B on CCVs generated by *cvpF*::Tn mutants prompted us to investigate the role of CvpF in autophagosome dynamics further. We probed the individual role of CvpF on LC3B-II increase in transfected cells. We analyzed the autophagy flux by western blotting on U2OS cells expressing



HA, HA-CvpF, or HA-CvpF^{Y425A} (Figure 4C). When bafilomycin A₁ blocks the autophagy flux, we observed a marked increase in LC3B-II and SQSTM1 in cells expressing CvpF and HA-CvpF^{Y425A} compared to cells expressing HA, with wild type CvpF having the greatest effect on SQSTM1 levels, indicating that CvpF stimulates the autophagy flux and that its membrane localization participates in this process (Figure 4C).

Next, we co-transfected HA-CvpF and HA-CvpF^{Y425A} with the tandem-fluorescent probe TF-LC3. This probe consists of an LC3B linked to GFP and RFP. Since acidic conditions quench GFP fluorescence, this probe labels autophagosomes in green and red, while autolysosomes appear only red. In transfected cells, HA-CvpF localizes to clustered vesicles, only displaying red fluorescence corresponding to autolysosomes (Figure S5A). Conversely, CvpF^{Y425A} displayed a diffuse localization, and transfected cells displayed non-acidified autophagosomes similarly to HA-transfected cells (Figure S5A). Upon addition of bafilomycin A₁, CvpF was still found present on clustered vesicles, but these were GFP- and RFP-positive (Figure S5B). In bafilomycin A₁-treated cells, HA and HA-CvpF^{Y425A}-transfected cells displayed non-acidified autophagosomes similarly to the mock-treated condition (Figure S5B). CvpF-dependent clustering of vesicles rendered the scoring of LC3B-positive puncta impossible. Of note, vesicular swelling and clustering triggered by overexpression of LAMP1-Flag did not affect the TF-LC3 probe signal in the presence or absence of bafilomycin A₁, indicating that CvpF alone can stimulate the formation of autophagosomes and autolysosomes. Furthermore, its membrane localization seems critical to act on this endosomal system.

Finally, to rule out the possibility that CvpF stimulates autophagy by inhibiting MTORC1, we stained U2OS cells transfected with HA, HA-CvpF, or HA-CvpF^{Y425A} for MTOR and we labeled lysosomes with LysoTracker (Figure S6A). The expression of CvpF or CvpF^{Y425A} did not affect the localization of MTOR on lysosomes, indicating that CvpF does not alter MTORC1 activity to stimulate autophagy.

CvpF interacts with the autophagy-related RAB GTPase RAB26

Yeast two-hybrid screening identified the small GTPase RAB26 as a candidate interactor of CvpF. Of note, RAB26 has been previously involved in lysosomal positioning [37], autophagosome maturation [18,19], and vesicle-mediated secretion of adrenergic receptors [38]. We, thus, validated the interaction using a co-immunoprecipitation

approach on U2OS cells co-expressing HA-CvpF and GFP-RAB26 (Figure 5A). The lack of interaction in cells co-expressing HA-CvpF together with GFP-tagged versions of RAB5, RAB7, RAB9, RAB11, or RAB37 (the closest homolog of RAB26 with 54% amino acid identity), indicated that the CvpF-RAB26 interaction is specific (Figure 5A). In agreement with the interactomics analysis, fluorescence microscopy indicated that CvpF and RAB26 localize at the same cellular compartments, and that expression of CvpF increases membrane targeting of RAB26 (Figure 5B). Of note, we still observed interactions in cells co-expressing CvpF^{Y425A} and RAB26, indicating that the membrane targeting of CvpF is not required for the interaction with RAB26 (Fig. S6B). However, ectopically expressed CvpF^{Y425A} does not alter GFP-RAB26 distribution in cells, indicating that the interaction of CvpF with membranes is required to relocalize RAB26 (Figure S6C). Further analysis using the CvpF truncations revealed that the domain 370–695 of CvpF is sufficient to relocalize RAB26 onto vesicles (Figure S7).

To investigate whether CvpF binds preferentially to active or inactive forms of RAB26, we generated GFP-tagged dominant-negative (GFP-RAB26^{T77N}), dominant-positive (GFP-RAB26^{Q123L}) and guanosine-free (GFP-RAB26^{N177I}) versions of RAB26. We co-expressed these constructs in U2OS cells, in combination with HA-CvpF for the co-immunoprecipitation assay or mCherry-CvpF, to investigate the respective intracellular localization of the two proteins. Interactomics analysis indicated that CvpF preferentially binds to inactive RAB26 (Figure 5C), which we confirmed by fluorescence microscopy. Indeed, co-expression of either GFP-RAB26^{T77N} or GFP-RAB26^{N177I} with mCherry-CvpF resulted in the membrane targeting of the small GTPase, conversely, we observed little or no overlapping between mCherry-CvpF and GFP-RAB26^{Q123L} (Figure 5D). Together, these observations suggest that CvpF might act as a guanosine exchange factor (GEF) or GDI displacement factor (GDF), anchoring and/or activating RAB26 on either early endosomal or pre-autophagosomal structures.

CvpF triggers the recruitment of RAB26 to CCVs

CvpF localization at CCVs (Figure 1A) and its interaction with RAB26 (Figure 5A) suggested that the small GTPase might be recruited at CCVs and be involved in vacuole biogenesis. To test whether RAB26 recruitment at CCVs is CvpF-dependent, we infected U2OS cells with *WT Coxiella*, *cvpF::Tn* or *cvpF::Tn Comp.* and transfected with a plasmid

Figure 2. CvpF participates in LC3B recruitment to CCVs but not in their acidification. (A) U2OS cells were infected with either *Coxiella WT* GFP (top panels), *cvpF::Tn* (middle panels) or the complemented *cvpF::Tn* strain (*cvpF::Tn Comp.*, bottom panels) (green) for 6 d, fixed and stained with anti-LAMP1 (pseudo-colored gray) and LysoTracker (red). (B) U2OS cells were infected as in A, and the presence of the LysoTracker probe in CCVs was scored for at least 80 cells. (C) U2OS cells were infected with either *Coxiella WT* GFP (top panels), *cvpF::Tn* (middle panels), or the complemented *cvpF::Tn* strain (*cvpF::Tn Comp.*, bottom panels) for 6 d, fixed and stained with anti-LAMP1 (pseudo-colored cyan) and anti-LC3B (red). The white line in the merged image indicates the position of the profile line used for the analysis of intensity distribution. Fluorescence intensity plotting of GFP (green), LC3B (red), and LAMP1 (blue) signals are shown on the right for each strain. (D) U2OS cells were infected as in C and the presence of LC3B on CCVs was scored for at least 80 cells. Values are mean \pm SD from 3 independent experiments (n.s. = non-significant, **** = $P < 0.0001$, one-way ANOVA, Dunnett's multiple comparison test). Scale bars: 10 μ m. (E) Pearson's correlation coefficient between LC3B and LAMP1 signals in images acquired in C (**** = $P < 0.0001$, one-way ANOVA, Sidak's multiple comparison test).

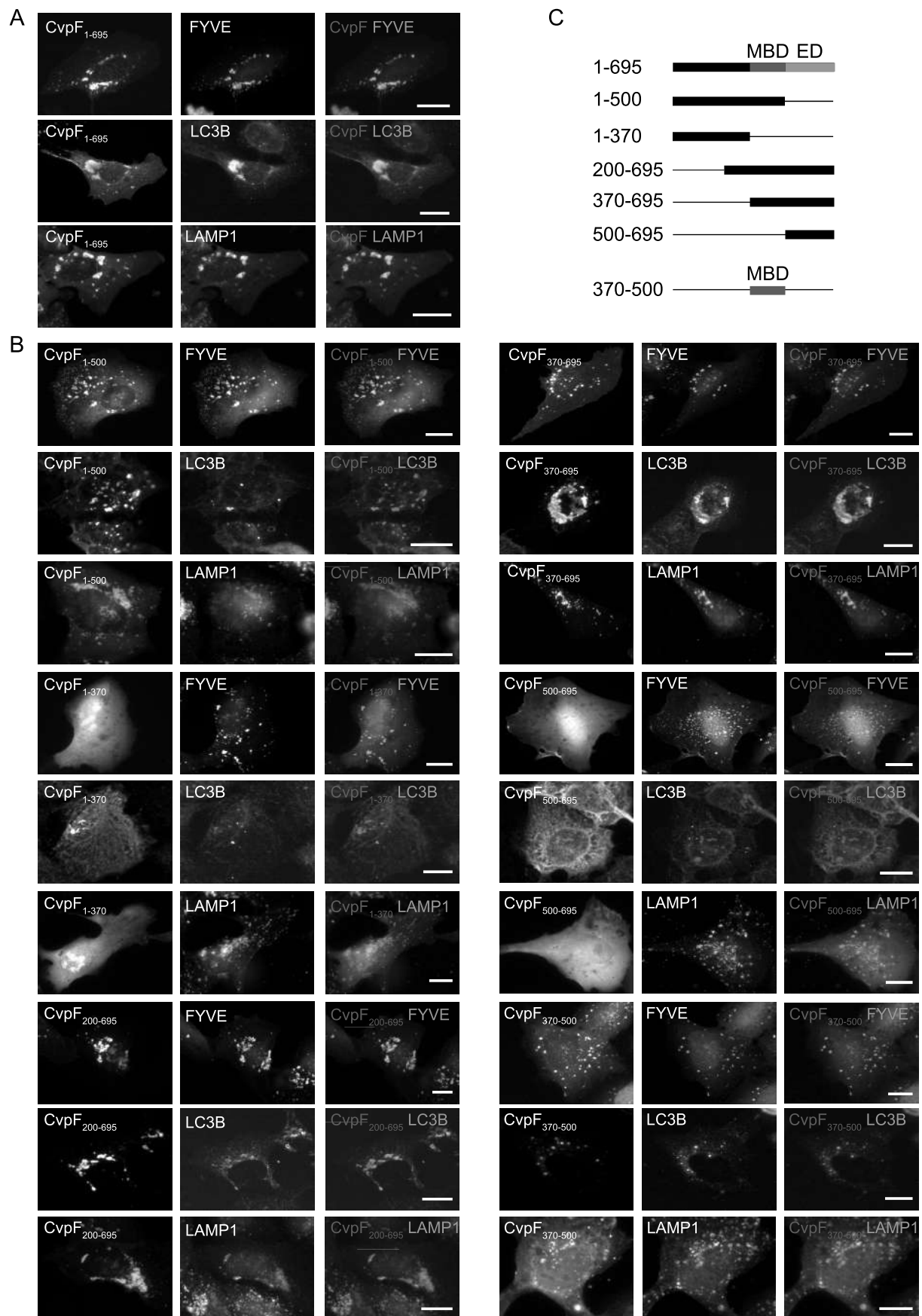


Figure 3. Ectopically expressed CvpF localizes to vesicles with autolysosomal features. (A) U2OS or U2OS GFP-FYVE cells were transfected with pLVX-mCherry-CvpF or pRK5-HA-CvpF (red). Cells were fixed and labeled either with anti-LC3B or anti-LAMP1 antibodies (green). HA-CvpF was labeled with an anti-HA antibody (red). (B) U2OS or U2OS GFP-FYVE cells were transiently transfected with plasmids pLVX-mCherry or pRK5-HA fused to CvpF₁₋₅₀₀, CvpF₁₋₃₇₀, CvpF₂₀₀₋₆₉₅, CvpF₃₇₀₋₆₉₅, CvpF₅₀₀₋₆₉₅, or CvpF₃₇₀₋₅₀₀ (red). Cells were fixed and labeled either with anti-LC3B or anti-LAMP1 antibodies (green). HA-tagged constructs were labeled with anti-HA antibody (red). (C) Schematic representation of CvpF fragments used in A and B. MBD: membrane-binding domain, ED: effector domain. Scale bars: 10 μ m.

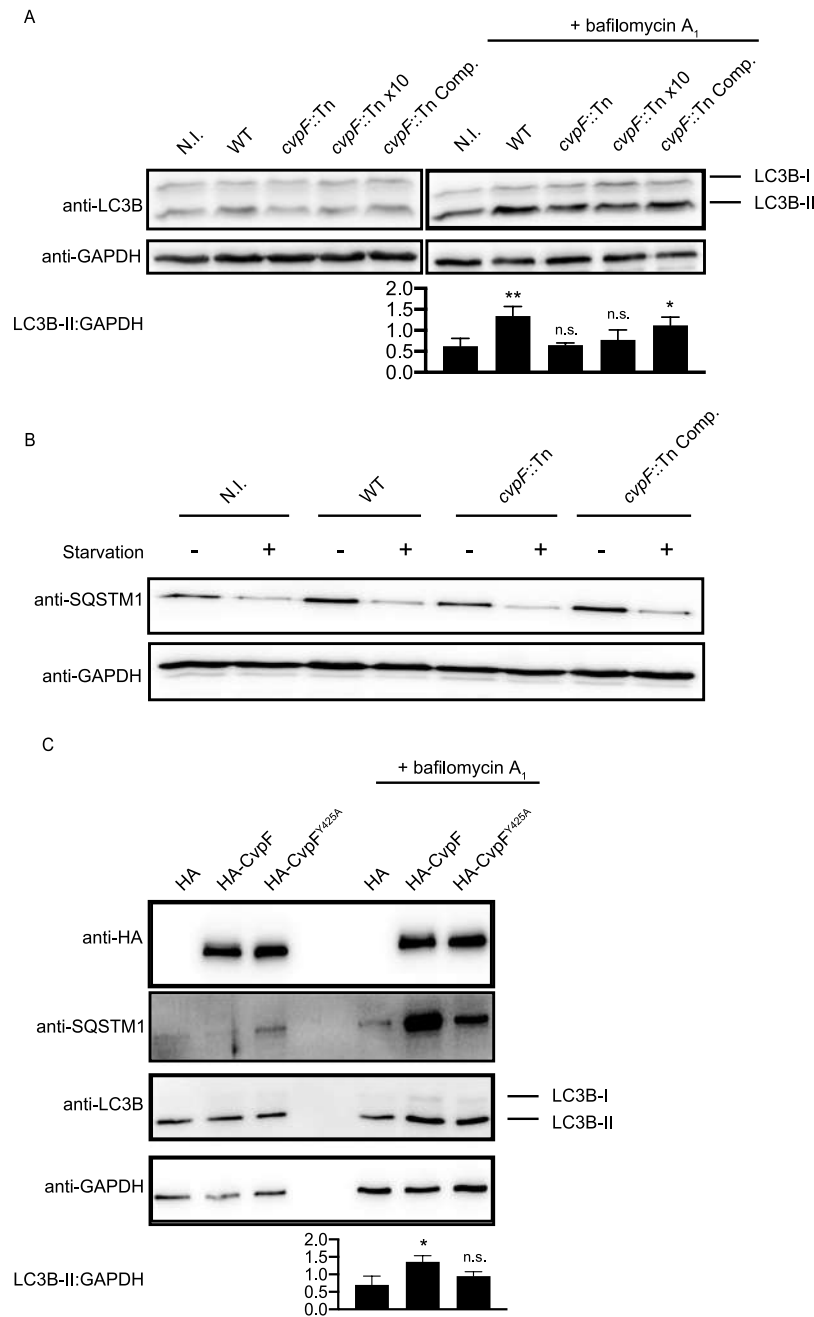


Figure 4. CvpF stimulates the formation of LC3B-II. (A) Immunoblot of lysates from U2OS cells left uninfected (N.I.) or infected with *Coxiella* WT GFP (WT), *cvpF::Tn*, 10 times *cvpF::Tn* (*cvpF::Tn* x10) or the complemented *cvpF::Tn* strain (*cvpF::Tn* Comp.) for 72 h in complete media. Bafilomycin A₁ (25 nM) was added to the media 3 h before lysis. Immunoblots were probed with antibodies against LC3B and GAPDH. The signal ratio of LC3B-II versus GAPDH is indicated for samples treated with bafilomycin A₁. (B) Immunoblot of lysates from U2OS cells left uninfected (N.I.) or infected with *Coxiella* WT GFP (WT), *cvpF::Tn*, or the complemented *cvpF::Tn* strain (*cvpF::Tn* Comp.) for 72 h in complete media. Starvation was triggered by incubation of cells in HBSS for 3 h before lysis. Immunoblots were probed with antibodies against SQSTM1 and GAPDH. (C) Immunoblot of lysates from U2OS cells transfected with pRK5-HA, pRK5-HA-CvpF or pRK5-HA-CvpF^{Y425A} mock-treated or treated with 25 nM bafilomycin A₁ for 1 h. The signal ratio of LC3B-II versus GAPDH is indicated for samples treated with bafilomycin A₁. Values are mean \pm SD from 3 independent experiments (n.s. = non-significant, ** = $P < 0.0021$, * = $P < 0.0033$, one-way ANOVA, Dunnett's multiple comparison test).

expressing GFP-RAB26 (Figure 6A). Indeed, GFP-RAB26 became recruited on $75.4 \pm 2.72\%$ of CCVs generated by WT *Coxiella* and $66.9 \pm 6.12\%$ of CCVs generated by *cvpF::Tn* Comp. strains but only $23.23 \pm 3.78\%$ of CCVs generated by *cvpF::Tn* mutants were positive for RAB26 (Figure 6B). Colocalization analysis between LAMP1 and RAB26 on CCVs generated by WT, *cvpF::Tn* and *cvpF::Tn* complemented

strains (Figure 6C) indicated that CvpF stimulates the presence of RAB26 at the CCV.

Inhibition of RAB26 activity alters LC3B recruitment to CCVs and CCV development

Active RAB26 has been shown to interact with ATG16L1 [18,19], which is key for LC3B anchoring to membranes.

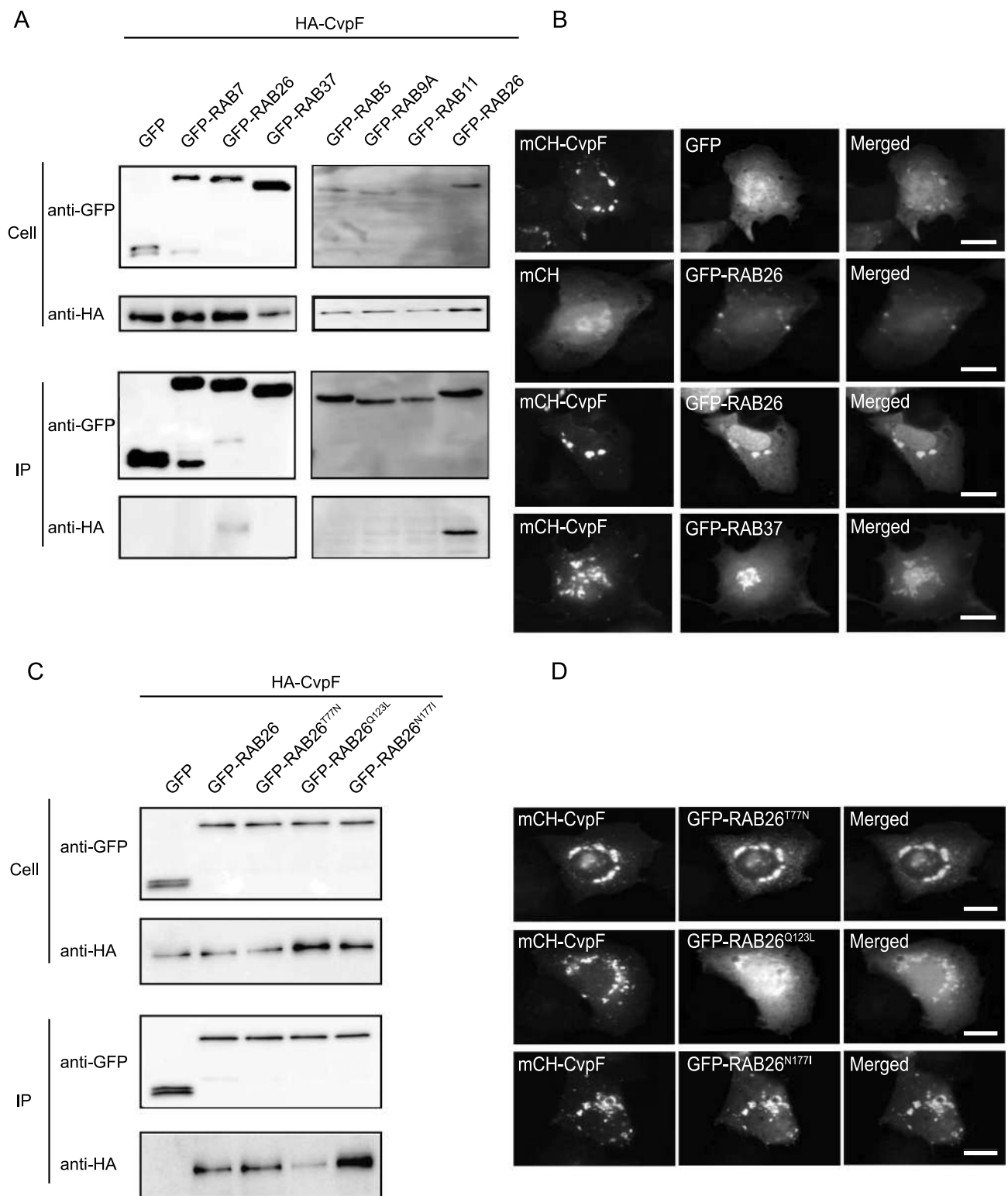
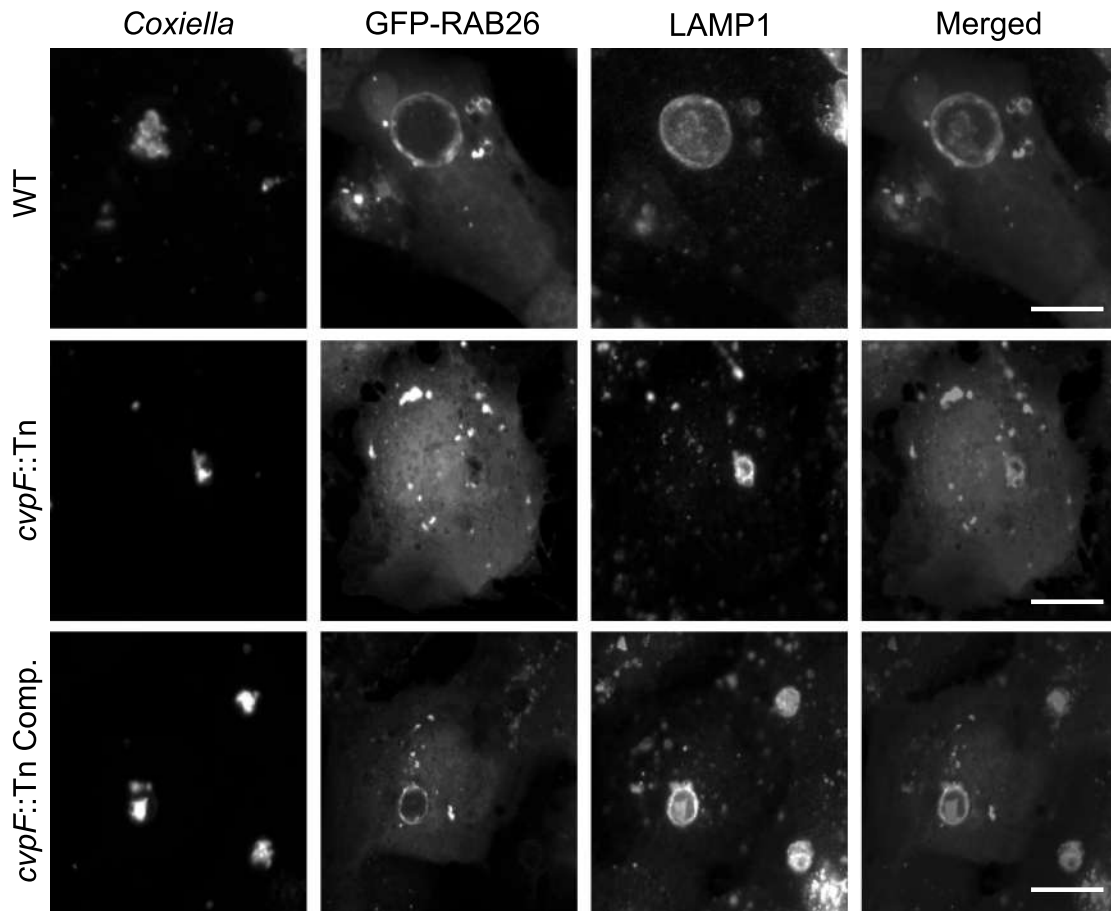


Figure 5. CvpF interacts specifically with RAB26. (A) A co-immunoprecipitation assay using U2OS cells co-transfected with pRK5-HA-CvpF and pLVX-GFP, pLVX-GFP-RAB5, pLVX-GFP-RAB7, pLVX-GFP-RAB9, pLVX-GFP-RAB11, pLVX-GFP-RAB26, pLVX-GFP-RAB37. RAB GTPases and CvpF were detected using anti-GFP and anti-HA antibodies, respectively. (B) U2OS cells were transfected with pLVX-mCherry or pLVX-mCherry-CvpF (red) and pLVX-GFP, pLVX-GFP-RAB26 or pLVX-GFP-RAB37 (green). (C) A co-immunoprecipitation assay using U2OS cells co-transfected with pRK5-HA-CvpF and pLVX-GFP, pLVX-GFP-RAB26, pLVX-GFP-RAB26^{T77N}, pLVX-GFP-RAB26^{Q123L}, pLVX-GFP-RAB26^{N177I}. The RAB GTPases and CvpF were detected using anti-GFP and anti-HA antibodies, respectively. (D) U2OS cells were transiently transfected with pLVX-mCherry-CvpF (red) and pLVX-GFP-RAB26^{T77N}, pLVX-GFP-RAB26^{Q123L} or pLVX-GFP-RAB26^{N177I} (green). Scale bars: 10 μ m.

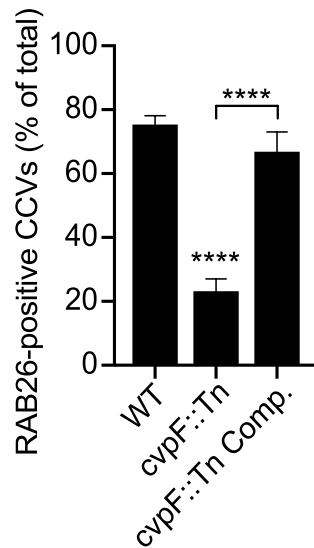
We, thus, determined the requirement of active RAB26 for CCV biogenesis and investigated the presence of the LC3B autophagy marker on CCVs in cells expressing GFP, GFP-RAB26, GFP-RAB26^{T77N}, GFP-RAB26^{Q123L}, and GFP-

RAB26^{N177I}. The LC3B signal on CCVs generated by *Coxiella* NMII became much reduced in cells transfected with the inactive forms of RAB26 (GFP-RAB26^{T77N} and GFP-RAB26^{N177I}) compared to cells expressing either RAB26 wild

A



B



C

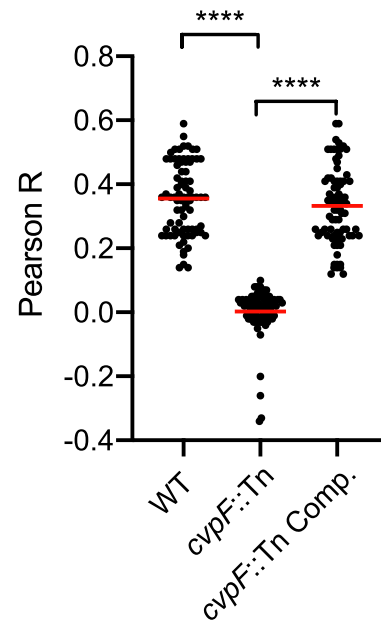


Figure 6. CvpF stimulates the recruitment of RAB26 to CCVs. (A) U2OS cells were infected with either *Coxiella* WT GFP (WT, top panels), *cvpF::Tn* (middle panels), or the complemented *cvpF::Tn* strain (*cvpF::Tn* Comp., bottom panels) and transfected with pLVX-GFP-RAB26 (green) 4 d post-infection. We fixed cells 12 h post-transfection and stained with anti-LAMP1 (red) and anti-*Coxiella* (blue) antibodies. (B) U2OS cells were infected, as in A, and the presence of RAB26 on CCVs was scored for at least 80 cells per condition. Values are mean \pm SD from 3 independent experiments (n.s. = non-significant, **** = $P < 0.0001$, one-way ANOVA, Bonferroni's multiple comparison test). Scale bars: 10 μ m. (C) Pearson's correlation coefficient between RAB26 and LAMP1 signals in images acquired in A (**** = $P < 0.0001$, one-way ANOVA, Sidak's multiple comparison test).

type (GFP-RAB26) or active RAB26 (GFP-RAB26^{Q123L}) (Figure 7A). Of note, loss of LC3B was accompanied by a reduction in the size of CCVs (Figure 7B).

To confirm the importance of RAB26 for CCV development, we inhibited endogenous RAB26 expression using the CRISPR-Cas9 genome editing system. We used three RAB26-targeting guides, and guide 5 was the most efficient in decreasing RAB26 expression (Figure 7C). We infected U2OS cells treated with either non-targeting guides or RAB26-targeting guide 5 with *WT Coxiella*, and we determined the CCV area and Genome Equivalents (GE). We observed a marked decrease in CCV area (Figure 7D), as well as bacterial replication (Figure 7E) in cells deficient in RAB26 expression, indicating that RAB26-mediated autophagy is key to the development of CCVs.

Co-expression of RAB26 with CvpF stimulates the formation of LC3B-II

To determine whether the interaction between CvpF and RAB26 stimulates the recruitment of LC3B onto vesicles, we transfected U2OS cells with HA-CvpF, in combination with either GFP, GFP-RAB26, GFP-RAB26^{T77N}, GFP-RAB26^{Q123L}, or GFP-RAB26^{N177I}. While the co-expression of RAB26 wild type and RAB26^{Q123L} with CvpF led to an increase of the LC3B signal onto vesicles, the concomitant expression of the dominant-negative and guanosine-free forms of RAB26 with CvpF led to a moderate increase of the LC3B signal (Figure 8). These observations indicate that active RAB26 can stimulate the recruitment of LC3B onto vesicles and that CvpF could activate RAB26 to trigger the recruitment of LC3B onto vesicles.

Discussion

Coxiella-containing vacuoles (CCVs) are unique compartments with autolysosomal features. Key to the generation of CCVs is the secretion of bacterial effectors that divert host cell mechanisms to shape an adequate environment for bacterial replication. Here, we identified a new *Coxiella* effector protein important for vacuole biogenesis and replication of the bacterium in epithelial and myeloid cell lines. As recent studies have highlighted, the fact that defective vacuole biogenesis impacts *Coxiella* virulence in insect and mammalian models of infection [12,34,39], we, thus, investigated the *in vivo* relevance of CvpF using the recently developed SCID mouse model. This model is capable of assessing two traits relevant to virulence, such as the ability to cause splenomegaly (a surrogate for inflammation) and the ability to replicate within the spleen (replication defect). The *cvpF*::Tn mutant was severely attenuated for both virulence readouts, and we found even less GE in the spleens than in the *dotA*::Tn mutant. We hypothesize that this is a result of the impaired vacuole synthesis, but it could be due to the ability of the *cvpF*::Tn mutant to secrete proteins, which may alert the innate immune system. In agreement with the *in vitro* observations, the complemented strain was able to partially rescue the ability of *cvpF*::Tn to replicate within the spleen and marginally increased the amount of splenomegaly.

Stimulation of autophagy leads to increased CCV size, suggesting that autophagy provides nutrients and membranes to the expanding CCV [28]. It has been shown that infection of cultured myeloid and epithelial cells with *Coxiella* wild type leads to increased lipidation of LC3B [35,40] and that this lipidation is dependent on the secretion of bacterial effectors [15,36]. Besides lipidation of LC3B, secretion of bacterial effectors via the T4SS is required for the acquisition of autophagosomes and autophagosomal markers to the CCV [12,35,39,40]. Here, we showed how the secreted effector CvpF diverts RAB26-dependent autophagy to favor the generation of *Coxiella*-containing vacuoles *in vitro*, and the virulence of the bacterium *in vivo*. Indeed, most of CCVs generated by the *cvpF*::Tn mutant are devoid of the autophagosomal marker LC3B, suggesting that CvpF could favor CCV biogenesis by manipulating autophagy. Interestingly, SQSTM1 levels are stabilized during *Coxiella* infections [40,41], and SQSTM1 is recruited to CCVs in a T4SS-dependent but LC3B-independent manner. We showed here an increase of steady-state levels of LC3B-II and SQSTM1 in cells infected with *WT Coxiella* and the *cvpF*::Tn complemented strains compared to cells infected with the *cvpF*::Tn mutant or in uninfected cells. This observation is similar to what is observed in HeLa cells infected with the *cig57*::Tn mutant [15]. Indeed, *Coxiella* effector Cig57 has been shown to influence autophagy via clathrin recruitment to CCVs, as *cig57*::Tn mutant CCVs display decreased levels of clathrin and LC3B [15,42]. However, contrary to CvpF, Cig57 alone was not capable of inducing LC3B lipidation [15]. This observation raises the possibility that CvpF and Cig57 could be functionally linked through the recruitment of host cell proteins RAB26 and clathrin, respectively, to CCVs.

Cells expressing HA-CvpF show decreased steady-state levels of SQSTM1 but unaltered levels of steady-state LC3B-II. The increased levels of SQSTM1 and LC3B-II in the presence of bafilomycin A₁ suggest that ectopically expressed CvpF could stimulate the degradation of SQSTM1 and the lipidation of LC3B-II. However, in the context of infection, multiple effectors are translocated that could counteract some of CvpF actions (i.e., SQSTM1 degradation, stimulation of SQSTM1 transcription). The fact that cells infected with the *cvpF*::Tn mutant display less SQSTM1 compared to cells infected with the *WT* strain could be the result of other *Coxiella* effectors. Overall, ectopically expressed CvpF stimulates the formation of LC3B-II but also the degradation of SQSTM1, suggesting that CvpF would be involved in the formation of autolysosomes, but other effectors could stabilize SQSTM1 during infection.

Several studies have shown that mature autophagosomes are recruited to the CCV [39,40] and that another effector protein, CvpB/Cig2, is important to recruit LC3B to CCVs and to maintain the CCV in an autolysosomal stage of maturation [35,39]. This is achieved via the CvpB-dependent stabilization of phosphatidylinositol 3-phosphate at CCVs [12]. Interestingly, in *cvpB/cig2*::Tn mutants, LC3B lipidation, and SQSTM1 levels are increased. This raises the possibility that *Coxiella* effectors may act in sequence to modify the lipid and protein signature of the CCV, and to alter the physiological behavior of the endosomal network. In this case, effectors such as CvpB and Cig57 would initiate CCV maturation

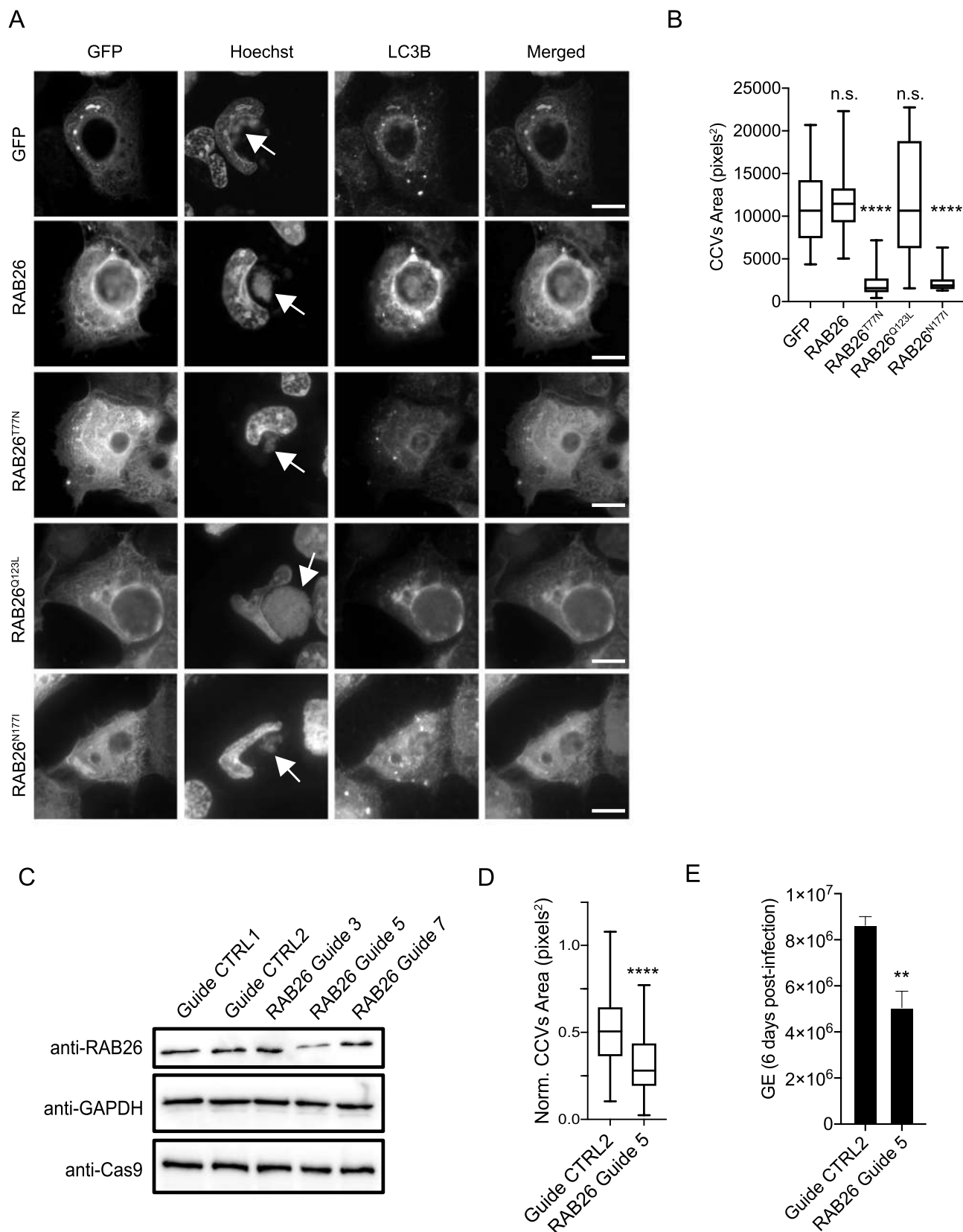


Figure 7. RAB26 activity is essential for CCV biogenesis. (A) U2OS cells infected with *Coxiella* NMII were transfected with pLVX-GFP, pLVX-GFP-RAB26, pLVX-GFP-RAB26^{T77N}, pLVX-GFP-RAB26^{Q123L} or pLVX-GFP-RAB26^{N177I} (green) 2 d post-infection. We fixed cells 24 h post-transfection and stained with anti-LC3B (red) and stained DNA using Hoechst 33,258 (blue). White arrows indicate *Coxiella* colonies. (B) Cells were treated as in A, and the CCV area was measured for at least 100 cells per condition. Values are mean \pm SD from 3 independent experiments (n.s. = non-significant, **** = $P < 0.0001$, one-way ANOVA, Dunnett's multiple comparison test). (C) Immunoblot of lysates from U2OS Cas9 cells expressing non-targeting guides (Guide CTRL1 and guide CTRL2) or RAB26-targeting guides (RAB26 Guide 3, 5 and 7). Immunoblots were probed with antibodies against RAB26, GAPDH and Cas9. (D) U2OS Cas9 cells expressing the non-targeting guide CTRL2 or the RAB26-targeting guide 5 were challenged for 6 d with *Coxiella* WT GFP (WT). The normalized CCV area for each condition was determined using the Cell Profiler software. (E) U2OS cells were challenged as in D and Genome Equivalents (GE) were determined by quantitative PCR. Values are mean \pm SD from 3 independent experiments (n.s. = non-significant, **** = $P < 0.0001$, ** = $P < 0.001$, unpaired t test). Scale bars: 10 μ m.

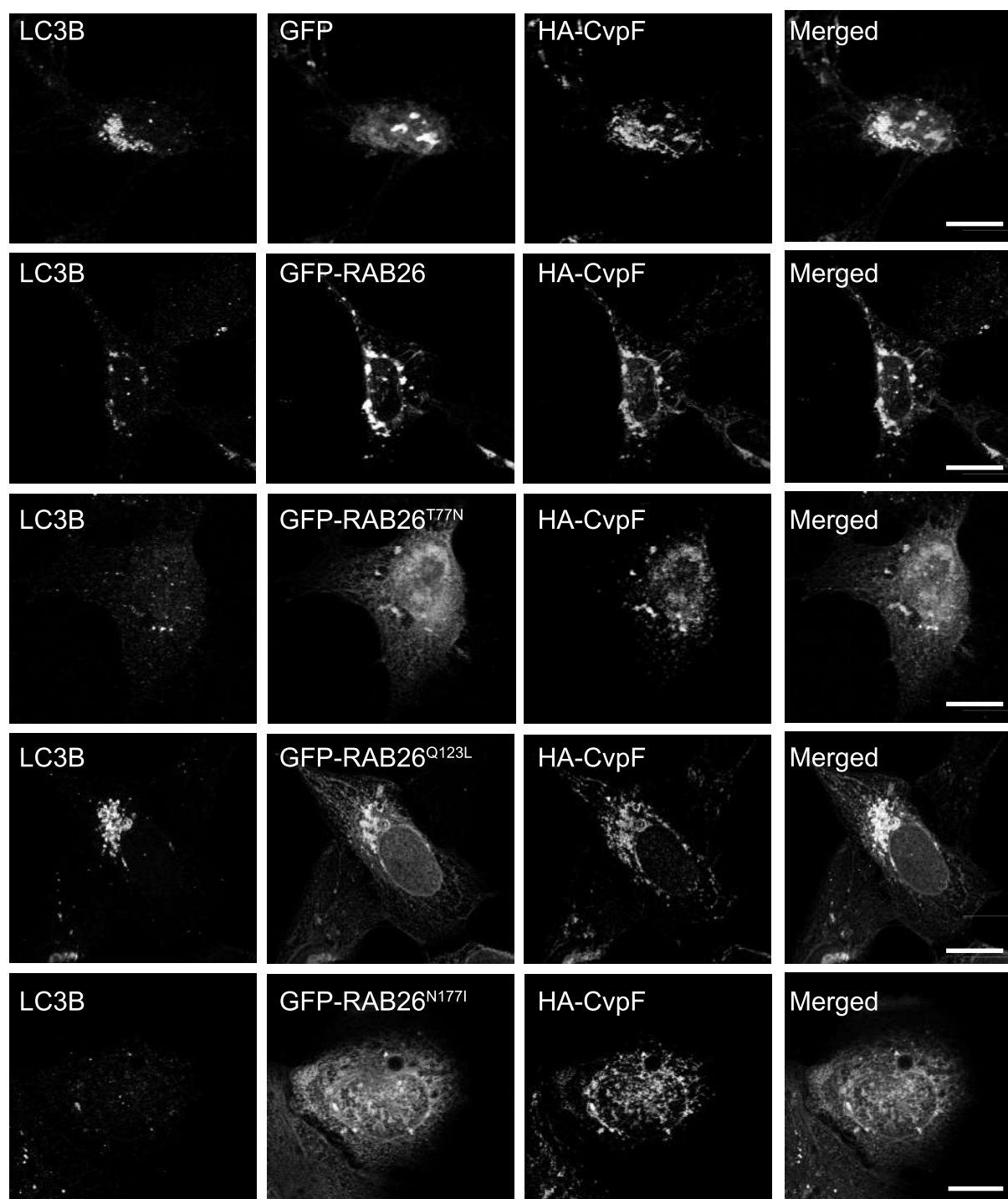


Figure 8. Co-expression of CvpF and RAB26 stimulates the formation of LC3B-positive endosomes. U2OS cells were transfected with pLVX-GFP, pLVX-GFP-RAB26, pLVX-GFP-RAB26^{T77N}, pLVX-GFP-RAB26^{Q123L}, or pLVX-GFP-RAB26^{N177I} (green) and pRK5-HA or pRK5-HA-CvpF. Cells were fixed and stained with anti-LC3B (red) and anti-HA (blue). Scale bars: 10 μ m.

events, and CvpF could then stimulate the autophagy flux to provide membranes and nutrients to expand CCVs and permit optimal *Coxiella* replication.

Ectopic expression showed that CvpF has a strong capacity to remodel the endosomal network by clustering early and late endosomal vesicles, as well as autophagosomal structures in the perinuclear area of transfected cells. Of note, the dynein-dependent movement of autophagosomes

is used in cells to promote their efficient encounter with lysosomes [43], a mechanism that could be used by CvpF to drive transport and maturation of vesicles toward an autolysosomal state. Interestingly, CvpF possesses an internal motif that corresponds to a putative eukaryotic-like endocytic sorting motif that could interact with adaptor complexes (APs), similar to the vacuolar effector CvpA [10]. Indeed, mutation of a critical tyrosine residue in this motif

led to the complete relocalization of CvpF to the cytosol of transfected cells. Furthermore, this tyrosine could also be part of an extended LC3-interacting region (LIR) motif (xx[WFY]xx[LIV]) [44]. However, direct interaction of CvpF with APs and LC3B still needs to be experimentally demonstrated.

Several RAB GTPases have been shown to decorate the CCV (RAB1 [29], RAB7 [26], and RAB24 [28]), all of them being important for its biogenesis. Importantly, CvpF is the first *Coxiella* effector protein to interact with RAB GTPases. Specific interaction of CvpF with RAB26 recruits the small GTPase to CCVs and RAB26-depletion, or inactivation decreases LC3B recruitment at CCVs, which is accompanied by a strong reduction in CCVs size, indicating that active RAB26 and RAB26-dependent stimulation of autophagy favor the development of CCVs. Accordingly, RAB26 participates in the transport of lysosomes to perinuclear regions [37] and autophagy [18,19], as its active form is capable of interacting with ATG16L1 to stimulate LC3B lipidation.

Intracellular pathogens commonly manipulate RAB GTPases for the establishment of their replicative niche [24]. For example, *Legionella pneumophila* secretes at least 7 effectors targeting the RAB GTPase RAB1 for the development of its vacuole [45,46]. CvpF preferentially interacts with the inactive form of RAB26 and stimulates its presence on endosomal vesicles, suggesting that CvpF may act either as a GDI Dissociation Factor (GDF) or Guanine Exchange Factor (GEF) for RAB26. This hypothesis remains to be experimentally validated. Interestingly, CvpF still localizes with inactive RAB26 in the perinuclear area, suggesting that the CvpF-dependent endosomal relocation does not rely on RAB26 activity.

Thus, in this study, we identified the first *Coxiella* effector protein capable of interacting with an autophagy-related RAB GTPase to stimulate the autophagy flux. With a repertoire of more than 130 effector proteins, *Coxiella* could possess additional RAB-modifying proteins that could favor its development in mammalian hosts. CvpF could open the way for the characterization of novel RAB-targeting effectors.

Material and methods

Bacterial strains, cell lines, and growth conditions

Strains used in this study are listed in Supplementary Table 1. *Coxiella burnetii* strains were grown in ACCM-2 [47] supplemented with kanamycin (Sigma-Aldrich, K1377; 340 µg/ml) or chloramphenicol (Sigma-Aldrich, C0378; 3 µg/ml), as appropriate in a humidified atmosphere of 5% CO₂ and 2.5% O₂ at 37°C. U2OS (ATCC, HTB-96), U2OS mCherry, U2OS GFP-FYVE (kindly provided by Dr. Tassula Proikas-Cezanne, Eberhard Karls University Tübingen, Germany), U2OS Cas9, and HEK293T (ATCC, CRL-11268) cell lines were routinely maintained in DMEM with GlutaMAX (GIBCO, 61965-026) containing 10% fetal calf serum (FCS; Sigma-Aldrich, F7524) and THP-1 (ATCC, TIB-202) cells were routinely maintained in RPMI with

GlutaMAX (GIBCO, 61,870-010) containing 10% FCS. All cells were grown in a humidified atmosphere of 5% CO₂ at 37°C. THP-1 cells were differentiated into macrophages by treatment with 25 ng/ml phorbol myristate acetate (PMA, Sigma-Aldrich, P8134) for 24 h. Cell growth medium was supplemented with 600 µg/ml of geneticin G418 (Gibco, 10131035), 10 µg/ml of blasticidin (InvivoGen, ant-bl-05) and/or 1 µg/ml of puromycin (Sigma-Aldrich, P8833) as appropriate.

Antibodies and reagents

Hoechst 33258 (94403), anti-mouse (12-349), and anti-rabbit (-12-348) HRP-conjugated antibodies, rabbit anti-LC3B (L8918), rabbit anti-LAMP1 (L1418), mouse anti-GAPDH (G8795), mouse anti-Flag (F1804) and bafilomycin A₁ (B1793) were purchased from Sigma-Aldrich. Rabbit monoclonal anti-GOLGA2/GM130 (ab52649) and rabbit polyclonal anti-RAB26 (ab187151) were purchased from AbCam. Mouse monoclonal anti-beta-lactamase (MA1-20370) was from ThermoFisher Scientific. Mouse anti-LC3B (ALX-803-080-C100) was from Enzo Life Sciences. Rabbit anti-HA (sc-7392) was from Santa Cruz Biotechnology, and mouse anti-HA (66006-1-Ig) was from Proteintech. Rabbit polyclonal anti-SQSTM1/p62 (GTX100685) was from GeneTex. Phalloidin coupled to Alexa Fluor 647 (A22287) and LysoTracker Red (L7528) were purchased from Life technologies. Rabbit anti-GFP (PABG1-20) was from Chromotek. Rabbit anti-MTOR (2983S) was from Cell Signaling Technology. Mouse anti-Cas9 (844302) was from BioLegend. Rabbit anti-*Coxiella* NMII antibodies [30] were generated by Covalab. Mouse and rabbit IgG conjugated to Alexa Fluor 488 (A-11029 and A-11008), 555 (A-21147 and A-21429), or 647 (A-21239 and A-21245), as well as Prolong Gold antifade mounting reagent (P36930) were purchased from Invitrogen. Paraformaldehyde (15700) was provided by Electron Microscopy Sciences, PA.

Plasmids

Plasmids and primers used in this study are listed in Supplementary Tables 2 and 3, respectively. DNA sequences were amplified by PCR using Phusion polymerase (New England Biolabs, M0530L) and gene-specific primers (Sigma-Aldrich). All site-directed mutagenesis was performed by PCR overlap extension with the mentioned primer pairs.

Complementation in *C. burnetii*

The operon comprising *cbu0625* promoter (600 nt upstream *cbu0625* start codon), *cbu0625*, and *cbu0626/cvpF* was amplified from *Coxiella* RSA439 NMII genomic DNA using Prom-0625-NheI-Fw and CvpF-XhoI-Rv and cloned into pUCR6K-miniTn7-Kan (kindly provided by Prof. Robert Heinzen, Rocky Mountain Laboratories, MT, USA) to generate Mini-Tn7-Kan-prom625-0625-0626. Preparation of electrocompetent *Coxiella cvpF::Tn* was performed as described in [33] and the bacteria were electroporated with an equimolar amount of Mini-Tn7-Kan-prom625-0625-0626 (carrying the transposon prom625-0625-0626) and pTnS2 (carrying the Tn7 transposase, kindly provided by Prof.

Robert Heinzen) plasmids prior to selection and amplification in ACCM-2 containing appropriate antibiotics.

Lentivirus production and stable cell line engineering

To produce lentiviral particles, HEK293T cells were cotransfected with an HIV-1 based genome coding plasmid (pLentiCas9-Blast [Addgene, 47948], pLentiGuide-Puro [Addgene, 68463], or pLVX-mCherry-C1 [Clontech, 632561]), pCMV-dR8.91 (HIV-1 GagPol, kindly provided by Dr. Antoine Gross, IRIM UMR9004 CNRS, Montpellier, France) and pMD.G (VSV-G, kindly provided by Dr. Antoine Gross, IRIM UMR9004 CNRS, Montpellier, France) at a ratio of 1:1:0.5, respectively. The medium was replaced after 6 h, and viral particles were harvested 42 h later, filtered on 0.45- μ m filters (Clearline, 146561), and directly used to transduce U2OS target cells. After 4 to 6 h, the transduction medium was replaced with fresh DMEM containing 10% FCS, and the relevant antibiotics were added 48 h later to select transduced U2OS Cas9 and U2OS mCherry cells.

Reverse transcription and PCR

Coxiella strains *Tn1832* (WT), *Tn248*, or *Tn248* Comp. were grown for 7 d in 5 ml of ACCM-2 containing the appropriate antibiotics. Bacteria were centrifuged for 30 min at 21,000 \times g at 4°C and total RNA was extracted using the RNA easy kit (Qiagen, 74104) or the Direct-zol RNA miniprep kit (Zymo Research, R2051), according to the manufacturer's recommendations. DNA was further removed using DNase I (New England Biolabs, M0303S). 1 μ g of total RNA was used for reverse transcription using the High Capacity cDNA reverse transcription kit (Applied Biosystems, 4368814) or the SuperScript VILO cDNA synthesis kit (Invitrogen, 11754-050) according to the manufacturer's recommendations. Gene-specific primers (Supplementary Table 3) were used to amplify the cDNA corresponding to *ompA* (*cbu1260*), *cbu0625*, and *cbu0626/cvpF*.

Real-time PCR

Lightcycler 480 SYBR Green I master mix (Thermo Fisher Scientific, 4887352001) was used for real-time PCR and readouts was acquired on a Lightcycler480 real-time system (Roche) according to the manufacturer's instructions. The relative levels of transcripts were calculated by the $\Delta\Delta$ CT threshold cycle (CT) method using *dotA* as the internal control. The relative levels of mRNA from the WT samples were adjusted to 1 and served as the basal control value. Each experiment was done in biological triplicate. For the calibration curve construction, aliquots of the plasmid pCR2.1::dotA (Provided by Dr. Robert Heinzen, 8×10^{10} copies/ μ l) in dilutions ranging from 8×10^2 to 8×10^9 copy numbers were applied. Three replicative runs of a *dotA* real-time PCR for all samples were performed. For the standard curves, the threshold cycle (Cq) values were calculated using the Lightcycler480 Software (Roche).

Immunofluorescence staining

Cells were either fixed in 3% paraformaldehyde in PBS (ThermoFisher Scientific, 14190-094) at room temperature for 30 min, or in methanol/acetone (1:1) at -20°C for 5 min. Samples were rinsed in PBS and incubated in BSS (0.5% BSA (Sigma-Aldrich, A2058), 50 mM NH₄Cl in PBS pH 7.4) or FBS (5% fetal bovine serum [Sigma-Aldrich, F7524] in PBS pH 7.4) blocking solutions. Primary and secondary antibodies were diluted in the respective blocking solutions and used for immunofluorescence staining.

Co-immunoprecipitation

U2OS cells were transfected with equimolar amounts of plasmids expressing GFP- and HA-tagged constructs. After 24 h, cells were trypsinized, washed twice in PBS and incubated in the co-IP buffer (20 mM Tris-HCl pH 7.6, 200 mM NaCl, 0.5 mM EDTA, 1% IGEPAL CA-630 [Sigma-Aldrich, I8896], Complete protease inhibitor [Roche, 11836170001]) on ice for 30 min. Following a 10-min spin at 21,000 \times g at 4°C, cell lysates were incubated with magnetic GFP-trap beads (Chromotek, gtma-20) for 1 h at 4°C on a roller. Beads were washed thrice with co-IP buffer, and proteins were collected in Laemmli buffer.

Beta-lactamase translocation assay

For *C. burnetii* effector translocation assays, cells were cultured in black, clear-bottomed, 96-well plates (Greiner Bio-One, 655,090), and infected with the appropriate *C. burnetii* strain (MOI of 100) for 24, 48, and 72 h. *C. burnetii* expressing β -lactamase alone was used as a negative control; *C. burnetii* expressing β -Lactamase-tagged CvpB was used as a positive control. Cell monolayers were loaded with the fluorescent substrate CCF4/AM (LiveBLazer-FRET B/G loading kit; Invitrogen, K1095) in a solution containing 15 mM probenecid (Sigma-Aldrich, P36400). Cells were incubated in the dark for 1 h at room temperature and imaged using an EVOS inverted fluorescence microscope (ThermoFisher Scientific, UK). Images were acquired using a DAPI and GFP filter cubes. The image analysis software CellProfiler (Broad Institute, MA) was used to segment and identify all cells in the sample (GFP) and positive cells (DAPI) and to calculate the intensity of fluorescence in each channel. The percentage of positive cells versus the total number of cells was then calculated and used to evaluate effector translocation.

Microscopy and image analysis

Samples were imaged with a Zeiss Axio Imager Z1 epifluorescence microscope (Carl Zeiss, Germany) connected to a CoolSNAP HQ² CCD camera (Teledyne Photometrics, Tucson, AZ). Images were acquired with 40x oil immersion objectives and processed with Metamorph (Molecular Devices, San Jose, CA). High throughput image acquisition was performed on an epifluorescence automated microscope (Cellomics, ThermoFisher Scientific, Pittsburgh, PA) equipped with a 20X objective. Image analysis was performed using the CellProfiler 3.0 software, as previously

described (Martinez *et al.*, 2015). Briefly, Hoechst 33258 (Sigma-Aldrich, 94403) staining, cytoplasmic mCherry fluorescence produced by U2OS mCherry cells and LAMP1 labeling were used to identify nucleus, cytoplasm, and lysosomal/late endosomal compartments, respectively. The GFP signal was used to identify *C. burnetii* colonies, and CCVs were segmented based on the LAMP1 antibody labeling and GFP fluorescence, respectively. After sorting non-infected and infected cells, a morphometrical analysis was carried out over a population of at least 200 objects (CCVs and/or *C. burnetii* colonies) per condition. Confocal microscopy was performed using a TCS SP8 HyVolution microscope (Leica, Germany) connected to a DFC9000 sCMOS camera or an SP5-SMD microscope (Leica, Germany). Images were acquired with 63x oil immersion objectives and processed with LAS-AF (Leica, Germany). Fluorescence was measured using Fiji analysis software (version 2.0.0) and the Multicolor line profile plot macro (University of Leicester). LC3B and RAB26 recruitment at CCVs were scored as follow: The mean \pm confidence interval (CI) Pearson's correlation coefficient between LAMP1 and the cellular marker of interest (LC3B or RAB26) was calculated using Icy analysis software from triplicate experiments representing a total of at least 80 CCVs per condition (WT, *cvpF::Tn*, *cvpF::Tn* Comp.). The mean + positive CI calculated from cells infected with the *cvpF::Tn* mutant was then taken as a threshold to calculate the percentage of CCVs positive for either marker.

Animal experiments

SCID (C.B-17/LcrHsd-*Prkdc*^{scid}) mice were handled and infected, as previously described [34]. All animal procedures were done in compliance with Texas A&M University IACUC (AUP#2016-0370). DNA was purified from infected organs, and primers and probe for IS1111 were used to determine Genome Equivalents (GE) using TaqMan real-time PCR.

Statistical analysis

Statistical analyses of data were performed using Prism software (GraphPad, San Diego, CA). For experiments requiring statistical analysis, an adapted statistical test was performed, as described in the corresponding figure legends.

Acknowledgments

This work was supported by the French National Research Agency (ANR; ANR-14-CE14-0012-01, project AttaQ) and by the ERA-NET Infect-ERA (ANR-13-IFEC-0003, project EUGENPATH). FAS is the recipient of a fellowship from the Agence Nationale Bourses Gabon (ANBG). We acknowledge the imaging facility MRI, member of the national infrastructure France-BioImaging supported by the French National Research Agency (ANR-10-INBS-04, «Investments for the future»). We thank Dr. Martine Biard-Piechaczyk, Dr. Lucile Espert, and Dr. Fabien Blanchet (IRIM CNRS UMR9004 Montpellier, France) for scientific advice and sharing material.

Disclosure statement

No potential conflict of interest was reported by the authors.

Funding

This work was supported by the Agence Nationale de la Recherche [ANR-13-IFEC-0003]; Agence Nationale de la Recherche [ANR-14-CE14-0012-01]; Agence Nationale de la Recherche [ANR-10-INBS-04].

ORCID

Erin Van Schaik  <http://orcid.org/0000-0003-2536-0857>
 Mélanie Burette  <http://orcid.org/0000-0001-5751-2208>
 Caroline Goujon  <http://orcid.org/0000-0001-8571-1108>
 Matteo Bonazzi  <http://orcid.org/0000-0001-5499-8759>

References

- [1] Quaglio GL, Demotes-Mainard J, Loddenkemper R. Emerging and re-emerging infectious diseases: a continuous challenge for Europe. *Eur Respir J*. 2012;40:1312–1314.
- [2] Waag DM, Fritz DL. Q fever. *Biodefense Res Methodol Anim Model*. Second Ed. 2012; 12:179–196.
- [3] Moffatt JH, Newton P, Newton HJ. *Coxiella burnetii*: turning hostility into a home. *Cell Microbiol*. 2015;17:621–631.
- [4] Lührmann A, Newton HJ, Bonazzi M. Beginning to understand the role of the type IV secretion system effector proteins in *Coxiella burnetii* pathogenesis. *Curr Top Microbiol Immunol*. 2017;413:243–268.
- [5] Voth DE, Heinzen RA. Lounging in a lysosome: the intracellular lifestyle of *Coxiella burnetii*. *Cell Microbiol*. 2007;9:829–840.
- [6] Carey KL, Newton HJ, Lührmann A, et al. The *Coxiella burnetii* Dot/Icm system delivers a unique repertoire of type IV effectors into host cells and is required for intracellular replication. *PLoS Pathog*. 2011;7(5):e1002056.
- [7] Newton HJ, McDonough JA, Roy CR. Effector protein translocation by the *Coxiella burnetii* Dot/Icm type iv secretion system requires endocytic maturation of the pathogen-occupied vacuole. *PLoS One*. 2013;8:e54566.
- [8] Larson CL, Martinez E, Beare PA, et al. Right on Q: genetics begin to unravel *Coxiella burnetii* host cell interactions. *Future Microbiol*. 2016;11:919–939.
- [9] Lührmann A, Nogueira CV, Carey KL, et al. Inhibition of pathogen-induced apoptosis by a *Coxiella burnetii* type IV effector protein. *Proc Natl Acad Sci U S A*. 2010;107:18997–19001.
- [10] Larson CL, Beare PA, Howe D, et al. *Coxiella burnetii* effector protein subverts clathrin mediated vesicular trafficking for pathogen vacuole biogenesis. *Proc Natl Acad Sci U S A*. 2013;110: E4770–9.
- [11] Larson CL, Beare PA, Voth DE, et al. *Coxiella burnetii* effector proteins that localize to the parasitophorous vacuole membrane promote intracellular replication. *Infect Immun*. 2015;83:661–670.
- [12] Martinez E, Allombert J, Cantet F, et al. *Coxiella burnetii* effector CvpB modulates phosphoinositide metabolism for optimal vacuole development. *Proc Natl Acad Sci U S A*. 2016;113:E3260–9.
- [13] Voth DE, Beare PA, Howe D, et al. The *Coxiella burnetii* cryptic plasmid is enriched in genes encoding type IV secretion system substrates. *J Bacteriol*. 2011;193:1493–1503.
- [14] Maturana P, Graham JG, Sharma UM, et al. Refining the plasmid-encoded type IV secretion system substrate repertoire of *Coxiella burnetii*. *J Bacteriol*. 2013;195:3269–3276.
- [15] Latomanski EA, Newton HJ. Interaction between autophagic vesicles and the *Coxiella*-containing vacuole requires CLTC (clathrin heavy chain). *Autophagy*. 2018;14:1710–1725.
- [16] Crabill E, Schofield WB, Newton HJ, et al. Dot/Icm-translocated proteins important for biogenesis of the *Coxiella burnetii*-containing vacuole identified by screening of an effector mutant sublibrary. *Infect Immun*. 2018;86:e00758–17.
- [17] Ao X, Zou L, Wu Y. Regulation of autophagy by the Rab GTPase network. *Cell Death Differ*. 2014;21:348–358.
- [18] Binotti B, Pavlos NJ, Riedel D, et al. The GTPase Rab26 links synaptic vesicles to the autophagy pathway. *Elife*. 2014;2015:1–23.

- [19] Dong W, He B, Qian H, et al. RAB26-dependent autophagy protects adherens junctional integrity in acute lung injury. *Autophagy*. 2018;14:1677–1692.
- [20] Song Y, Shang D, Cheng H, et al. The small GTPase RAB37 functions as an organizer for autophagosome biogenesis. *Autophagy*. 2018;14:727–729.
- [21] Sheng Y, Song Y, Li Z, et al. RAB37 interacts directly with ATG5 and promotes autophagosome formation via regulating ATG5-12-16 complex assembly. *Cell Death Differ*. 2018;25:918–934.
- [22] Spanò S, Galán JE. Taking control: hijacking of RAB GTPases by intracellular bacterial pathogens. *Small GTPases*. 2018;9:182–191.
- [23] Stein MP, Müller MP, Wandering-Ness A. Bacterial pathogens commandeer RAB GTPases to establish intracellular niches. *Traffic*. 2012;13:1565–1588.
- [24] Martinez E, Siadous FA, Bonazzi M. Tiny architects: biogenesis of intracellular replicative niches by bacterial pathogens. *FEMS Microbiol Rev*. 2018;42:425–447.
- [25] McDonough JAJ, Newton HJHH, Klum S, et al. Host pathways important for *Coxiella burnetii* infection revealed by genome-wide RNA interference screening. *MBio*. 2013;4:e00606–12.
- [26] Berón W, Gutierrez MG, Rabinovitch M, et al. *Coxiella burnetii* localizes in a Rab7-labeled compartment with autophagic characteristics. *Infect Immun*. 2002;70:5816–5821.
- [27] Romano PS, Gutierrez MG, Berón W, et al. The autophagic pathway is actively modulated by phase II *Coxiella burnetii* to efficiently replicate in the host cell. *Cell Microbiol*. 2007;9:891–909.
- [28] Gutierrez MG, Vázquez CL, Munafó DB, et al. Autophagy induction favours the generation and maturation of the *Coxiella*-replicative vacuoles. *Cell Microbiol*. 2005;7:981–993.
- [29] Campoy EM, Martín Zoppino FC, Colombo MI. The early secretory pathway contributes to the growth of the *Coxiella*-replicative niche. *Infect Immun*. 2011;79:402–413.
- [30] Martinez E, Cantet F, Fava L, et al. Identification of OmpA, a *Coxiella burnetii* protein involved in host cell invasion, by multi-phenotypic high-content screening. *PLoS Pathog*. 2014;10:e1004013.
- [31] Zusman T, Aloni G, Halperin E, et al. The response regulator PmrA is a major regulator of the icm/dot type IV secretion system in *Legionella pneumophila* and *Coxiella burnetii*. *Mol Microbiol*. 2007;63:1508–1523.
- [32] Lifshitz Z, Burstein D, Peeri M, et al. Computational modeling and experimental validation of the *Legionella* and *Coxiella* virulence-related type-IVB secretion signal. *Proc Natl Acad Sci U S A*. 2013;110:E707–15.
- [33] Martinez E, Cantet F, Bonazzi M. Generation and multi-phenotypic high-content screening of *Coxiella burnetii* transposon mutants. *J Vis Exp*. 2015;2015:4–6.
- [34] van Schaik EJ, Case ED, Martinez E, et al. The SCID mouse model for identifying virulence determinants in *Coxiella burnetii*. *Front Cell Infect Microbiol*. 2017;7:25.
- [35] Newton HJ, Kohler LJ, McDonough JA, et al. A screen of *Coxiella burnetii* mutants reveals important roles for Dot/Icm effectors and host autophagy in vacuole biogenesis. *PLoS Pathog*. 2014;10(7):e1004286.
- [36] Larson CL, Sandoz KM, Cockrell DC, et al. Noncanonical Inhibition of mTORC1 by *Coxiella burnetii* promotes replication within a phagolysosome-like vacuole. *MBio*. 2019;10(1):e02816–18.
- [37] Jin RU, Mills JC. RAB26 coordinates lysosome traffic and mitochondrial localization. *J Cell Sci*. 2014;127:1018–1032.
- [38] Lambert NA, Lan T-H, Li C, et al. Rab26 modulates the cell surface transport of α_2 -adrenergic receptors from the golgi. *J Biol Chem*. 2012;287:42784–42794.
- [39] Kohler LJ, Reed SR, Sarraf SA, et al. Effector protein *cig2* decreases host tolerance of infection by directing constitutive fusion of autophagosomes with the *Coxiella*-containing vacuole. *MBio*. 2016;7:1–14.
- [40] Winchell CG, Graham JG, Kurten RC, et al. *Coxiella burnetii* type IV secretion-dependent recruitment of macrophage autophagosomes. *Infect Immun*. 2014;82:2229–2238.
- [41] Winchell CG, Dragan AL, Brann KR, et al. *Coxiella burnetii* subverts p62/sequestosome 1 and activates Nrf2 signaling in human macrophages. *Infect Immun*. 2018;86:e00608–17.
- [42] Latomanski EA, Newton P, Khoo CA, et al. The effector Cig57 hijacks FCHO-mediated vesicular trafficking to facilitate intracellular replication of *Coxiella burnetii*. *PLoS Pathog*. 2016;12(12):e1006101.
- [43] Kimura S, Noda T, Yoshimori T. Dynein-dependent movement of autophagosomes mediates efficient encounters with lysosomes. *Cell Struct Funct*. 2008;33:109–122.
- [44] Kalvari I, Tsompanis S, Mulakkal NC, et al. iLIR: a web resource for prediction of Atg8-family interacting proteins. *Autophagy*. 2014;10:913–925.
- [45] Goody RS, Itzen A. Modulation of small Gtpases by *Legionella*. *Curr Top Microbiol Immunol*. 2013;376:117–133.
- [46] Wang Z, McCloskey A, Cheng S, et al. Regulation of the small GTPase Rab1 function by a bacterial glucosyltransferase. *Cell Discov*. 2018;4:53.
- [47] Omsland A, Beare PA, Hill J, et al. Isolation from animal tissue and genetic transformation of *Coxiella burnetii* are facilitated by an improved axenic growth medium. *Appl Environ Microbiol*. 2011;77:3720–3725.

The secreted protein kinase CstK from *Coxiella burnetii* influences vacuole development and interacts with the GTPase-activating host protein TBC1D5

Received for publication, July 9, 2019, and in revised form, April 14, 2020 Published, Papers in Press, April 17, 2020, DOI 10.1074/jbc.RA119.010112

Eric Martinez^{†1}, Sylvaine Huc-Brandt^{§1}, Solène Brelle[§], Julie Allombert[†],  Franck Cantet[†], Laila Gannoun-Zaki[§],  Mélanie Burette[†],  Marianne Martin[§],  François Letourneur[§], Matteo Bonazzi^{†2}, and Virginie Molle^{§3}

From the [†]Institut de Recherche en Infectiologie de Montpellier, Université de Montpellier, CNRS, UMR 9004, Montpellier, France and [§]Laboratory of Pathogen Host Interactions, Université de Montpellier, CNRS, UMR 5235, Montpellier, France

Edited by Ursula Jakob

The intracellular bacterial pathogen *Coxiella burnetii* is the etiological agent of the emerging zoonosis Q fever. Crucial to its pathogenesis is type 4b secretion system-mediated secretion of bacterial effectors into host cells that subvert host cell membrane trafficking, leading to the biogenesis of a parasitophorous vacuole for intracellular replication. The characterization of prokaryotic serine/threonine protein kinases in bacterial pathogens is emerging as an important strategy to better understand host–pathogen interactions. In this study, we investigated CstK (for *Coxiella* Ser/Thr kinase), a protein kinase identified in *C. burnetii* by *in silico* analysis. We demonstrate that this putative protein kinase undergoes autophosphorylation on Thr and Tyr residues and phosphorylates a classical eukaryotic protein kinase substrate *in vitro*. This dual Thr–Tyr kinase activity is also observed for a eukaryotic dual-specificity Tyr phosphorylation-regulated kinase class. We found that CstK is translocated during infections and localizes to *Coxiella*-containing vacuoles (CCVs). Moreover, a CstK-overexpressing *C. burnetii* strain displayed a severe CCV development phenotype, suggesting that CstK fine-tunes CCV biogenesis during the infection. Protein–protein interaction experiments identified the Rab7 GTPase-activating protein TBC1D5 as a candidate CstK-specific target, suggesting a role for this host GTPase-activating protein in *Coxiella* infections. Indeed, CstK co-localized with TBC1D5 in non-infected cells, and TBC1D5 was recruited to CCVs in infected cells. Accordingly, TBC1D5 depletion from infected cells significantly affected CCV development. Our results indicate that CstK functions as a bacterial effector protein that interacts with the host protein TBC1D5 during vacuole biogenesis and intracellular replication.

Signal transduction is an essential and universal function that allows all cells, from prokaryotes to eukaryotes, to translate environmental signals to adaptive changes. By this mechanism, extracellular inputs propagate through complex signaling networks whose activity is often regulated by reversible protein phosphorylation. Signaling mediated by serine/threonine/tyrosine protein phosphorylation has been extensively studied in eukaryotes; however, its relevance in prokaryotes has only begun to be appreciated. The recent discovery that bacteria also use Ser/Thr/Tyr kinase-based signaling pathways has opened new perspectives to study environmental adaptation, especially in the case of bacterial pathogens, with respect to host infection (1). Thus, advances in genetic strategies and genome sequencing have revealed the existence of “eukaryotic-like” serine/threonine protein kinases (STPKs)⁴ and phosphatases in a number of prokaryotic organisms (2), including pathogens such as *Streptococcus* spp. (3–6), *Mycobacteria* (7–12), *Yersinia* spp. (13, 14), *Listeria monocytogenes* (15, 16), *Pseudomonas aeruginosa* (17), *Enterococcus faecalis* (18), or *Staphylococcus aureus* (19, 20). Consequently, the study of STPKs in human bacterial pathogens is emerging as an important strategy to better understand host–pathogen interactions and develop new, targeted antimicrobial therapies. However, if on one hand it is clear that STPKs and phosphatases regulate important functions in bacterial pathogens, their signal transduction mechanism remains ill-defined and restricted to a limited number of microbes.

Importantly, STPKs expressed by pathogenic bacteria can either act as key regulators of important microbial processes or be translocated by secretion systems to interact with host substrates, thereby subverting essential host functions including the immune response, cell shape, and integrity (21). Phosphorylation of host substrates has been demonstrated for some bacterial STPKs, whereas others seem to require their kinase activity, but their phosphorylated substrates remain to be identified (21). Therefore, biochemical mechanisms of these pathogen-directed targeted perturbations in the host cell–signaling network are being actively investigated, and STPKs are proving to

This work was supported by grants from the ATIP/AVENIR Program (to V. M. and M. Bonazzi), the Region Occitanie (to S. B. and V. M.), Marie Curie Action Career Integration Grant 293731 (to E. M. and M. Bonazzi), and Agence Nationale de la Recherche Grant ANR-14-CE14-0012-01 through project AttaQ (to M. Bonazzi). The authors declare that they have no conflicts of interest with the contents of this article.

This article contains Table S1 and Figs. S1 and S2.

¹ These authors contributed equally to this work.

² To whom correspondence may be addressed. Tel.: 3-4-34-35-94-59; E-mail: matteo.bonazzi@irim.cnrs.fr.

³ To whom correspondence may be addressed. Tel.: 33-4-67-14-47-25; E-mail: virginie.molle@umontpellier.fr.

⁴ The abbreviations used are: STPK, serine/threonine protein kinase; IPTG, isopropyl β-D-thiogalactopyranoside; HA, hemagglutinin; CCV, *Coxiella*-containing vacuole; BLAM, β-lactamase; GST, glutathione S-transferase; MBP, myelin basic protein; qRT-PCR, quantitative RT-PCR; ROI, region of interest; ANOVA, analysis of variance.

This is an Open Access article under the CC BY license.

 ASBMB

CstK affects *C. burnetii* vacuole biogenesis

be molecular switches that play key roles in host–pathogen interactions (21).

Among emerging human pathogens, *Coxiella burnetii* is a highly infectious bacterium, responsible for the zoonosis Q fever, a debilitating flu-like disease leading to large outbreaks with a severe health and economic burden (22–24). The efficiency of infections by *C. burnetii* is likely associated with the remarkable capacity of this bacterium to adapt to environmental as well as intracellular stress. Indeed, outside the host, *C. burnetii* generates pseudospores that facilitate its airborne dissemination. *C. burnetii* has developed a unique adaptation to the host, being the only bacterium that thrives in an acidic compartment containing active lysosomal enzymes. Upon host cell invasion, bacteria reside within membrane-bound compartments that passively traffic through the endocytic maturation pathway, progressively acquiring early and late endocytic markers such as Rab5 and Rab7, respectively (25). Fusion of *Coxiella*-containing vacuoles (CCVs) with late endosomes and lysosomes is accompanied by the acidification of the endosomal environment, which is required to activate the translocation of bacterial effector proteins by a Dot/Icm type 4b secretion system (26). Some of these effectors modulate important signaling pathways of infected cells, including apoptosis and inflammasome activation (27–29), whereas others are essential for the development of the intracellular replicative niche. Among these, CvpB and CvpF have been recently implicated in the manipulation of autophagy for optimal vacuole development (30–33). *C. burnetii* genome analysis revealed a close homology to the facultative intracellular pathogen *Legionella pneumophila*, in particular at the level of Dot/Icm core genes (34). *In silico* analysis identified over 100 candidate effector proteins encoded in the *C. burnetii* genome, some of which have been validated for secretion using either *C. burnetii* or *L. pneumophila* as a surrogate model (26, 35, 36).

In this study, we investigated the candidate effector CBU_0175, which encodes a unique putative *Coxiella* Ser/Thr kinase (CstK). We demonstrated CstK translocation by *C. burnetii* during infection, and we reported its localization at CCVs. *In vitro* kinase assays revealed that CstK undergoes autophosphorylation on Thr and Tyr residues and displays a *bona fide* kinase activity toward a test substrate of eukaryotic protein kinases. Furthermore, the identification of the Rab7 GTP-activating protein TBC1D5 as a CstK interactor suggests that this protein might be involved during infection to facilitate CCVs biogenesis. Indeed, TBC1D5 is actively recruited at CCVs during *Coxiella* infections, and TBC1D5-targeting siRNAs significantly affect CCVs development. Our data provide the first evidence that a *C. burnetii* secreted kinase might control host cell infection.

Results

C. burnetii genome encodes a single putative protein kinase

In silico analysis of the virulent *C. burnetii* strain RSA493 NMI genome revealed only one gene encoding a putative STPK. To date, no STPKs have been characterized in this organism. This gene was named *cstK* for *C. burnetii* serine threonine kinase and encodes a 246-amino acid protein with an estimated

molecular mass of 31 kDa. The gene coding for *cstK* is flanked by genes CBU_0174 (which encodes an hypothetical protein) and CBU_0176, a gene coding for the serine protease domain-containing protein degP.1. Of note, these genes are not part of an operon (Fig. 1A). InterProScan analysis of CstK revealed the presence of most of the essential amino acids and sequence subdomains characterizing the Hanks family of eukaryotic-like protein kinases (37). CstK shares a common eukaryotic protein kinase superfamily fold with two lobes and a Gly-rich loop. These protein kinases include the central core of the catalytic domain and the invariant lysine residue in the consensus motif within subdomain II, which is usually involved in the phosphate transfer reaction and required for the autophosphorylating activity of eukaryotic STPKs (Fig. 1A) (37–39). The activation loop in the catalytic domain is particularly short in CstK, and the DFG motif is substituted by a GLG motif. Interestingly, the transmembrane domain usually present in classical prokaryotic STPKs is lacking in CstK; thus, it is a so-called cytoplasmic STPK.

CstK is a Dot/Icm effector protein

Bioinformatics analysis using the prediction software S4TE 2.0 (40) indicated that CstK harbors features corresponding to secreted effector proteins, including a promoter motif typically found in effector proteins from intravacuolar bacterial pathogens, suggesting that CstK is indeed a *Coxiella* effector protein (Fig. 1A). Consistently, previous studies by Chen *et al.* (36) have shown that CstK is secreted in a type 4b secretion system–dependent manner by the surrogate host *L. pneumophila*, albeit with low efficiency. To validate CstK secretion in *C. burnetii*, we engineered plasmids encoding, either CstK or CvpB (a known *C. burnetii* effector protein) (30), fused to β -lactamase (BLAM) and expressed in WT *Coxiella* Tn1832 (a *C. burnetii* transposon mutant expressing GFP and that phenocopies WT *C. burnetii*) or the Dot/Icm-defective *dotA::Tn* mutant, also expressing GFP. By means of a BLAM secretion assay, we could observe that BLAM-CstK was secreted by WT *Coxiella* at 48 and 72 h, but not at 24 h postinfection (Fig. 1B). Secretion of BLAM-CvpB or BLAM-CstK was not detectable in cells infected with the *dotA::Tn* strain, indicating that both CvpB and CstK are *C. burnetii* Dot/Icm substrates (Fig. 1B). Next, the intracellular localization of CstK was investigated by ectopically expressing HA-tagged CstK either in noninfected or WT *C. burnetii*-infected U2OS cells. In noninfected cells, CstK localized at intracellular compartments that were negative for the lysosomal marker LAMP1, whereas it was recruited at CCVs (as revealed by the co-localization with LAMP1) in infected cells (Fig. 1C).

CstK displays autokinase and protein kinase activities

To determine whether CstK is a functional protein kinase, this protein was overproduced in *Escherichia coli* and purified as a recombinant protein fused to glutathione S-transferase (GST) tag. The purified tagged CstK protein (Fig. 2A, upper panel) was then assayed for autokinase activity in the presence of the phosphate donor [γ -³³P]ATP. As shown in Fig. 2A (lower panel), CstK incorporated radioactive phosphate from [γ -³³P]ATP, generating a radioactive signal corresponding to

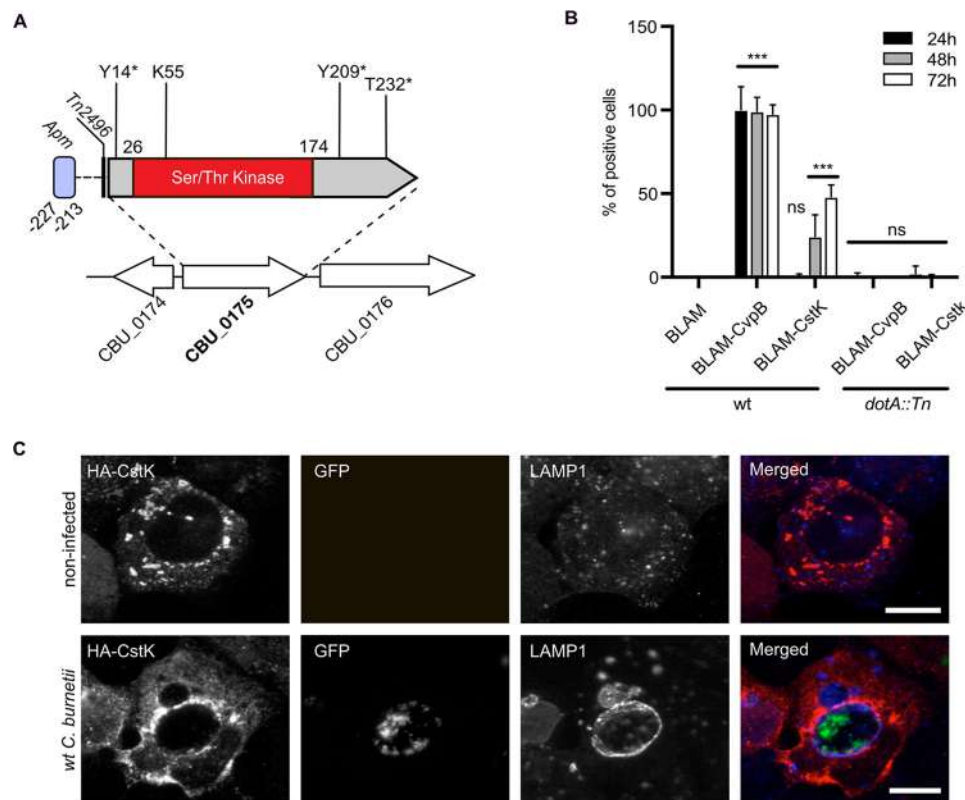


Figure 1. CstK is a Dot/Icm effector protein. A, schematic representation of CstK. A conserved promoter-binding domain is predicted between amino acids –227 and –213 (Apm), and the transposon insertion site for Tn2496 is indicated. The kinase domain is predicted between amino acids 26 and 174 and is shown in red. The conserved lysine residue is indicated, and the phosphorylated sites are indicated by an asterisk. B, BLAM secretion assay. U2OS cells were infected for 24, 48, or 72 h (black, gray, and white bars, respectively) with WT *C. burnetii* or the *dotA::Tn* mutant transformed with vectors expressing BLAM (negative control), BLAM-CvpB (positive control), or BLAM-CstK. Protein translocation was probed using the CCF-4 substrate. The average percentage of cells positive for cleaved CCF-4 as compared with the total number of cells was assessed. The values are means \pm S.D. from three independent experiments. ns, nonsignificant; ***, $p < 0.0001$, one-way ANOVA, Dunnett's multiple comparison test. C, U2OS cells ectopically expressing HA-tagged CstK (red) were either left untreated (top panels) or challenged with WT *C. burnetii* expressing GFP (green) for 3 days. Lysosomal compartments were labeled using anti-LAMP1 antibodies (blue). Scale bars, 10 μ m.

the expected size of the protein isoform, strongly suggesting that this kinase undergoes autophosphorylation. To confirm CstK autophosphorylation and exclude the possibility that contaminant kinase activities from *E. coli* extracts might phosphorylate CstK, we mutated the conserved Lys⁵⁵ residue present in subdomain II into CstK by site-directed mutagenesis. Indeed protein sequence analysis revealed that Lys⁵⁵ in CstK is similarly positioned as a conserved Lys residue usually involved in the phosphotransfer reaction and also required for the autophosphorylating activity of eukaryotic-like STPKs (37, 38). Thus, Lys⁵⁵ was substituted by a Met residue, the mutated form of CstK, CstK_K55M, was purified as described above (Fig. 2A, upper panel), and it was then tested for autophosphorylation in the presence of [γ -³²P]ATP. As expected, no radioactive signal could be detected (Fig. 2A, lower panel), thus establishing that CstK displayed autophosphorylation activity. A kinetic analysis of CstK phosphorylation was next performed to determine the initial CstK phosphorylation rate (Fig. 2B). Incorporation of γ -phosphate occurred rapidly, reaching \sim 50% of its maximum rate within 5 min of reaction. This autokinase activity depended on bivalent cations such as Mg²⁺ and Mn²⁺ in the range of 5 mM, thus in correlation with concentrations required for canonical STPK activity, as shown in Fig. 2C, and abolished by addition of 20 mM EDTA chelating all the divalent cations available (data not shown).

The recombinant CstK protein was further characterized by studying its ability to phosphorylate exogenous proteins and was thus assayed for *in vitro* phosphorylation of the general eukaryotic protein kinase substrate, myelin basic protein (MBP), in the presence of [γ -³²P]ATP. MBP is a commonly used substrate for both Ser/Thr and Tyr kinases. A radiolabeled signal at the expected 18-kDa molecular mass of MBP was detected, thus demonstrating that CstK phosphorylates protein substrates such as MBP (Fig. 2A). As expected, the CstK_K55M mutant did not phosphorylate MBP. Altogether, these data indicate that *in vitro*, CstK possesses intrinsic autophosphorylation activity and displays kinase functions for exogenous substrates.

Identification of CstK autophosphorylation sites

To determine the specificity of this kinase, we next identified its autophosphorylation sites. A MS approach was used because this technique allows precise characterization of post-translational modifications including phosphorylation (41, 42). NanoLC/nanospray/tandem MS (LC-ESI/MS/MS) was applied for the identification of phosphorylated peptides and for localization of phosphorylation sites in CstK. This approach led to 97% of sequence coverage, whereas the remaining residues uncovered did not include Ser, Thr, or Tyr residues.

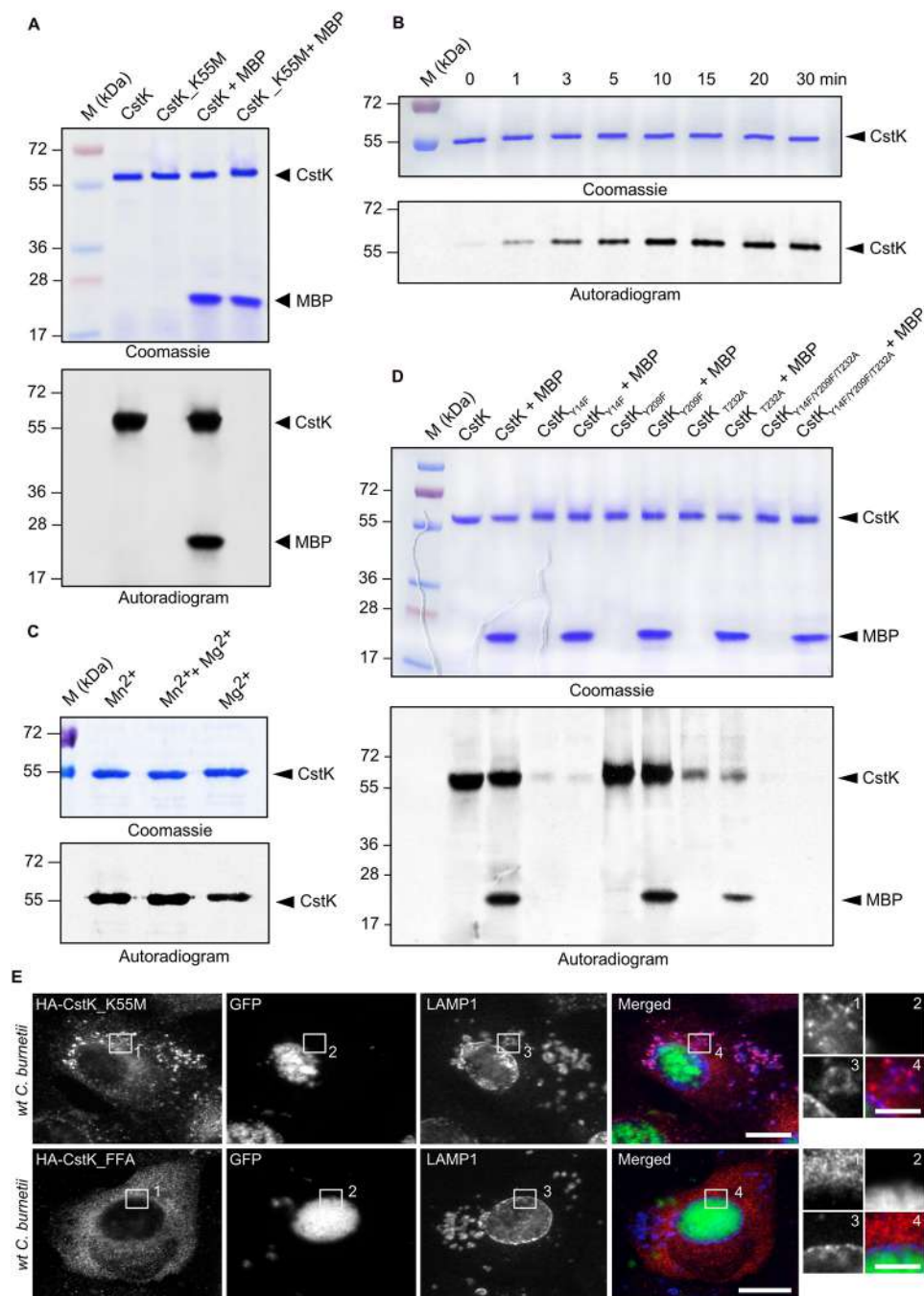


Figure 2. A, biochemical characterization of CstK. Recombinant CstK derivatives were overproduced, purified on GSH-Sepharose 4B matrix, submitted to gel electrophoresis, and stained with Coomassie Blue (upper panel). *In vitro* phosphorylation assays were performed with [γ -³³P]ATP for 30 min and the eukaryotic substrate myelin basic protein (MBP) when required. Proteins were analyzed by SDS-PAGE, and radioactive bands were revealed by autoradiography (lower panel). The upper bands illustrate the autokinase activity of CstK, and the lower bands represent phosphorylated MBP. Standard proteins of known molecular masses were run in parallel. B, a kinetic analysis was performed by incubation of CstK with [γ -³³P]ATP for different times. Proteins were analyzed by SDS-PAGE, and radioactive bands were revealed by autoradiography. C, effects of cations on autokinase activity of CstK. Purified CstK protein was subjected to *in vitro* autophosphorylation assays in the presence of 50 μ M ATP [γ -³³P]ATP and 5 mM of Mg²⁺ or Mn²⁺. Phosphoproteins were separated by SDS-PAGE and then revealed by autoradiography. D, *in vitro* phosphorylation of CstK mutant derivatives. The mutated variants CstK_Y14F (harboring a Tyr to Phe substitution at Tyr¹⁴), CstK_Y209F (harboring a Tyr to Phe substitution at Tyr²⁰⁹), CstK_T232A (harboring a Thr to Ala substitution at Thr²³²), and CstK_Y14F/Y209F/T232A (harboring all three substitutions) were incubated in the presence of [γ -³³P]ATP with or without the eukaryotic substrate MBP. The samples were separated by SDS-PAGE, stained with Coomassie Blue (upper panel), and visualized by autoradiography (lower panel). The upper bands illustrate the autokinase activity of CstK, and the lower bands represent phosphorylated MBP. Standard proteins of known molecular masses were run in parallel (kDa lane). E, U2OS cells ectopically expressing either HA-tagged CstK_K55M or CstK_FFA (red) were challenged with WT *C. burnetii* expressing GFP (green) for 3 days. Lysosomal compartments were labeled using anti-LAMP1 antibodies (blue). Scale bars, 10 μ m. Inset, magnification scale bars, 4 μ m.

As detailed in Table 1, analysis of tryptic digests allowed the characterization of three phosphorylation sites in CstK. Surprisingly, unlike classical Ser/Thr or Tyr kinases, CstK was phos-

phorylated on two Tyr residues (Tyr¹⁴ and Tyr²⁰⁹), in addition to one Thr site (Thr²³²). Because protein sequence analysis did not reveal a classical activation loop in this kinase, the contri-

Table 1**Phosphoacceptors identified after phosphorylation of *C. burnetii* CstK**

Sequences of the phosphorylated peptides identified in CstK as determined by mass spectrometry following tryptic digestion are indicated, and phosphorylated residues (pT or pY) are shown in bold type.

Phosphorylated tryptic peptide sequence of CstK	Number of detected phosphate groups LC/MS/MS	Phosphorylated residue
⁸ LSVADF p YDLKK ¹⁸	1	Tyr ¹⁴
²²⁸ EQFN p TAGHLR ²³⁷	1	Thr ²³²
²⁰⁹ p YCNPHIK ²¹⁵	1	Tyr ²⁰⁹

bution of Thr²³², Tyr¹⁴, and Tyr²⁰⁹ to CstK kinase activity was individually assessed. Hence, these residues were mutated either to phenylalanine to replace tyrosine residues or alanine to replace threonine residue, generating the single mutants CstK_Y14F, CstK_Y209F, and CstK_T232A, as well as the CstK_Y14F/Y209F/T232A triple mutant (CstK_FFA). Next, *in vitro* kinase assays with [γ -³³P]ATP were carried out and revealed that maximum loss in CstK autophosphorylation activity was observed in the CstK_Y14F mutant (Fig. 2D), suggesting that this site is central for CstK activation. In contrast, the CstK_Y209F mutant exhibited a slight hyperphosphorylation, which might indicate that Tyr²⁰⁹ only plays an accessory role in controlling CstK autophosphorylation (Fig. 2D). Finally, the CstK_T232A mutant showed a reduced CstK phosphorylation and displayed diminished kinase activity toward the exogenous substrate MBP (Fig. 2D). Note that mutating all three autophosphorylation sites fully abrogated CstK kinase activity (Fig. 2D). These results indicate that Tyr¹⁴ and Thr²³² are the major phosphorylation sites in CstK and strongly suggest that CstK might be a dual specificity (Thr/Tyr) kinase.

CstK activity and phosphorylated state affect its intracellular localization

Next, we ectopically expressed HA-tagged CstK, CstK_K55M, and CstK_FFA derivatives in noninfected and *C. burnetii*-infected U2OS cells to investigate its intracellular localization. CstK mainly localized at vesicular compartments in noninfected cells and accumulated at CCVs upon *C. burnetii* infection, suggesting an active role in the biogenesis of this compartment (Fig. 1C). Interestingly, the inactive CstK_K55M mutant localized at vesicular structures positive for the lysosomal marker LAMP1 but not at CCVs, whereas the nonphosphorylated CstK_FFA displayed a diffuse localization in the cytosol of transfected cells (Fig. 2E). Overall, these data suggest that the kinase activity and phosphorylated state of CstK play an important role in its localization in cells.

CstK regulates vacuole development and *C. burnetii* replication within infected cells

As a first step toward the understanding of CstK functions in the course of infection and to appreciate the extent to which this kinase is required for growth and viability of *C. burnetii*, we attempted to inactivate the corresponding chromosomal gene. Unfortunately, after several attempts we were unable to generate a null mutant, suggesting that *cstK* might be essential. However, we had previously isolated a *C. burnetii* mutant (*Tn2496*) carrying a transposon insertion allowing GFP expression at position 156,783, 32 bp upstream of the starting codon of *cstK*

(43) (Fig. 1A). To determine the effect of this transposon insertion on *cstK* gene expression, we assessed the expression level of *cstK* mRNA from WT *C. burnetii* and *Tn2496* strains. Surprisingly, *cstK* expression was significantly up-regulated in the mutant strain, suggesting that the transposon insertion may have released a transcriptional negative regulation (Fig. 3A). This suggested that a putative transcriptional regulator might bind the *cstK* promoter and control its activity during host invasion.

We next examined the effects of CstK overexpression on *C. burnetii* infections by challenging Vero cells with WT *C. burnetii*, the Dot/Icm-defective *dotA::Tn* mutant, or the *Tn2496* mutant. Intracellular growth of the CstK-overexpressing strain was significantly reduced over 7 days of infection with an intermediate phenotype between WT and the *dotA::Tn* mutant (Fig. 3B). Accordingly, multiparametric phenotypic profile analysis of the *Tn2496* mutant indicated that this strain exhibited a major defect in CCV development as compared with WT *C. burnetii* (Fig. 3, C and D). To further investigate the effects of CstK overexpression on *C. burnetii* infections, GFP-expressing *C. burnetii* were transformed with plasmids expressing HA-tagged WT CstK or its corresponding mutants (CstK_K55M and CstK_FFA) under the control of an IPTG promoter. U2OS cells expressing cytoplasmic mCherry were challenged with the three *C. burnetii* strains in the presence or absence of IPTG. After 6 days of infection, the cells were fixed, labeled with Hoechst and anti-LAMP1 antibody to visualize host cells nuclei and CCVs, respectively, and processed for automated image analysis. In all cases, the overexpression of CstK was detrimental for CCVs biogenesis and bacterial replication (Fig. 3E). Next, U2OS cells were challenged with WT *C. burnetii*, the GFP-expressing *Tn2496* mutant strain, or a combination of the two for 6 days (Fig. 3F). The cells were then fixed and labeled with an anti-*C. burnetii* antibody to label both bacteria strains and incubated with Hoechst to visualize host cells nuclei (Fig. 3F). Automated image analysis was then used to determine the effects of CstK overexpression on the replication of WT bacteria, *in trans*. Co-infections resulted in a significant increase in the size of *Tn2496* colonies, indicating that WT *C. burnetii* can partially restore the growth of the CstK-overexpressing strain (Fig. 3G). However, a significant decrease in the size of bacterial colonies labeled by the anti-*C. burnetii* antibodies indicated that CstK overexpression has a detrimental effect in *trans* on the development of WT bacteria (Fig. 3G). Of note, vacuoles harboring WT or mutant colonies alone were never observed in co-infection experiments. Therefore, we concluded that CstK participates in the formation of the *C. burnetii* replicative vacuole and that its expression must be finely tuned for optimal intracellular replication.

CstK specifically interacts with host cell proteins

Because CstK is a secreted protein, we assume that this kinase would interfere with host cell signal transduction pathways to subvert host cell defenses to the benefit of the bacteria. To identify host cell proteins that could interact with CstK, we made use of the model amoeba *Dictyostelium discoideum*. *D. discoideum* is a eukaryotic professional phagocyte amenable to genetic and biochemical studies. Lysate from cells overex-

CstK affects *C. burnetii* vacuole biogenesis

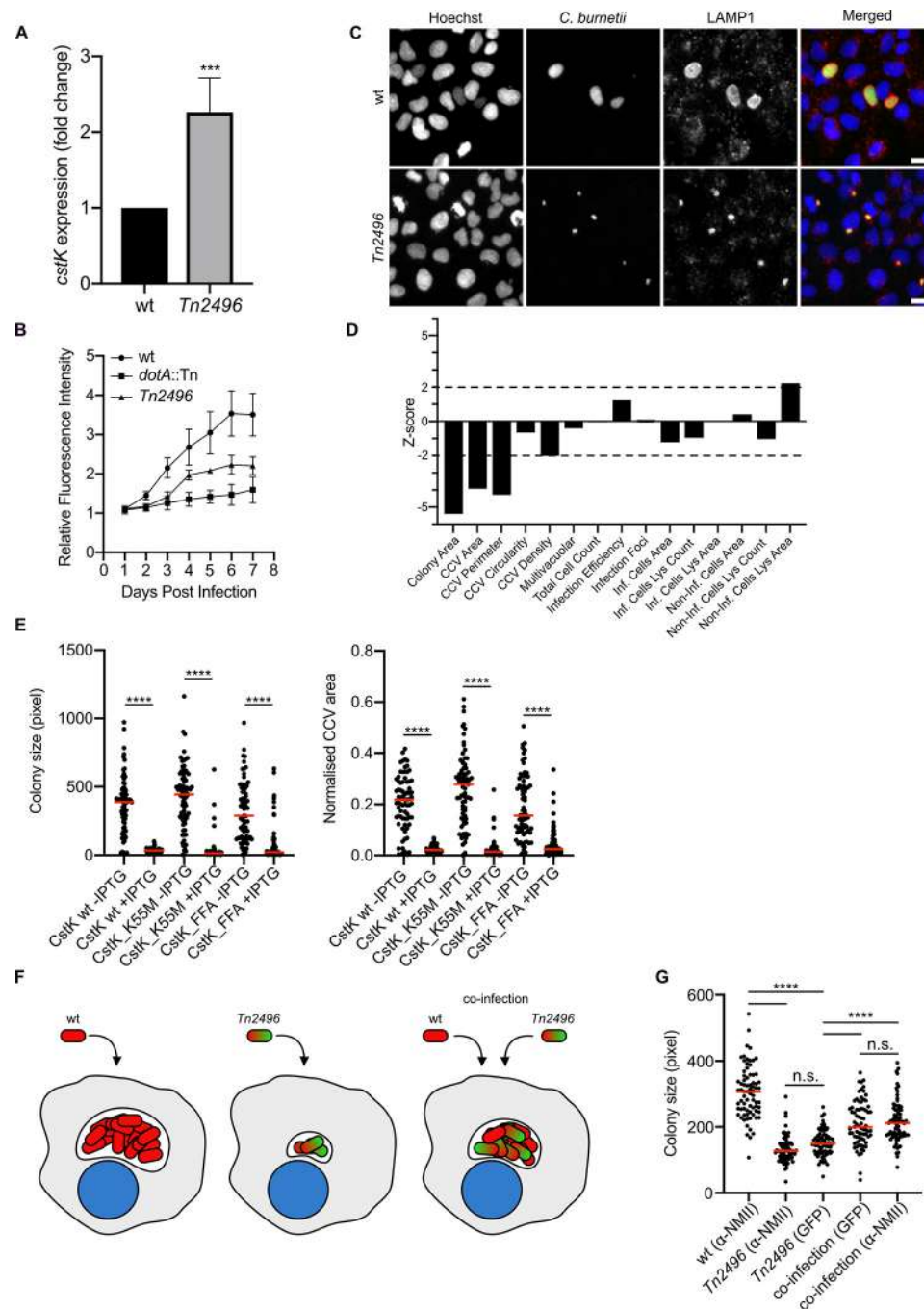


Figure 3. CstK regulates vacuole development and *C. burnetii* replication within infected cells. A, expression of *cstK* was measured by qRT-PCR from cultures of either WT *C. burnetii* or the Tn2496 mutant strain. The values are means \pm S.E. of four independent experiments. ***, $p < 0.001$, unpaired *t* test. B, Vero cells were challenged with WT *C. burnetii*, the *dotA::Tn* mutant, or the Tn2496 mutant strains, all expressing GFP. Intracellular replication was monitored over 7 days of infection by monitoring the GFP fluorescence using a microplate reader. The values are means \pm S.D. from three independent experiments. C, U2OS cells were challenged with either WT *C. burnetii* or the Tn2496 mutant strain, both expressing GFP (green). 7 days postinfection, the cells were fixed and labeled with an anti-LAMP1 antibody (red) and Hoechst (blue) to visualize CCVs and host cell nuclei, respectively. Scale bars, 10 μ m. D, an average of 50,000 cells were automatically imaged and analyzed from triplicate experiments for each condition illustrated in C, and the phenotypic profile of the Tn2496 mutant was compared with that of WT *C. burnetii* and expressed as z scores over 15 independent features. E, GFP-expressing *C. burnetii* transformed with plasmids encoding WT CstK, the K55M, or the FFA mutants, all under the regulation of an IPTG-inducible promoters were used to infect U2OS cells for 6 days, in the presence or absence of IPTG. The cells were then fixed and labeled as in C, and an average of 50,000 cells was automatically imaged and analyzed for each condition. The mean sizes of *C. burnetii* colonies and CCVs were calculated (red bars). F, U2OS cells were challenged with WT *C. burnetii*, the GFP-expressing mutant Tn2496, or a combination of the two strains for 6 days. The cells were then fixed and labeled with anti-*C. burnetii* antibodies (anti-NMII) to label both strains. G, an average of 50,000 cells were automatically imaged and analyzed for each condition illustrated in F, and the mean size of *C. burnetii* colonies was calculated (red bars). n.s., nonsignificant; ****, $p < 0.0001$, one-way ANOVA, Dunnett's multiple comparison test.

pressing CstK tagged with a C-terminal FLAG epitope (CstK-FLAG) was incubated with beads coupled to an anti-FLAG antibody. The beads were extensively washed, and

bound proteins were separated by SDS-PAGE before MS analysis. Among the putative interactants of CstK identified by this approach, some were discarded on the basis of their

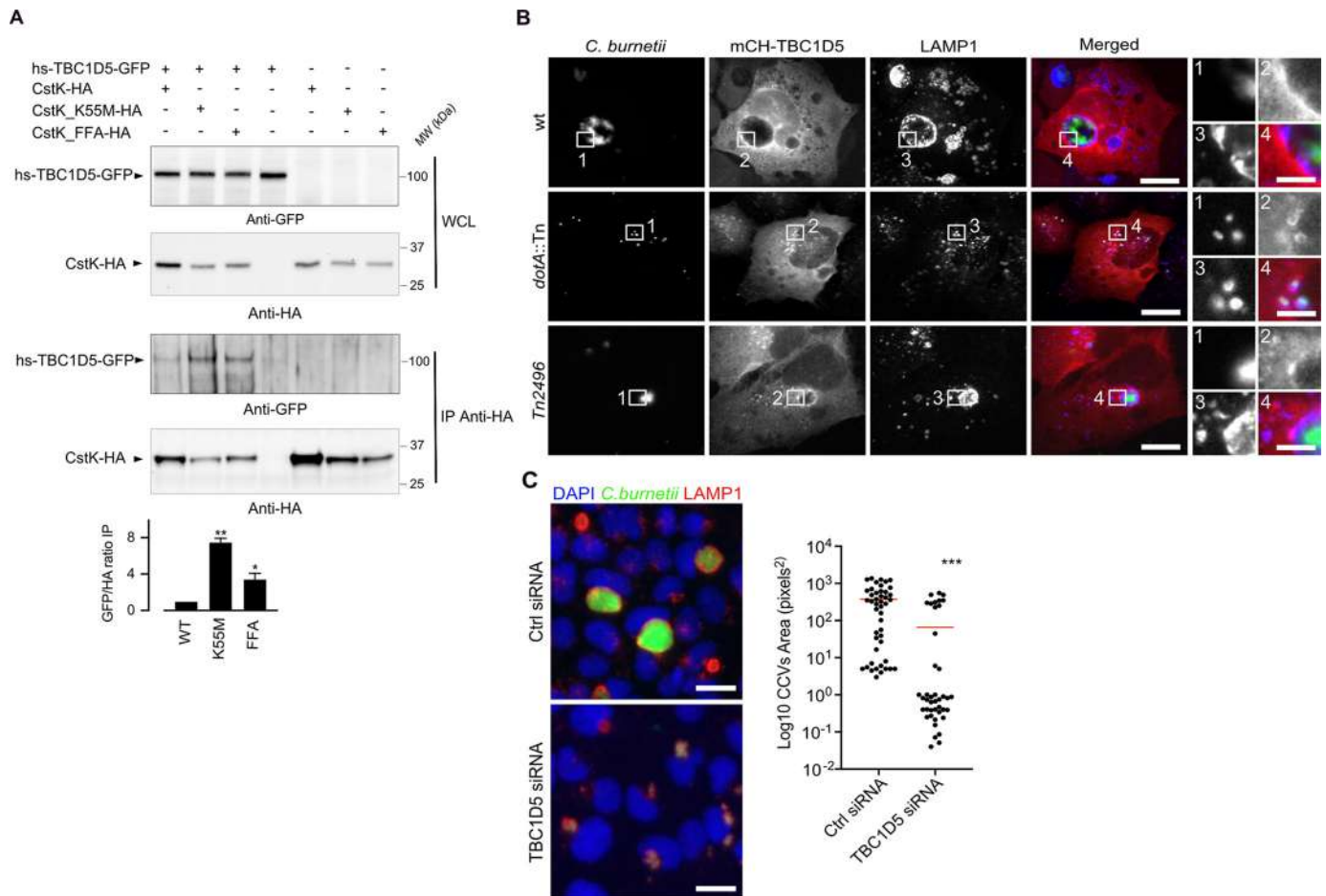


Figure 4. CstK interacts with TBC1D5. A, The interaction between CstK and the human TBC1D5 has been confirmed after cotransfection of HEK-293T cells to express each HA-tagged CstK derivatives with GFP-tagged Hs-TBC1D5. Cells have been lysed and HA-tagged CstK derivatives have been trapped on anti-HA magnetic beads (Pierce). Beads were washed, eluted by boiling, and bound proteins were revealed by Western blot analysis. Anti-HA antibody confirms the immunoprecipitation of CstK derivatives. For the densitometry graph, Regions of Interest (ROIs) were obtained from each band of interest and the intensity was measured (ctrl for “control” and WCL for “whole cell lysates”). B, Hs-TBC1D5 localization during infection was monitored in U2OS cells expressing mCherry-tagged Hs-TBC1D5 (red) challenged for 4 days either with wt *C. burnetii*, the Dot/Icm-defective *dotA::Tn* mutant or the CstK-overexpressing mutant *Tn2496*, all expressing GFP (green). Lysosomal compartments were labelled with anti-LAMP1 antibodies (blue). Scale bars 10 μ m. Inset magnification scale bars 4 μ m. C, The role of TBC1D5 in *C. burnetii* infections was investigated using siRNA to deplete Hs-TBC1D5 in U2OS prior to challenge with GFP-expressing wt *C. burnetii*. The size of CCVs was automatically calculated over an average of 150000 cells per condition. Red bars indicate medians. ***, $p < 0.0001$; **, $p < 0.001$; *, $p < 0.01$; one-way ANOVA, Dunnett’s multiple comparison test. Scale bars 10 μ m.

intracellular localization, whereas other retained candidates were mostly involved in the endocytic pathway (Table S1). Among these, the Rab GTPase-activating protein/TBC domain-containing protein, DDB_G0280253 (UniProtKB Q54VM3), is a 136.4-kDa protein homologous to mammalian TBC1D5 (dictyBase), a GTPase-activating protein for Rab7a and Rab7b (44–46) that acts as a molecular switch between the endosomal and the autophagy pathway (47). Given the recently reported implication of TBC1D5 in the biogenesis of *L. pneumophila*-containing vacuoles (48) and the role of autophagy in the biogenesis of CCVs (25, 31, 49), we aimed at validating the interaction between human TBC1D5 (Hs-TBC1D5) and CstK in HEK-293T cells. The cells co-expressing Hs-TBC1D5-GFP and HA-CstK or CstK mutants were used for immunoprecipitation using anti-HA beads. WT and CstK derivatives were detected as co-immunoprecipitated in the presence of Hs-TBC1D5-GFP, thus confirming that Hs-TBC1D5 is a *bona fide* CstK interactant (Fig. 4A). Significantly higher levels of TBC1D5 were co-

immunoprecipitated by the CstK mutants, suggesting that the interaction might be increased in the absence of phosphorylation turnover of the kinase (Fig. 4A, bottom panel). Interestingly, the interaction is not dependent on the phosphorylation status of CstK because the K55M mutant and the triple FFA mutant are still able to interact. Other candidates identified by MS are currently being investigated.

TBC1D5 is recruited at CCVs and regulates their biogenesis

Given its recently reported role in the development of *L. pneumophila*-containing vacuoles, we investigated the localization of TBC1D5 in U2OS cells infected with WT *C. burnetii*, the CstK-overexpressing strain *Tn2496*, or the Dot/Icm-defective mutant *dotA::Tn*. Consistent with previous studies demonstrating a role in the activation of Rab7a and b, TBC1D5 seems to accumulate specifically at CCVs in a Dot/Icm-independent manner because the eukaryotic protein was found at CCVs generated by all *C. burnetii* (WT, the *Tn2496*, and the *dotA::Tn*; Fig. 4B and Fig. S1). Next, we used siRNA to deplete

CstK affects *C. burnetii* vacuole biogenesis

cells of TBC1D5 prior to *C. burnetii* infection, to investigate a possible role in CCVs development and intracellular bacterial replication. Indeed, vacuole development was significantly reduced in cells exposed to Hs-TBC1D5-targeted siRNAs as opposed to cells treated with nontargeting siRNA oligonucleotides (Fig. 4C).

TBC1D5 is not phosphorylated *in vitro* by recombinant CstK

We assessed whether CstK might phosphorylate the recombinant Hs-TBC1D5. Despite the *in silico* prediction of several Ser/Thr and Tyr phosphorylatable residues in Hs-TBC1D5, we failed to detect Hs-TBC1D5 phosphorylation using several *in vitro* kinases assays (Fig. S2). In addition, Hs-TBC1D5 phosphorylation status was also investigated upon transfection with CstK or its inactive derivative (K55M) followed by Hs-TBC1D5 immunoprecipitation. No phosphorylation could be detected in our experimental conditions.

Discussion

Bacterial Ser/Thr/Tyr kinases expressed by pathogenic bacteria can either act as key regulators of important microbial processes or be translocated by secretion systems to interact with host substrates; thereby our results provide the first biochemical analysis of the secreted *C. burnetii* kinase CstK and its involvement in the process of infection and CCVs development. Importantly, CstK presents important differences as compared with classical Ser/Thr kinases. In particular, we provided evidence that CstK is a dual kinase able to autophosphorylate on Thr and Tyr residues. Moreover, the observation that a transposon insertion 32 bp upstream of the *cstK* starting codon leads to an increase in the levels of *cstK* mRNAs was indicative of the presence of a negative transcriptional regulation of gene expression, suggesting a fine-tuning of the levels of CstK. Indeed, the *Tn2496* mutant displays a severe CCV biogenesis defect when used to challenge U2OS cells, highlighting the importance of regulating *cstK* expression during *C. burnetii* infections. Accordingly, inducing the expression of WT CstK in WT *C. burnetii* severely impairs CCVs development and bacterial replication. Co-infection experiments demonstrated that CstK overexpression can also act *in trans*, by perturbing the intracellular replication of WT *C. burnetii*. The identification of candidate eukaryotic interactors of CstK further corroborated a role of the bacterial kinase in subverting host functions during infection. Here we confirmed that CstK interacts with TBC1D5, but we failed to detect phosphorylation of the eukaryotic target by CstK. However, we cannot exclude that TBC1D5 is a genuine CstK substrate *in vivo* because the lack of phosphorylation of host interactors of bacterial STPKs is not uncommon. Interaction between STPKs and host proteins might well perturb protein interaction networks at play in host cells (21). Indeed, the induced overexpression of CstK mutants lacking kinase activity in WT *C. burnetii* impaired CCVs development to the same extent as the overexpression of WT CstK. The biochemical mechanisms of these pathogen-directed targeted perturbations of host cell–signaling networks are being actively investigated. Regardless, siRNA depletion of TBC1D5 in *C. burnetii*-infected cells points at a role of the eukaryotic protein in CCVs development. In mammals, TBC1D5 was sug-

gested to function as a molecular switch between endosomal and autophagy pathways. Indeed TBC1D5 associates the retromer VPS29 subunit involved in endosomal trafficking, and upon autophagy induction, the autophagy ubiquitin-like protein LC3 can displace VPS29, thus orienting TBC1D5 functions toward autophagy instead of endosomal functions (47). It is thus tempting to propose that CstK might interfere with this tight regulation between TBC1D5, LC3, and VPS29 and redirect TBC1D5 functions to support efficient *C. burnetii* intracellular replication. Further work will need to be carried out to decipher how CstK recognizes these host substrates and how they participate in the establishment of *C. burnetii* parasitophorous vacuoles. Another perspective of this work is the opening of a new field of investigation for future drug development to fight this pathogen. Because CstK seems to be essential, specific inhibitors of this kinase preventing *C. burnetii* growth would be extremely useful for the development of new therapies.

Experimental procedures

Bacterial strains and growth conditions

Bacterial strains and plasmids are described in Table 2. Strains used for cloning and expression of recombinant proteins were *E. coli* TOP10 (Invitrogen) and *E. coli* BL21 (DE3)Star (Stratagene), respectively. *E. coli* cells were grown and maintained at 25 °C in LB medium supplemented with 100 µg/ml ampicillin when required. *C. burnetii* RSA439 NMII and transposon mutants *Tn1832*, *Tn2496*, and *dotA::Tn* were grown in ACCM-2 (45) supplemented with chloramphenicol (3 mg/ml) in a humidified atmosphere of 5% CO₂ and 2.5% O₂ at 37 °C.

Cloning, expression, and purification of CstK derivatives

The *cstK* (*CBU_0175*) gene was amplified by PCR using *C. burnetii* RSA439 NMII chromosomal DNA as a template with the primers listed in Table 3 containing a BamHI and HindIII restriction site, respectively. The corresponding amplified product was digested with BamHI and HindIII and ligated into the bacterial pGEX(M) plasmid, which includes a N-terminal GST tag, thus generating pGEX(M)-*cstK*. pGEX(M)-*cstK* derivatives harboring different mutations were generated by using the QuikChange site-directed mutagenesis kit (Stratagene, La Jolla, CA) and resulted in the construction of plasmids detailed in Table 3. For overexpression assays, *cstK* and its derivatives were cloned in the pJA-LACO-4xHA vector (30) using KpnI and BamHI restriction sites. All constructs were verified by DNA sequencing. Transformed *E. coli* BL21 Star cells with pGEX(M)-*cstK* derivatives were grown at 16 °C in LB medium containing 1 g/liter of glucose and 100 µg/ml of ampicillin and protein synthesis induced with 0.5 mM IPTG overnight. Bacteria were disrupted by sonication (Branson, digital sonifier) and centrifuged at 14,000 rpm for 25 min. Purifications of the GST-tagged recombinants were performed as described by the manufacturer (GE Healthcare). *cstK* coding sequence was also optimized for mammalian cell expression (GenScript), amplified by PCR, and cloned into pDAXA-3C (50) containing a FLAG tag for C-terminal fusion. After sequencing, the plasmid was linearized by the restriction

Table 2
Strains and plasmids used in this study

Strain or plasmid	Genotype or description	Source or reference
<i>E. coli</i> strains		
<i>E. coli</i> TOP10	<i>E. coli</i> derivative ultra-competent cells used for general cloning; F [−] mcrA D(mrr-hsdRMS-mcrBC) f80dlacZΔM15 D lacX74 endA1 recA1araD139 D (ara, leu)7697 galU galK rpsL nupG--tonA	Invitrogen
<i>E. coli</i> BL21(DE3)Star	F2 <i>ompT hsdSB</i> (rB2 mB2) <i>gal dcm</i> (DE3); used to express recombinant proteins in <i>E. coli</i>	Stratagene
<i>C. burnetii</i> strains		
<i>C. burnetii</i> RSA439 NMII	WT <i>C. burnetii</i> RSA439 NMII nonfluorescent	Ref. 55
<i>C. burnetii</i> Tn2496	<i>C. burnetii</i> RSA439 NMII carrying an Himar1-CAT-GFP cassette 32 bp upstream of CBU_0175, expressing GFP	This study
<i>C. burnetii</i> Tn1832	<i>C. burnetii</i> RSA439 NMII carrying an Himar1-CAT-GFP cassette in the intergenic region between CBU_1847b and CBU_1849, expressing GFP	Ref. 43
<i>C. burnetii</i> Tn292	<i>C. burnetii</i> RSA439 NMII carrying an Himar1-CAT-GFP cassette in CBU_1648 (<i>dotA</i>), expressing GFP	Ref. 43
Plasmids		
pGEX(M)	pGEX with a 321-bp EcoRI/BamHI fragment from pET19b introducing a HindIII site in the pGEX polylinker	Ref. 56
pGEX(M) _{cstK}	pGEX(M) derivative used to express GST-tagged fusion of CstK (Amp ^R)	This study
pGEX(M) _{cstK_K55M}	pGEX(M) derivative used to express GST-tagged fusion of CstK_K55 M (Amp ^R)	This study
pGEX(M) _{cstK_Y14F}	pGEX(M) derivative used to express GST-tagged fusion of CstK_Y14F (Amp ^R)	This study
pGEX(M) _{cstK_Y209F}	pGEX(M) derivative used to express GST-tagged fusion of CstK_Y209F (Amp ^R)	This study
pGEX(M) _{cstK_T232A}	pGEX(M) derivative used to express GST-tagged fusion of CstK_T232A (Amp ^R)	This study
pGEX(M) _{cstK_Y14F/Y209F/T232A}	pGEX(M) derivative used to express GST-tagged fusion of CstK_Y14F/Y209F/T232A (Amp ^R)	This study
peGFPN1	Vector used for mammalian expression of C-terminal GFP-tagged fusion proteins	Addgene
peGFPN1_Hs-TBC1D5-GFP	peGFP-N1 derivative used to express C-terminal GFP-tagged fusion of Hs_TBC1D5 for mammalian expression	This study
pmCH_Hs-TBC1D5-mCherry	pmCH derivative used to express C-terminal mCherry-tagged fusion of Hs_TBC1D5 for mammalian expression	This study
pRK5_HA_cstKopt	pRK5_HA derivative used to express N-terminal HA-tagged fusion of CstK codon-optimized for mammalian expression	This study
pRK5_HA_cstK_K55Mopt	pRK5_HA derivative used to express N-terminal HA-tagged fusion of <i>cstK_K55M</i> codon-optimized for mammalian expression	This study
pRK5_HA_cstK_FFaopt	pRK5_HA derivative used to express N-terminal HA-tagged fusion of <i>cstK_FFA</i> codon-optimized for mammalian expression	This study
pXDC61K-Blam	Vector with IPTG-inducible expression of β-lactamase	Ref. 57
pXDC61K-Blam-cvpB	pXDC61K-Blam derivative used to express Blam-tagged fusion of CvpB	This study
pXDC61K-Blam-cstK	pXDC61K-Blam derivative used to express Blam-tagged fusion of CstK	This study
pJA-LACO-4×HA	Vector with IPTG-inducible expression of 4 × HA-tagged proteins	Ref. 30
pJA-LACO-4×HA-cstK	Vector with IPTG-inducible expression of 4 × HA-tagged <i>cstK</i>	This study
pJA-LACO-4×HA-cstK_K55M	Vector with IPTG-inducible expression of 4 × HA-tagged <i>cstK_K55M</i>	This study
pJA-LACO-4×HA-cstK_FFA	Vector with IPTG-inducible expression of 4 × HA-tagged <i>cstK_FFA</i>	This study
<i>D. discoideum</i> plasmids		
pDXA-3C_cstK-FLAG	Vector for overexpression of CstK with a C-terminal FLAG tag in <i>D. discoideum</i>	This study
pDXA-3C_DdTBC1D5-myc	vector for expression of myc-DdTBC1D5 in <i>D. discoideum</i>	This study

enzyme ScaI and transfected in *D. discoideum* as described (51). Clone selection was made with 10 mg/ml of G418, and protein expression was assayed by Western blotting analysis of *D. discoideum* crude extract with an anti-FLAG rabbit polyclonal antibody (GenScript). For ectopic expression assays, *cstK*, *cstK_K55M*, and *cstK_FFA* with optimized codons (IDT) were cloned in pRK5-HA using the primer pair CstKopt-BamHI-Fw/CstKopt-EcoRI-Rv.

Cloning, expression, and purification of TBC1D5 derivatives

The *D. discoideum* GFP-tagged TBC1D5 was previously generated (48). Cells were grown at 22 °C in HL5 medium as previously described (51). Human TBC1D5 coding sequence was obtained from the hORFeome v8.1 (ORF 2659, Q92609, fully sequenced cloned human ORFs in Gateway Entry clones ready for transfer to Gateway-compatible expression

vectors). HsTBC1D5 coding sequence has been recombined into pEGFP-N1 RfC Destination vector by Gateway reaction (MGC Platform Montpellier), thus generating pEGFP-N1_HsTBC1D5 coding for HsTBC1D5 with a C-terminal GFP tag. pmCH_Hs-TBC1D5-mCherry has been generated by the same method (MGC Platform Montpellier).

RNA extraction and quantitative RT-PCR (qRT-PCR)

50 ml of *C. burnetii* culture was harvested, resuspended in 600 μl of RNA protect reagent (Qiagen) and incubated for 5 min at room temperature. Bacteria were centrifuged and resuspended in 200 μl of TE (10 mM Tris-HCl, 1 mM EDTA, pH 8) containing 1 mg/ml lysozyme. Bacterial suspension was incubated at room temperature for 5 min, and bacteria were disrupted by vigorous vortexing for 10 s every 2 min. 700 μl of lysis buffer from RNA easy kit (Qiagen) were added to the bacterial

Table 3**Primers used in this study**

Restriction sites are underlined and specified in parentheses. Mutagenized codons are shown in bold type.

Primer	5' to 3' sequence
NtermCstK	TATGGATCCTTAATGGCTTATATGAGGCTTAGT (BamHI)
CtermCstK	TATAAGCTTTTAATCCCATTCATATTTTC (HindIII)
RvCstK K55M	ATAAAGAGC AT CGCCGCTCG
FwCstKY14F	CTTAGTGTGGCTGACTTT TTT GATTGAAGAAGGGCAAG
FwCstKY209F	GGGGCGACGGCTATCGCT TTCT GTAAACCCACATAAAG
FwCstKT232A	CATTCGTGAACAGTTTAAT GCT GCGGGCCATTTCGATTAC
CstKopt-BamHI-Fw	GAAGGATCCCTGATGGCGTATATGCGTCTGAG
CstKopt-EcoRI-Rv	CTTGAATTCCTAGTCCCACTCGATGTTTCCAGATG
CstK-KpnI-Fw	AGGGGTACCTTAATGGCTTATATGAGGCTTAGT
CstK-BamHI-Rv	AGGGGATCCCTAATTAATCCCATTCATATTTTCTAA
CvpB-KpnI-Fw	GATGGTACCAGCAGACAGCCATCATTG
CvpB-KpnI-Fw	GATGGTACCAGCAGACAGCCATCATTG
RT-PCR primers	
DotA-F	GCTCCAGCATTCATCCAGT
DotA-R	GGCACTTAACAGCCCTCAT
CstK-F	GGCAAGGTATTAGGGCGGAA
CstK-R	GGGATTCTCACCATTGGCCT

suspension, and disruption was completed by vortexing vigorously. RNA was purified with the RNA easy kit according to the manufacturer's instructions. DNA was further removed using DNase I (Invitrogen). cDNA was produced using Superscript III reverse transcriptase (Invitrogen). Controls without reverse transcriptase were done on each RNA sample to rule out possible DNA contamination. Quantitative real-time PCR was performed using LightCycler 480 SYBR Green I Master (Roche) and a 480 light cycler instrument (Roche). PCR conditions were as follows: 3 min of denaturation at 98 °C, 45 cycles of 98 °C for 5 s, 60 °C for 10 s, and 72 °C for 10 s. The *dotA* gene was used as internal control. The sequences of primers used for qRT-PCR are listed in Table 3. The expression level of *cstK* in the WT strain was set at 100, and the expression levels of *cstK* in the *Tn2496* mutant were normalized to the WT levels.

In vitro kinase assays

In vitro phosphorylation was performed with 4 µg of WT CstK or CstK derivatives in 20 µl of buffer P (25 mM Tris-HCl, pH 7.0, 1 mM DTT, 5 mM MnCl₂, 1 mM EDTA, 50 µM ATP) with 200 µCi ml⁻¹ (65 nM; γ-³³P]ATP; PerkinElmer, ref: NEG 602H250UC, 3000 Ci mmol⁻¹) for 30 min at 37 °C. For substrate phosphorylation, 4 µg of MBP (Sigma) and 4 µg of CstK were used. Each reaction mixture was stopped by addition of an equal volume of Laemmli buffer, and the mixture was heated at 100 °C for 5 min. After electrophoresis, the gels were soaked in 16% TCA for 10 min at 90 °C and dried. Radioactive proteins were visualized by autoradiography using direct exposure to films.

Mass spectrometry analysis

For MS analysis, CstK was phosphorylated as described above, except that [γ-³³P]ATP was replaced with 5 mM cold ATP. Subsequent MS analyses were performed as previously reported (52, 53). Briefly, the samples were submitted to trypsin digestion and analyzed using an Ultimate 3000 nano-RSLC (Thermo Scientific, San Jose, CA) coupled on line with a quadrupole Orbitrap Q Exactive HF mass spectrometer via a nano-electrospray ionization source (Thermo Scientific). The samples were injected and loaded on a C18 Acclaim PepMap100 trap-column (Thermo Scientific) and separated on a C18

Acclaim Pepmap100 nano-column (Thermo Scientific). MS data were acquired in a data-dependent strategy selecting the fragmentation events based on the 20 most abundant precursor ions in the survey scan (350–1600 Th). The resolution of the survey scan was 60,000 at *m/z* 200 Th, and for MS/MS scan the resolution was set to 15,000 at *m/z* 200 Th. Peptides selected for MS/MS acquisition were then placed on an exclusion list for 30 s using the dynamic exclusion mode to limit duplicate spectra. Data files were then analyzed with Proteome Discover 2.2 using the SEQUEST HT algorithm against the Uniprot *D. discoideum*, which included the sequence of CstK.

***C. burnetii* infections**

U2OS epithelial cells were challenged with *C. burnetii* RSA439 NMII, the transposon mutants *Tn1832*, *dotA::Tn*, or *Tn2496* as previously described (38, 49). For co-infection experiments, the cells were challenged with a 1:1 ratio of *C. burnetii* RSA439 NMII and *Tn2496* transposon mutant. For gene silencing, U2OS cells were seeded at 2,000 cells/well in black, clear-bottomed, 96-well plates in triplicate and transfected with siRNA oligonucleotides 24 h later by using the RNAiMAX transfection reagent (Thermo Fisher Scientific) according to the manufacturer's recommendations. At 24 h post-transfection, the cells were challenged with *C. burnetii* (MOI of 100) and further incubated for 5 days. The cells were then fixed and processed for immunofluorescence. Where appropriate, anti-LAMP1 antibodies were used to label lysosomes and CCVs as previously described (54). Samples were imaged with a Zeiss Axio Imager Z1 epifluorescence microscope (Carl Zeiss) connected to a CoolSNAP HQ² CCD camera (Teledyne Photometrics, Tucson, AZ). Images were acquired with 40× oil immersion objectives and processed with Metamorph (Molecular Devices, San Jose, CA). For phenotypic screening, the samples were imaged with an ArrayScan VTI Live epifluorescence automated microscope (Cellomics) equipped with an ORCA-ER CCD camera (Hamamatsu). 25 fields/well were acquired for image analysis. ImageJ and ICY software were used for image analysis and quantifications. Phenotypic profiles (expressed as *z* scores) were calculated using CellProfiler, from triplicate experiments as previously described (54) following median based normalization of 96-well plates. Plates effects were cor-

rected by the median value across wells that are annotated as control.

***β*-Lactamase translocation assay**

Effector proteins translocation assays were performed as previously described (30). Briefly, *C. burnetii* Tn1832 (WT) and *dotA::Tn* were transformed with pXDC-Blam (negative control), pXDC-Blam-CvpB (positive control), or pXDC-Blam-CstK. Each strain was used to infect U2OS epithelial cells. After 24, 48, or 72 h of infection, the cells were loaded with the fluorescent substrate CCF4/AM (LiveBLAzer-FRET B/G loading kit; Invitrogen) in Hanks' balanced salt solution (20 mM HEPES, pH 7.3) containing 15 mM probenecid (Sigma). The cells were incubated in the dark for 1 h at room temperature and imaged using an EVOS inverted fluorescence microscope. Images were acquired using 4',6'-diamino-2-phenylindole and GFP filter cubes. The image analysis software CellProfiler was used to segment and identify all cells in the sample (GFP) and positive cells (4',6'-diamino-2-phenylindole) and to calculate the intensity of fluorescence in each channel. The percentage of positive cells *versus* the total number of infected cells was then calculated and used to evaluate effector translocation.

Immunoprecipitation from *D. discoideum* lysates

For immunoprecipitation assays, 2×10^7 cells were lysed in lysis buffer (50 mM Tris-HCl, pH 7.5, 300 mM NaCl, 0.5% Nonidet P-40, protease inhibitors (Roche)) and cleared by centrifugation for 15 min at 14,000 rpm in a microfuge. Lysate supernatants were incubated overnight at 4 °C with anti-FLAG mAb coated on agarose beads (Genscript). The beads were then washed five times in wash buffer (50 mM Tris-HCl, pH 7.5, 300 mM NaCl, 0.1% Nonidet P-40) and once in PBS. Bound proteins were migrated on SDS-PAGE and analyzed by LC-MS/MS.

Cell culture, heterologous expression, and anti-HA immunoprecipitation

HEK-293T cells were grown in DMEM (Gibco) containing 10% (v/v) FBS, 1% GlutaMAX (Gibco, 200 mM stock), 0.5% penicillin/streptomycin (Gibco, 10,000 units/ml stock) and maintained under standard conditions at 37 °C in a humidified atmosphere containing 5% CO₂. The cells were transiently transfected using the jetPEI transfection reagent (Polyplus-Transfection Inc.) to express either Hs-TBC1D5-GFP, CstK_HA derivatives, or each CstK derivatives with TBC1D5_GFP protein. The cells were used 24 h after transfection for immunoprecipitation assay. Transfected cells were washed two times in cold PBS and lysed in lysis buffer (50 mM Tris, 150 mM NaCl, 0.5 mM EDTA, 0.5% Nonidet P-40, protease, and phosphatases inhibitors (Roche)). Cleared lysate (950 μl, ~1 mg of total proteins) were incubated with anti HA magnetic Beads (Pierce) for 30 min at room temperature under gentle rotation. The beads were washed three times in lysis buffer, boiled in 2× Laemmli sample buffer and loaded on ExpressPlus™ PAGE gels (Genscript). The eluted proteins were visualized by Western blotting with the following antibodies: anti-HA from Chromotek, anti-GFP from Torrey Pines, donkey anti-rat, or anti-rabbit from Jackson ImmunoResearch.

Densitometry

Regions of Interest (ROIs) were obtained from each band of interest, and the intensity was measured using ImageLab (From Bio-Rad). For each band, the same ROI was used for background calculation and removal from areas adjacent to each band.

Author contributions—E. M., S. H.-B., S. B., J. A., M. Burette, M. M., F. L., M. Bonazzi, and V. M. conceptualization; E. M., S. H.-B., S. B., J. A., F. C., M. Burette, M. M., F. L., M. Bonazzi, and V. M. data curation; E. M., S. H.-B., S. B., J. A., F. C., L. G.-Z., M. Burette, M. M., F. L., M. Bonazzi, and V. M. formal analysis; E. M., S. H.-B., S. B., J. A., L. G.-Z., M. Burette, M. M., F. L., M. Bonazzi, and V. M. investigation; E. M., S. H.-B., S. B., J. A., F. C., M. Burette, M. M., F. L., M. Bonazzi, and V. M. methodology; E. M., M. Burette, M. M., F. L., M. Bonazzi, and V. M. project administration; E. M., M. Burette, M. M., F. L., M. Bonazzi, and V. M. writing-review and editing; S. H.-B., S. B., M. Burette, M. M., F. L., M. Bonazzi, and V. M. writing-original draft; F. L., M. Bonazzi, and V. M. funding acquisition.

Acknowledgments—We thank the Montpellier RIO imaging facility at the University of Montpellier, a member of the national infrastructure France-BioImaging, which is supported by the French National Research Agency through Grant ANR-10-INBS-04 ("Investments for the Future"). We acknowledge the contribution of the Protein Science Facility of the Structure Fédérative de Recherche Biosciences through Grant UMS3444 (to CNRS, US8/INSERM, ENS de Lyon, UCBL), especially Frédéric Delolme and Adeline Page, who performed the MS analysis.

References

1. Stancik, I. A., Sestak, M. S., Ji, B., Axelson-Fisk, M., Franjevic, D., Jers, C., Domazet-Lošo, T., and Mijakovic, I. (2018) Serine/threonine protein kinases from bacteria, archaea and eukarya share a common evolutionary origin deeply rooted in the tree of life. *J. Mol. Biol.* **430**, 27–32 [CrossRef](#) [Medline](#)
2. Janczarek, M., Vinardell, J. M., Lipa, P., and Karaš, M. (2018) Hanks-type serine/threonine protein kinases and phosphatases in bacteria: roles in signaling and adaptation to various environments. *Int. J. Mol. Sci.* **19**, E2872 [Medline](#)
3. Rajagopal, L., Clancy, A., and Rubens, C. E. (2003) A eukaryotic type serine/threonine kinase and phosphatase in *Streptococcus agalactiae* reversibly phosphorylate an inorganic pyrophosphatase and affect growth, cell segregation, and virulence. *J. Biol. Chem.* **278**, 14429–14441 [CrossRef](#) [Medline](#)
4. Hussain, H., Branny, P., and Allan, E. (2006) A eukaryotic-type serine/threonine protein kinase is required for biofilm formation, genetic competence, and acid resistance in *Streptococcus mutans*. *J. Bacteriol.* **188**, 1628–1632 [CrossRef](#) [Medline](#)
5. Echenique, J., Kadioglu, A., Romao, S., Andrew, P. W., and Trombe, M. C. (2004) Protein serine/threonine kinase StkP positively controls virulence and competence in *Streptococcus pneumoniae*. *Infect. Immun.* **72**, 2434–2437 [CrossRef](#) [Medline](#)
6. Jin, H., and Pancholi, V. (2006) Identification and biochemical characterization of a eukaryotic-type serine/threonine kinase and its cognate phosphatase in *Streptococcus pyogenes*: their biological functions and substrate identification. *J. Mol. Biol.* **357**, 1351–1372 [CrossRef](#) [Medline](#)
7. Av-Gay, Y., and Everett, M. (2000) The eukaryotic-like Ser/Thr protein kinases of *Mycobacterium tuberculosis*. *Trends Microbiol.* **8**, 238–244 [CrossRef](#) [Medline](#)
8. Chaba, R., Raje, M., and Chakraborti, P. K. (2002) Evidence that a eukaryotic-type serine/threonine protein kinase from *Mycobacterium tubercu-*

- losis regulates morphological changes associated with cell division. *Eur. J. Biochem.* **269**, 1078–1085 [CrossRef Medline](#)
9. Wehenkel, A., Bellinzoni, M., Graña, M., Duran, R., Villarino, A., Fernandez, P., Andre-Leroux, G., England, P., Takiff, H., Cerveñansky, C., Cole, S. T., and Alzari, P. M. (2008) Mycobacterial Ser/Thr protein kinases and phosphatases: physiological roles and therapeutic potential. *Biochim. Biophys. Acta* **1784**, 193–202 [CrossRef Medline](#)
10. Molle, V., and Kremer, L. (2010) Division and cell envelope regulation by Ser/Thr phosphorylation: *Mycobacterium* shows the way. *Mol. Microbiol.* **75**, 1064–1077 [CrossRef Medline](#)
11. Alber, T. (2009) Signaling mechanisms of the *Mycobacterium tuberculosis* receptor Ser/Thr protein kinases. *Curr. Opin. Struct. Biol.* **19**, 650–657 [CrossRef Medline](#)
12. Greenstein, A. E., Grundner, C., Echols, N., Gay, L. M., Lombana, T. N., Miecskowski, C. A., Pullen, K. E., Sung, P. Y., and Alber, T. (2005) Structure/function studies of Ser/Thr and Tyr protein phosphorylation in *Mycobacterium tuberculosis*. *J. Mol. Microbiol. Biotechnol.* **9**, 167–181 [CrossRef Medline](#)
13. Galyov, E. E., Håkansson, S., Forsberg, A., and Wolf-Watz, H. (1993) A secreted protein kinase of *Yersinia pseudotuberculosis* is an indispensable virulence determinant. *Nature* **361**, 730–732 [CrossRef Medline](#)
14. Håkansson, S., Galyov, E. E., Rosqvist, R., and Wolf-Watz, H. (1996) The *Yersinia* YpkA Ser/Thr kinase is translocated and subsequently targeted to the inner surface of the HeLa cell plasma membrane. *Mol. Microbiol.* **20**, 593–603 [CrossRef Medline](#)
15. Archambaud, C., Gouin, E., Pizarro-Cerda, J., Cossart, P., and Dussurget, O. (2005) Translation elongation factor EF-Tu is a target for Stp, a serine-threonine phosphatase involved in virulence of *Listeria monocytogenes*. *Mol. Microbiol.* **56**, 383–396 [CrossRef Medline](#)
16. Lima, A., Durán, R., Schujman, G. E., Marchissio, M. J., Portela, M. M., Obal, G., Pritsch, O., de Mendoza, D., and Cerveñansky, C. (2011) Serine/threonine protein kinase PrkA of the human pathogen *Listeria monocytogenes*: biochemical characterization and identification of interacting partners through proteomic approaches. *J. Proteomics* **74**, 1720–1734 [CrossRef Medline](#)
17. Wang, J., Li, C., Yang, H., Mushegian, A., and Jin, S. (1998) A novel serine/threonine protein kinase homologue of *Pseudomonas aeruginosa* is specifically inducible within the host infection site and is required for full virulence in neutropenic mice. *J. Bacteriol.* **180**, 6764–6768 [CrossRef Medline](#)
18. Kristich, C. J., Wells, C. L., and Dunny, G. M. (2007) A eukaryotic-type Ser/Thr kinase in *Enterococcus faecalis* mediates antimicrobial resistance and intestinal persistence. *Proc. Natl. Acad. Sci. U.S.A.* **104**, 3508–3513 [CrossRef Medline](#)
19. Beltrami, A. M., Mukhopadhyay, C. D., and Pancholi, V. (2009) Modulation of cell wall structure and antimicrobial susceptibility by a *Staphylococcus aureus* eukaryote-like serine/threonine kinase and phosphatase. *Infect. Immun.* **77**, 1406–1416 [CrossRef Medline](#)
20. Truong-Bolduc, Q. C., Ding, Y., and Hooper, D. C. (2008) Posttranslational modification influences the effects of MgrA on norA expression in *Staphylococcus aureus*. *J. Bacteriol.* **190**, 7375–7381 [CrossRef Medline](#)
21. Canova, M. J., and Molle, V. (2014) Bacterial serine/threonine protein kinases in host–pathogen interactions. *J. Biol. Chem.* **289**, 9473–9479 [CrossRef Medline](#)
22. Kazar, J. (2005) *Coxiella burnetii* infection. *Ann. N.Y. Acad. Sci.* **1063**, 105–114 [CrossRef Medline](#)
23. Arricau-Bouvery, N., and Rodolakis, A. (2005) Is Q fever an emerging or re-emerging zoonosis? *Vet. Res.* **36**, 327–349 [CrossRef Medline](#)
24. Madariaga, M. G., Rezai, K., Trenholme, G. M., and Weinstein, R. A. (2003) Q fever: a biological weapon in your backyard. *Lancet Infect. Dis.* **3**, 709–721 [CrossRef Medline](#)
25. Berón, W., Gutiérrez, M. G., Rabinovitch, M., and Colombo, M. I. (2002) *Coxiella burnetii* localizes in a Rab7-labeled compartment with autophagic characteristics. *Infect. Immun.* **70**, 5816–5821 [CrossRef Medline](#)
26. Newton, H. J., McDonough, J. A., and Roy, C. R. (2013) Effector protein translocation by the *Coxiella burnetii* Dot/Icm type IV secretion system requires endocytic maturation of the pathogen-occupied vacuole. *PLoS One* **8**, e54566 [CrossRef Medline](#)
27. Lührmann, A., Nogueira, C. V., Carey, K. L., and Roy, C. R. (2010) Inhibition of pathogen-induced apoptosis by a *Coxiella burnetii* type IV effector protein. *Proc. Natl. Acad. Sci. U.S.A.* **107**, 18997–19001 [CrossRef Medline](#)
28. Klingenberg, L., Eckart, R. A., Berens, C., and Lührmann, A. (2013) The *Coxiella burnetii* type IV secretion system substrate CaeB inhibits intrinsic apoptosis at the mitochondrial level. *Cell Microbiol.* **15**, 675–687 [CrossRef Medline](#)
29. Cunha, L. D., Ribeiro, J. M., Fernandes, T. D., Massis, L. M., Khoo, C. A., Moffatt, J. H., Newton, H. J., Roy, C. R., and Zamboni, D. S. (2015) Inhibition of inflammasome activation by *Coxiella burnetii* type IV secretion system effector IcaA. *Nat. Commun.* **6**, 10205 [CrossRef Medline](#)
30. Martinez, E., Allombert, J., Cantet, F., Lakhani, A., Yandrapalli, N., Neyret, A., Norville, I. H., Favard, C., Muriaux, D., and Bonazzi, M. (2016) *Coxiella burnetii* effector CvpB modulates phosphoinositide metabolism for optimal vacuole development. *Proc. Natl. Acad. Sci. U.S.A.* **113**, E3260–E3269 [CrossRef Medline](#)
31. Siadous, F. A., Cantet, F., Van Schaik, E., Burette, M., Allombert, J., Lakhani, A., Bonaventure, B., Goujon, C., Samuel, J., Bonazzi, M., and Martinez, E. (2020) *Coxiella* effector protein CvpF subverts RAB26-dependent autophagy to promote vacuole biogenesis and virulence. *Autophagy*, 1–17
32. Newton, H. J., Kohler, L. J., McDonough, J. A., Temoche-Diaz, M., Crabill, E., Hartland, E. L., and Roy, C. R. (2014) A screen of *Coxiella burnetii* mutants reveals important roles for Dot/Icm effectors and host autophagy in vacuole biogenesis. *PLoS Pathog.* **10**, e1004286 [CrossRef Medline](#)
33. Latomanski, E. A., Newton, P., Khoo, C. A., and Newton, H. J. (2016) The effector Cig57 hijacks FCHO-mediated vesicular trafficking to facilitate intracellular replication of *Coxiella burnetii*. *PLoS Pathog.* **12**, e1006101 [CrossRef Medline](#)
34. Vogel, J. P. (2004) Turning a tiger into a house cat: using *Legionella pneumophila* to study *Coxiella burnetii*. *Trends Microbiol.* **12**, 103–105 [CrossRef Medline](#)
35. Carey, K. L., Newton, H. J., Lührmann, A., and Roy, C. R. (2011) The *Coxiella burnetii* Dot/Icm system delivers a unique repertoire of type IV effectors into host cells and is required for intracellular replication. *PLoS Pathog.* **7**, e1002056 [CrossRef Medline](#)
36. Chen, C., Banga, S., Mertens, K., Weber, M. M., Gorbashieva, I., Tan, Y., Luo, Z. Q., and Samuel, J. E. (2010) Large-scale identification and translocation of type IV secretion substrates by *Coxiella burnetii*. *Proc. Natl. Acad. Sci. U.S.A.* **107**, 21755–21760 [CrossRef Medline](#)
37. Hanks, S. K., and Hunter, T. (1995) Protein kinases 6: the eukaryotic protein kinase superfamily: kinase (catalytic) domain structure and classification. *FASEB J.* **9**, 576–596 [CrossRef Medline](#)
38. Hanks, S. K., Quinn, A. M., and Hunter, T. (1988) The protein kinase family: conserved features and deduced phylogeny of the catalytic domains. *Science* **241**, 42–52 [CrossRef Medline](#)
39. Carrera, A. C., Alexandrov, K., and Roberts, T. M. (1993) The conserved lysine of the catalytic domain of protein kinases is actively involved in the phosphotransfer reaction and not required for anchoring ATP. *Proc. Natl. Acad. Sci. U.S.A.* **90**, 442–446 [CrossRef Medline](#)
40. Noroy, C., Lefrançois, T., and Meyer, D. F. (2019) Searching algorithm for type IV effector proteins (S4TE) 2.0: improved tools for type IV effector prediction, analysis and comparison. *PLoS Comput. Biol.* **15**, e1006847 [CrossRef Medline](#)
41. Fiuzza, M., Canova, M. J., Zanella-Cléon, I., Becchi, M., Cozzzone, A. J., Mateos, L. M., Kremer, L., Gil, J. A., and Molle, V. (2008) From the characterization of the four serine/threonine protein kinases (PknA/B/G/L) of *Corynebacterium glutamicum* toward the role of PknA and PknB in cell division. *J. Biol. Chem.* **283**, 18099–18112 [CrossRef Medline](#)
42. Molle, V., Leiba, J., Zanella-Cléon, I., Becchi, M., and Kremer, L. (2010) An improved method to unravel phosphoacceptors in Ser/Thr protein kinase-phosphorylated substrates. *Proteomics* **10**, 3910–3915 [CrossRef Medline](#)
43. Martinez, E., Cantet, F., Fava, L., Norville, I., and Bonazzi, M. (2014) Identification of OmpA, a *Coxiella burnetii* protein involved in host cell invasion, by multi-phenotypic high-content screening. *PLoS Pathog.* **10**, e1004013 [CrossRef Medline](#)
44. Borg Distefano, M., Hofstad Haugen, L., Wang, Y., Perdreau-Dahl, H., Kjos, I., Jia, D., Morth, J. P., Neefjes, J., Bakke, O., and Progida, C. (2018)

- TBC1D5 controls the GTPase cycle of Rab7b. *J. Cell Sci.* **131**, jcs216630 [CrossRef Medline](#)
45. Seaman, M. N. J., Mukadam, A. S., and Breusegem, S. Y. (2018) Inhibition of TBC1D5 activates Rab7a and can enhance the function of the retromer cargo-selective complex. *J. Cell Sci.* **131**, jcs217398 [CrossRef Medline](#)
 46. Sun, M., Luong, G., Plastikwala, F., and Sun, Y. (2020) Control of Rab7a activity and localization through endosomal type I γ PIP 5-kinase is required for endosome maturation and lysosome function. *FASEB J.* **34**, 2730–2748 [CrossRef Medline](#)
 47. Popovic, D., and Dikic, I. (2014) TBC1D5 and the AP2 complex regulate ATG9 trafficking and initiation of autophagy. *EMBO Reports* **15**, 392–401 [CrossRef Medline](#)
 48. Bärlocher, K., Hutter, C. A. J., Swart, A. L., Steiner, B., Welin, A., Hohl, M., Letourneur, F., Seeger, M. A., and Hilbi, H. (2017) Structural insights into *Legionella* RidL-Vps29 retromer subunit interaction reveal displacement of the regulator TBC1D5. *Nat. Commun.* **8**, 1543 [CrossRef Medline](#)
 49. McDonough, J. A., Newton, H. J., Klum, S., Swiss, R., Agaisse, H., and Roy, C. R. (2013) Host pathways important for *Coxiella burnetii* infection revealed by genome-wide RNA interference screening. *mBio* **4**, e00606-12 [Medline](#)
 50. Manstein, D. J., Schuster, H. P., Morandini, P., and Hunt, D. M. (1995) Cloning vectors for the production of proteins in *Dictyostelium discoideum*. *Gene* **162**, 129–134 [CrossRef Medline](#)
 51. Alibaud, L., Cosson, P., and Benghezal, M. (2003) *Dictyostelium discoideum* transformation by oscillating electric field electroporation. *Bio-Techniques* **35**, 78–80, 82–83 [CrossRef Medline](#)
 52. Brelle, S., Baronian, G., Huc-Brandt, S., Zaki, L. G., Cohen-Gonsaud, M., Bischoff, M., and Molle, V. (2016) Phosphorylation-mediated regulation of the *Staphylococcus aureus* secreted tyrosine phosphatase PtpA. *Biochem. Biophys. Res. Commun.* **469**, 619–625 [CrossRef Medline](#)
 53. Baronian, G., Ginda, K., Berry, L., Cohen-Gonsaud, M., Zakrzewska-Czerwińska, J., Jakimowicz, D., and Molle, V. (2015) Phosphorylation of *Mycobacterium tuberculosis* ParB participates in regulating the ParABS chromosome segregation system. *PLoS One* **10**, e0119907 [CrossRef Medline](#)
 54. Martinez, E., Cantet, F., and Bonazzi, M. (2015) Generation and multiphenotypic high-content screening of *Coxiella burnetii* transposon mutants. *J. Vis. Exp.* e52851 [CrossRef Medline](#)
 55. Beare, P. A., Sandoz, K. M., Omsland, A., Rockey, D. D., and Heinzen, R. A. (2011) Advances in genetic manipulation of obligate intracellular bacterial pathogens. *Front. Microbiol.* **2**, 97 [Medline](#)
 56. Molle, V., Kremer, L., Girard-Blanc, C., Besra, G. S., Cozzzone, A. J., and Prost, J. F. (2003) An FHA phosphoprotein recognition domain mediates protein EmbR phosphorylation by PknH, a Ser/Thr protein kinase from *Mycobacterium tuberculosis*. *Biochemistry* **42**, 15300–15309 [CrossRef Medline](#)
 57. Charpentier, E., Anton, A. I., Barry, P., Alfonso, B., Fang, Y., and Novick, R. P. (2004) Novel cassette-based shuttle vector system for gram-positive bacteria. *Appl. Environ. Microbiol.* **70**, 6076–6085 [CrossRef Medline](#)